1 Introduction to vibration-absorbing isolators

Vibration isolation is a procedure through which the transmission of oscillating disturbances or forces is reduced. This involves the insertion of a flexible member between the two vibrating bodies as shown in Figure 1.1. Most commonly this will be between the equipment and its supporting structure, where the vibration is emanating from either of the two and transmission to the other is undesirable. It can easily be anticipated that a very soft isolator will achieve this goal. However, the design of such an isolator is complicated by the fact that the equipment needs to be kept at a constant relative displacement to the structure at low frequencies.

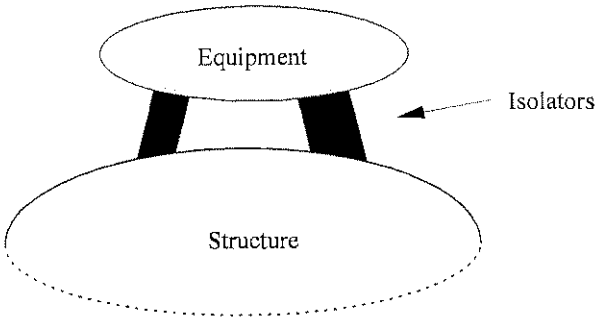

Figure 1.1: Isolation system

Miller & Ahmadian (1992) summarized the function of an isolator:

> *"In the simplest of terms, the ideal mount would have infinite stiffness at low frequencies and zero dynamic stiffness in the frequency range or the disturbance."*

Mead (2000) agreed:

> *"The study of vibration isolation must view the whole system in its three parts – the source system in which the vibration is generated, the receiver system in which the vibration is unwanted, and the interconnecting isolation system which must hold them together with adequate static stiffness and strength,* ***but with the smallest possible dynamic stiffness.***"

This goal can be illustrated graphically as shown in Figure 1.2.

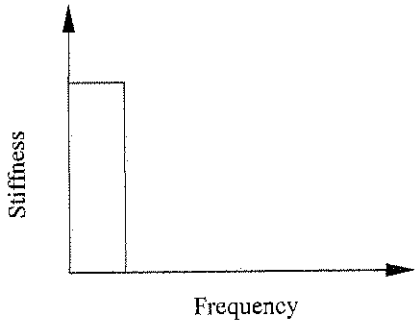

Figure 1.2: Stiffness *vs.* frequency relationship of an ideal isolator

As can be expected this discontinuous behaviour cannot be realised in practical systems. The goal of this thesis is to further our understanding of mechanical systems that can approximate this ideal isolator behaviour. Because of this approximation, a particular type of isolator will not necessarily be the best in all situations and additional parameters, such as the characteristics of the input, must be considered in order to arrive at an optimal solution.

Thus, when choosing a suitable isolator for a certain application it is important to define the isolation objective. One common aim would be to reduce the acceleration of sensitive equipment. This might be defined as a root-mean-square (rms) vibration criterion. Another aim might be to increase fatigne life. A further aim, which will be explored more fully in this thesis, relates to human vibration. In this case the output spectrum needs to be evaluated in terms of the ISO 5349 specification on hand-transmitted vibration. The optimal isolator choice will therefore depend on both the input spectrum as well as the evaluation criteria used. In cases where the excitation is tonal or narrow band an isolator with low dynamic stiffness at that frequency could be the best choice. In practice, however, random noise and harmonics will accompany most realistic inputs making the optimal choice less straightforward. The isolation philosophy is described graphically in Figure 1.3.

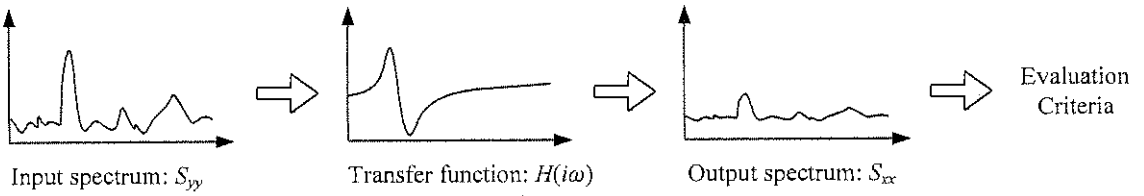

Figure 1.3: Isolation philosophy

A subset of tonal-excitation problems pertains to systems where the excitation frequency varies over a limited band. These changes can be a result of environmental changes such as ambient temperature or operational changes such as load. One possible solution to such a problem is to create an isolator that will continuously change its properties such that the region of lowest dynamic stiffness coincides with the excitation frequency. Such an isolator can be realised in a number of ways, the most general being an active isolator. It is, however, also possible to construct a passive isolator with adaptive properties (termed an adaptive isolator). Figure 1.4 illustrates how the adaptive algorithm seeks to minimise the objective of the isolator assuming that the input is stationary.

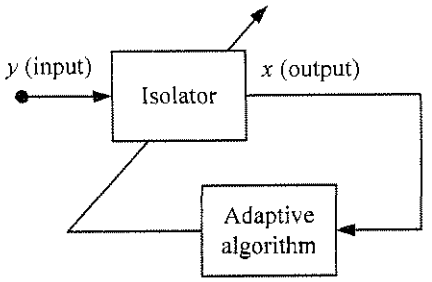

Figure 1.4: Adaptive isolator

The purpose of this chapter is to classify isolators in order to clarify the contribution of the thesis. The classification is not intended to be exhaustive, but examples will be given to illustrate isolator properties. Three approaches are identified namely passive, adaptive and active techniques. Passive

isolators are defined as resilient devices having no power requirements. Adaptive isolators can change its properties with some small power cost, while active isolators have a large power requirement. Passive techniques to reduce the dynamic stiffness of isolators will be introduced. These techniques are closely related to vibration absorbers and will therefore be termed vibration-absorbing isolators (VAI). The chapter will close by stating the aims of the research.

1.1 Background

In order to study the stiffness of isolators as a function of frequency it is necessary to define some terminology. Static stiffness refers to the deflection of the isolator when subjected to a constant force such as the weight of the equipment. Dynamic stiffness concerns the deflection when the system is moving and can be expressed as a function of frequency and is defined for frequencies larger than zero. The common definition of dynamic stiffness is the inverse of the direct receptance; F/Y in Figure 1.5 where the X, and Y refers to the excitation amplitude (Mead, 2000). It is, however, convenient to use the blocked ($X = 0$) transfer dynamic stiffness (F_T/Y) since it is independent of the mass of the attachment equipment (m_e). It is also possible to define the unblocked dynamic stiffness as $F_T/(X-Y)$. This has some advantages, which will be explored later. In this chapter a comparison of various isolation techniques will be discussed and it will be shown that the blocked transfer dynamic stiffness is a convenient measure to use. For the sake of brevity the blocked transfer dynamic stiffness will simply be referred to as the dynamic stiffness. When the dynamic stiffness is divided by the static stiffness the result is termed the normalised dynamic stiffness. This is an appropriate non-dimensional quantity.

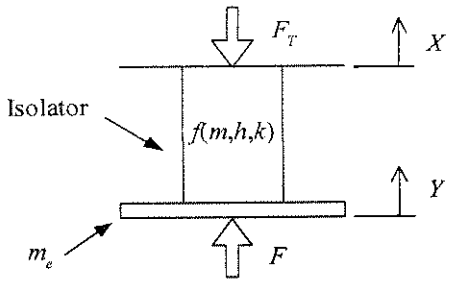

Figure 1.5: The definition of dynamic stiffness

For the system shown in Figure 1.5 the blocked and unblocked normalised dynamic stiffness lead to the same expressions (assuming the isolator mass is insignificant):

$$\frac{F_{T,unblocked}}{k(Y-X)} = 1 + i\eta \tag{1.1}$$

$$\frac{F_{T,blocked}}{kY} = 1 + i\eta \tag{1.2}$$

For some of the systems described later the blocked and unblocked dynamic stiffness is not equal. The unblocked dynamic stiffness has the advantage that it can be used to derive the system transmissibility. On the other hand, the blocked dynamic stiffness has the advantage that it only contains the properties of the isolator and not of the system being isolated. Therefore, it is independent of the natural

frequency of the system and as such explains the available parameters to reduce the transfer of motion clearly.

This study will further be limited to lumped-parameter systems i.e. rigid isolated masses suspended on massless isolators as shown in Figure 1.1. Such an approach is especially valid for low frequencies, which is the focus of this work. It will also be assumed that the resilient elements are massless, that is, massless spring and damping elements. The total isolation system need not be massless as it could include discrete masses, but these are expressly placed there to change the dynamics of the system and not to better idealise the spring or damping element behaviour. Due to the inclusion of masses the applied force (F) will not be equal to the transmitted force (F_T).

Most vibration texts consider both the transfer of force from a vibrating machine to its base as well as the transmission from a vibrating base to sensitive equipment. The first case is concerned with the force transmissibility, while the second considers motion transmissibility. For a single degree of freedom system the conclusions drawn from these two cases are essentially identical i.e. that the isolator stiffness should be as low as possible. This thesis will be limited to the motion transmissibility problem, without losing generality.

Several models exist to describe damping. The models that will be used in this work are:

1. Viscous damping $F_d = c\dot{x}$
2. Hysteretic damping $F_d = hx = k\eta x$
3. Coulomb or friction damping $F_d = -\text{sign}(\dot{x})\mu N$

When comparing the normalised dynamic stiffness of isolators in the frequency domain it is convenient to use hysteretic damping. It is not possible to use viscous damping for this purpose since non-dimensionalisation becomes impossible due to the addition of displacement and velocity units. In addition, although the linear viscous description of damping is mathematically convenient it is often not very realistic and it has been found that hysteretic damping better describes many common isolator materials, for instance, rubber (Rivin, 2001). In some cases time-domain simulation is used and in such cases the use of viscous damping will be necessary.

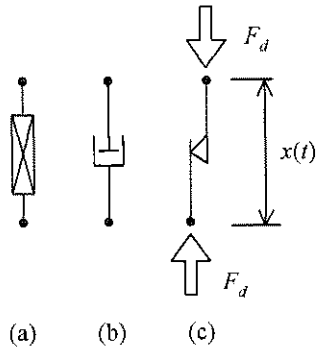

Figure 1.6: Damping models (a) hysteretic damper (b) viscous damper (c) Coulomb damper

Several models exist that describe the properties of an isolator. The most common element is the well-known Kelvin solid shown in Figure 1.7(c). Often elastomer behaviour is frequency dependent and can more accurately be described by the model shown in Figure 1.7(d) (Rivin, 2001).

The normalised dynamic stiffness for this model is [Equation (A.3)]:

$$\frac{F_T}{kY} = 1 + \frac{k'}{k}\frac{i\omega\frac{c}{k}}{\frac{k'}{k} + i\omega\frac{c}{k}} \tag{1.3}$$

The excitation (and response) is assumed to be of the form $y(t) = Ye^{i\omega t}$. To increase the readability of the thesis the derivation of the majority of the equations will be shown in appendices. Each chapter has its own appendix (i.e. Chapter 1, Appendix A etc.). References will indicate the equation in the relevant section of the appendix where the derivation can be found.

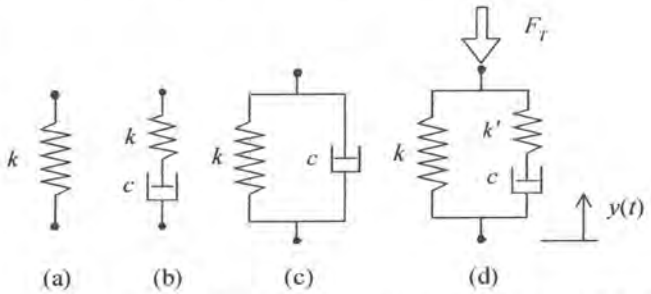

Figure 1.7: (a) Hook, (b) Maxwell, (c) Kelvin and (d) relaxation models (Rivin, 2001)

At low frequencies the model behaves as if the stiffness k' has no effect since the velocity across the damper is small. As the frequency increases the damper becomes solid and the stiffness k' appears parallel to stiffness k. The effect of frequency can be seen in Figure 1.8. This model does not take into account the effect of amplitude and temperature.

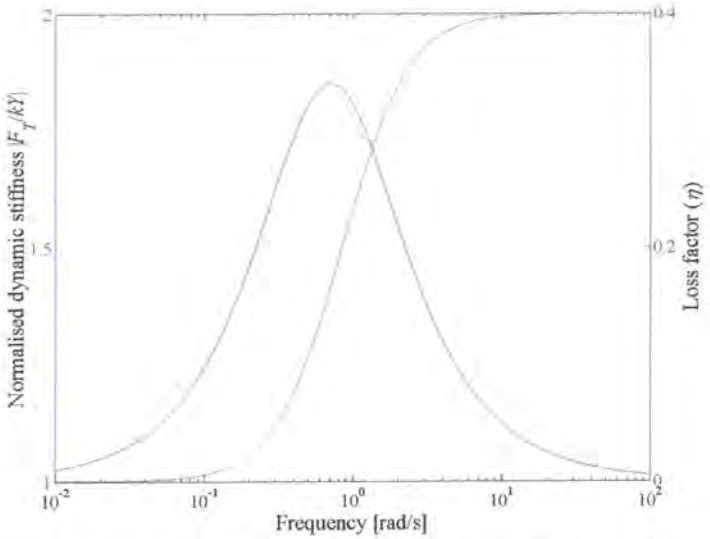

Figure 1.8: Normalised dynamic stiffness and loss factor of a relaxation model ($c/k = 1$ and $k'/k = 1$)

The quantities plotted in Figure 1.8 are the absolute values of the complex normalised dynamic stiffness and the loss factor. The loss factor is defined as the ratio of the imaginary and real parts of the complex dynamic stiffness as shown in Figure 1.9.

The loss factor is:

$$\eta = \frac{\mathrm{Im}\left(\frac{F_T}{kY}\right)}{\mathrm{Re}\left(\frac{F_T}{kY}\right)} = \tan(\theta) \tag{1.4}$$

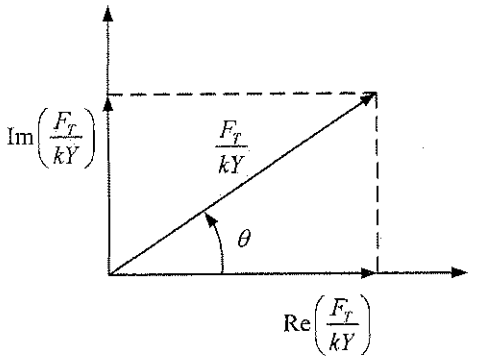

Figure 1.9: Complex dynamic stiffness phasor

Traditionally, isolation is discussed with reference to the single degree of freedom absolute transmissibility rather than dynamic stiffness (Rao, 1990). The single degree of freedom model is shown in Figure 1.10.

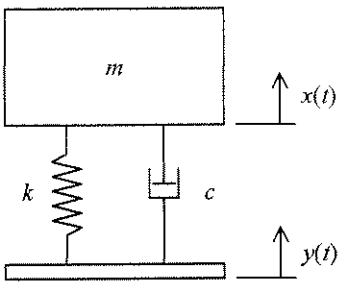

Figure 1.10: Mechanical model of a single degree of freedom isolator model

The transmissibility for a system with viscous damping is:

$$\frac{X}{Y} = \frac{1 + i2\frac{\omega}{\omega_n}\zeta}{1 + i2\frac{\omega}{\omega_n}\zeta - \left(\frac{\omega}{\omega_n}\right)^2} \tag{1.5}$$

where ζ is the damping ratio and ω_n the natural frequency. When using hysteretic damping the transmissibility is:

$$\frac{X}{Y} = \frac{1 + i\eta}{1 + i\eta - \left(\frac{\omega}{\omega_n}\right)^2} \tag{1.6}$$

For both these cases isolation occurs if the excitation frequency is larger than $\sqrt{2}\,\omega_n$ as shown in Figure 1.11.

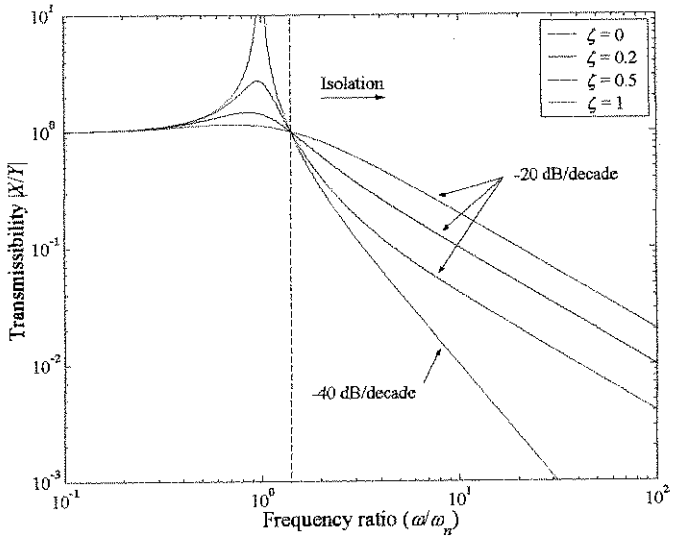

Figure 1.11: Single degree of freedom system transmissibility

In cases where the "rattle space" between of the isolated mass and its foundation is limited, the relative transmissibility is of importance. It is defined as $(X\text{-}Y)/Y$ and is related to the absolute transmissibility through:

$$\begin{aligned} T_r\big|_{REL} &= \frac{X-Y}{Y} \\ &= \frac{X}{Y} - 1 \\ &= T_r\big|_{ABS} - 1 \end{aligned} \tag{1.7}$$

In this thesis the absolute transmissibility will be used exclusively and will simply be referred to as the transmissibility. The relationship between the system transmissibility and the unblocked dynamic stiffness can be found by considering the force balance on the isolated mass as shown in Figure 1.12. The force acting on the mass can be calculated using the unblocked dynamic stiffness in Equation (1.1).

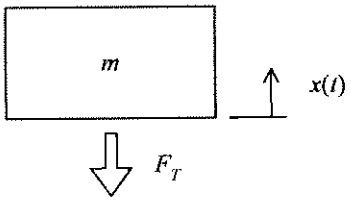

Figure 1.12: Force balance for the calculation of transmissibility

The result of the force balance is the transmissibility as shown before in Equation (1.6):

$$\begin{aligned} \sum F = F_T &= m\ddot{x} \\ k(1+i\eta)(Y-X) &= -\omega^2 mX \\ \frac{X}{Y} &= \frac{1+i\eta}{1+i\eta-\left(\frac{\omega}{\omega_n}\right)^2} \end{aligned} \tag{1.8}$$

By analysing several systems it was found that the blocked dynamic stiffness is a convenient method of comparison. In most cases it highlights the important parameters better than the transmissibility would have. There are, however, some exceptions where the transmissibility is modified by other factors than the dynamic stiffness, notably by "skyhook" damping and non-linear isolators. In such cases the effects will be explained by using transmissibility. The unblocked dynamic stiffness is only useful when the relationship between dynamic stiffness and transmissibility needs to be explained. In the following paragraphs the results of several unique derivations will be shown. These derivations relied heavily on existing vibration absorber literature, but had to be significantly adapted to fit the field of isolators.

1.2 Isolators

1.2.1 Passive isolators

Passive vibration isolation concepts can most easily be explained with reference to the basic isolator model shown in Figure 1.13.

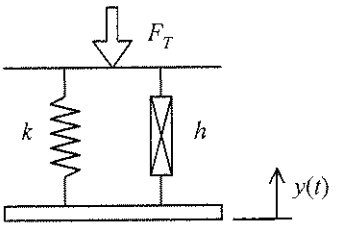

Figure 1.13: Mechanical model of a vibration isolator

The normalised dynamic stiffness is defined as the force transmitted by the isolator when a prescribed displacement (y) is applied:

$$\frac{F_T}{kY} = 1 + i\eta \tag{1.9}$$

Clearly, the normalised dynamic stiffness can never be less than 1 for a passive isolator. Additionally, materials tests have shown that for elastomers the loss factor will be a function of frequency and will generally increase with frequency resulting in an even more unfavourable situation as was shown in Figure 1.8 (Oyadiji & Tomlinson, 1994). Miller and Ahmadian (1992) also showed that elastomer an isolator's stiffness increases with frequency. Equation (1.9) implies that the stiffness must be as low as possible. There are, however, practical limits to the lowest stiffness that can be achieved in isolators. Improving these limits is not within the scope of this work and therefore, throughout this comparison, it will be assumed that the stiffness is as low as the technology used will allow.

The passive isolator can be augmented by adding an intermediate mass that will reduce the dynamic stiffness at high frequencies (Rivin, 2001). These devices are also known as two-stage mounts. The intermediate mass is inserted as shown in Figure 1.14. The stiffness values are chosen such that the normalised dynamic stiffness at zero Hz is the same as for the previous case, which allows fair comparison.

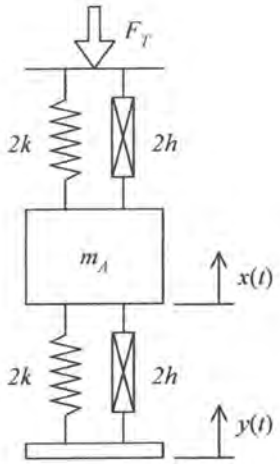

Figure 1.14: Mechanical model of an intermediate mass isolator

The normalised dynamic stiffness for this system is [Equation (A.9)]:

$$\frac{F_T}{kY} = \frac{(1+i\eta)^2}{1+i\eta-\left(\frac{\omega}{\omega_n}\right)^2} \qquad (1.10)$$

where: $\omega_n = \sqrt{\frac{4k}{m_A}}$

In Figure 1.15 it can be seen that the normalised dynamic stiffness will be less than one for all frequencies higher than $\sqrt{2}\,\omega_n$. The slope of the curve at high frequencies is -40 dB/decade, but this comes at the price of an area of high stiffness at low frequency. When the figure is compared to Figure 1.2 the approximation to the goal set out for this work is clear. By choosing the intermediate mass as large as possible the natural frequency of the isolator decreases and the isolation performance is optimised.

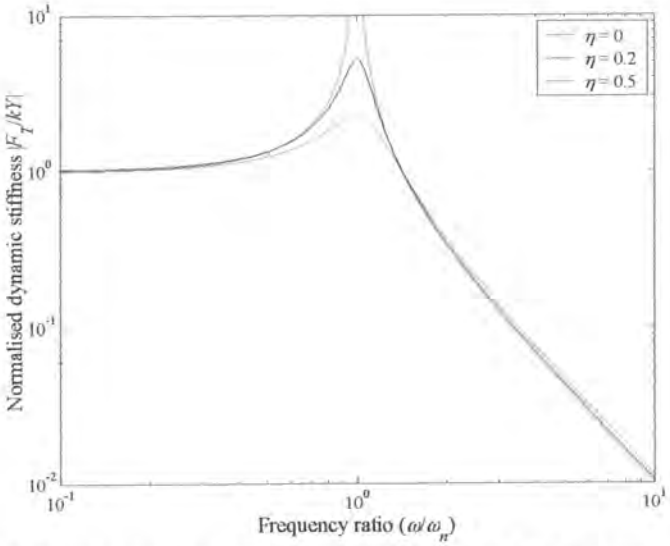

Figure 1.15: Normalised dynamic stiffness of an isolator with an intermediate mass

Several practical isolators display non-linear behaviour. This is often a consequence of their construction and not necessarily a performance requirement, as is the case with air springs. It is, however, possible to exploit non-linear behaviour to improve isolator performance. Two types of non-linear behaviour in isolators are identified. Firstly, a non-linear load-deflection characteristic is termed static non-linearity (Rivin, 2001). Examples of static non-linearity include Belleville springs, constant natural frequency isolators and motion-limiting bumpers (Babitsky & Veprik, 1998). Secondly, stiffness as well as damping that is frequency and amplitude dependent are categorised as dynamic non-linearities. Elastomeric materials commonly used for isolators exhibit this kind of behaviour as was illustrated in Figure 1.8.

An important aspect regarding non-linear behaviour of a single degree of freedom system with Duffing type stiffness is that the amplitude-frequency characteristic of the system "bends" at the natural frequency. This behaviour reduces the response at the natural frequency without the addition of damping, but at high amplitudes subharmonic oscillations will deteriorate isolation performance. Subharmonic oscillations cannot occur in systems where the damping exceeds a critical value depending on type and degree of non-linearity as well as amplitude of excitation (Rivin, 2001).

1.2.2 Adaptive isolators

Adaptive isolation entails the variation of stiffness and damping as shown in Figure 1.16. Adaptive isolation is also often termed semi-active isolation (Yu *et al.*, 2001).

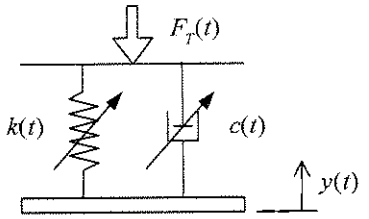

Figure 1.16: Mechanical model of a semi-active isolator

It is immediately clear that such a device cannot be used to reduce the normalised dynamic stiffness of the isolator. As such, these devices are not useful during steady state but can have advantages during transients. For instance, it is possible to increase the damping during start-up and rundown to reduce the response, while lowering damping when the excitation frequency is higher than $\sqrt{2}\,\omega_n$. Other instances where such devices can be used are in cases with conflicting requirements such as automotive suspensions, which need to be soft for comfort and hard to counteract body forces resulting from acceleration, braking and cornering. Cases where isolation is not the primary aim of the isolator falls outside the scope of this work.

1.2.3 Active isolators

Active isolation of vibration can be categorised as either feedback or feedforward techniques. Feedback control uses the response of the system as the input to the controller while feedforward control estimates the input directly. Generally, deterministic excitation is treated with feedforward

control and random excitation with feedback control (Fuller *et al.*, 1996). Two feedback techniques will be described. Absolute velocity feedback will be presented first (also termed "skyhook" damping). This is a well-known and effective technique to reduce system response at resonance (Karnopp, 1995). This technique does not reduce the dynamic stiffness, as does the second technique, which uses absolute input feedback.

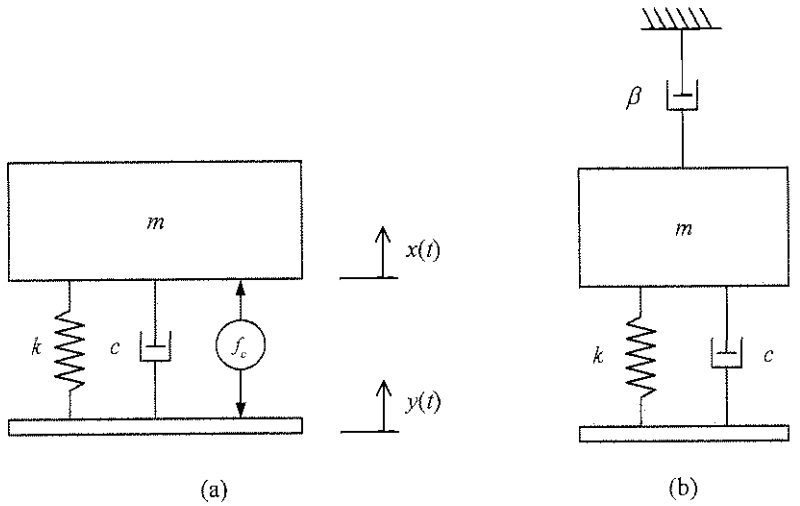

Figure 1.17: Mechanical model of an (a) active vibration isolator with absolute velocity feedback and (b) equivalent skyhook damper system

The control force (f_c) is a function of negative absolute velocity:

$$f_c(t) = -\beta \dot{x} \tag{1.11}$$

The system transmissibility is [Equation (A.14)]:

$$\frac{X}{Y} = \frac{1 + i2\dfrac{\omega}{\omega_n}\zeta}{1 + i2\dfrac{\omega}{\omega_n}\left(\zeta + \zeta_\beta\right) - \left(\dfrac{\omega}{\omega_n}\right)^2} \tag{1.12}$$

where: $\zeta = \dfrac{c}{2m\omega_n}$, $\zeta_\beta = \dfrac{\beta}{2m\omega_n}$

The most advantageous situation occurs when the system damping (ζ) is zero. In this case the high frequency roll-off remains -40 dB/decade regardless of the addition of damping by the control force as shown in Figure 1.18. If system damping exists the high frequency roll-off will be -20 dB/decade.

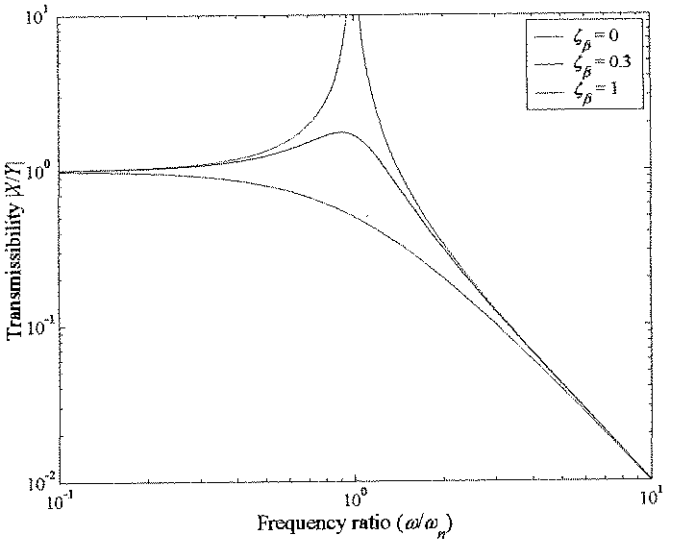

Figure 1.18: Transmissibility of an isolator with active damping ($\zeta = 0$)

Although many other active vibration isolator concepts exist, one is of particular interest since it is possible to arrange it in such a way that a system equivalent to the amplified vibration-absorbing isolator to be discussed in §1.4, is obtained. The model for this isolator is shown in Figure 1.19. It uses the input characteristics for the control force.

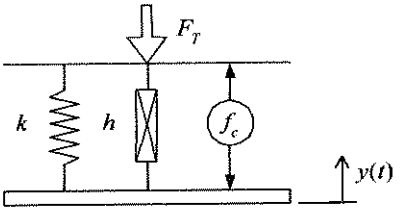

Figure 1.19: Mechanical model of an active isolator

The control force is:

$$f_c(t) = \alpha\ddot{y} + (\gamma + i\beta)y \tag{1.13}$$

where the parameters α, β and γ represent the gains.

The normalised dynamic stiffness is [Equation (A.18)]:

$$\frac{F_T}{(k+\gamma)Y} = 1 + i\frac{k\eta + \beta}{k+\gamma} - \left(\frac{\omega}{\omega_i'}\right)^2 \tag{1.14}$$

where: $\omega_i' = \sqrt{\dfrac{k+\gamma}{\alpha}}$

The undamped dynamic stiffness will be a minimum at the isolation frequency ω_i' as shown in Figure 1.20. It is possible to change the isolation frequency by varying the stiffness and acceleration feedback gains. Additionally, negative complex damping feedback can be used to reduce inevitable system

damping. These effects will be discussed in more detail in §1.4.2, which describes an adaptive device with similar properties but with some advantages, for instance, lower power requirement.

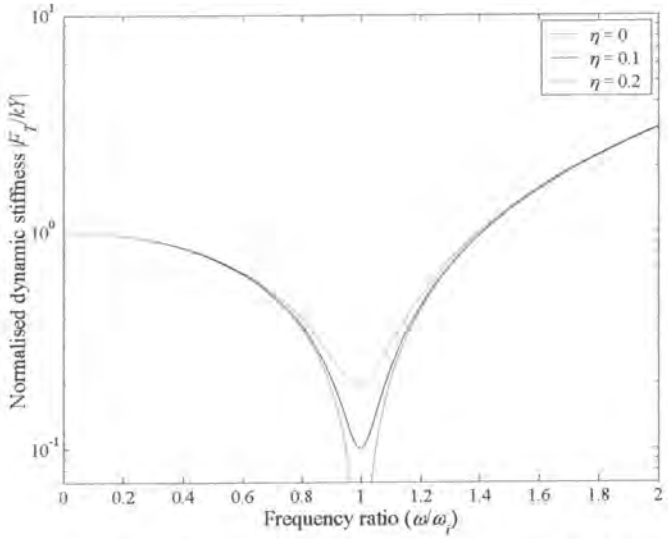

Figure 1.20: Normalised dynamic stiffness for an active isolator with absolute input acceleration feedback ($\alpha/k = 1$, $\gamma = 0$ and $\beta = 0$)

1.3 Vibration-absorbing isolators

Vibration absorbers are devices used to reduce the response of a structure by fixing a secondary spring mass system to the structure as shown in Figure 1.21. The first recorded use of vibration absorbers was to control the rolling motion of ships at sea (Watts, 1883). The vibration absorber was patented by Frahm (1909). The first theoretical analysis was done by Ormondroyd and Den Hartog (1928).

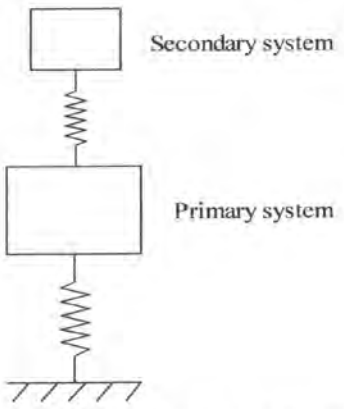

Figure 1.21: Vibration absorber

The secondary system is often called an auxiliary system. The objective of the absorber is to minimise the motion of the primary mass. This is achieved by tuning the natural frequency of the absorber to coincide with the excitation frequency. The result is a two degree of freedom system with zero response at the tuned frequency if no damping is present. Although vibration absorbers are classified as vibration control devices (Rao, 1990) they are not isolators since they are not fitted in the load path.

It is, however, possible to use a vibration absorber as part of a two-stage isolator as shown in Figure 1.22. This type of vibration control strategy is classified as nodalization by Mead (2000). He noted the similarity between nodalization and vibration isolators and the fact that it reacts the exciting force of the source by its own inertia forces.

Some authors (Mead, 2000 and Kidner and Brennan, 1999) prefer the term neutralizer to that of absorber because in their opinion "absorber" implies that the energy is dissipated. Ideally, in a low damping absorber, no energy will be dissipated. However, the word absorber is deeply entrenched in the literature and the device could therefore be called a Vibration-Absorbing Isolator (VAI) or a vibration-neutralizing isolator. In this work the term vibration-absorbing isolator will be used to describe the device. The relationship between the VAI and the vibration absorber is evident and the literature on vibration absorbers is extensive. A large proportion is applicable to the VAI, as will be shown next.

1.3.1 Passive vibration-absorbing isolators

The passive VAI is shown in Figure 1.22. Subscript A describes the intermediate (primary) mass and B the absorber (secondary) mass.

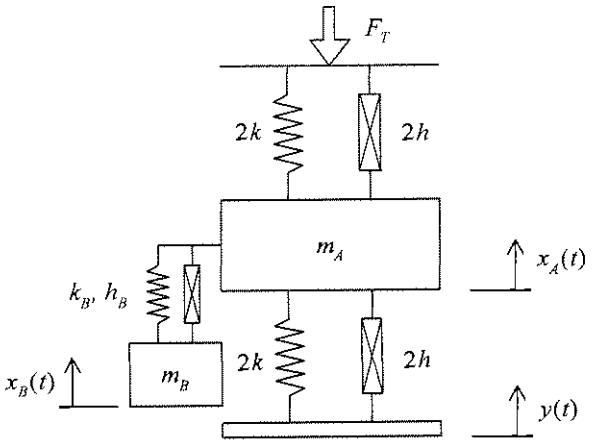

Figure 1.22: Mechanical model of a passive vibration-absorbing isolator ($h_B = \eta_B k_B$ and $h = \eta k$)

The normalised dynamic stiffness is given by [Equation (A.28)]:

$$\frac{F_T}{kY} = \frac{1 + i\eta_B - \left(\frac{\omega}{\omega_B}\right)^2}{\left[1 + i\eta + \frac{1}{4}\frac{k_B}{k}(1 + i\eta_B) - \left(\frac{\omega}{\omega_A}\right)^2\right]\left[1 + i\eta_B - \left(\frac{\omega}{\omega_B}\right)^2\right] - \frac{1}{4}\frac{k_B}{k}(1 + i\eta_B)} \tag{1.15}$$

where: $\omega_A = \sqrt{\frac{4k}{m_A}}$, $\omega_B = \sqrt{\frac{k_B}{m_B}}$

The main concern with the use of such a device is the small bandwidth over which the dynamic stiffness is low. Here the bandwidth is defined as the frequency range for which the normalized

dynamic stiffness is below 1 since that is the baseline for the best possible passive isolator. In Figure 1.23 it can be seen that the addition of damping decreases this bandwidth. Of course damping will be beneficial if the excitation frequency strays from the anticipated value.

The low-stiffness bandwidth could also be increased by increasing the mass ratio (m_B/m_A) as is shown in Figure 1.24. For a vibration absorber this will be difficult to do since the primary system mass is normally fixed and large. For the VAI it will be possible to choose a low intermediate mass (m_A) and therefore a large mass ratio is possible.

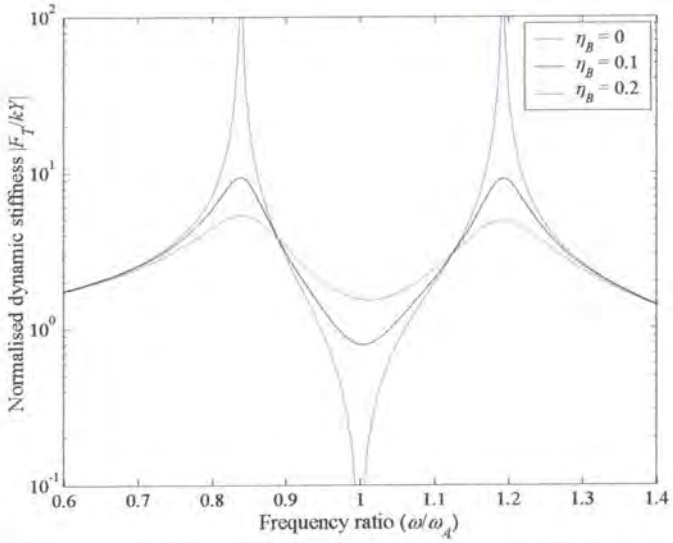

Figure 1.23: Normalised dynamic stiffness of a vibration-absorbing isolator as a function of absorber loss factor ($m_B/m_A = 1/8$, $\omega_A = \omega_B$ and $\eta = 0$)

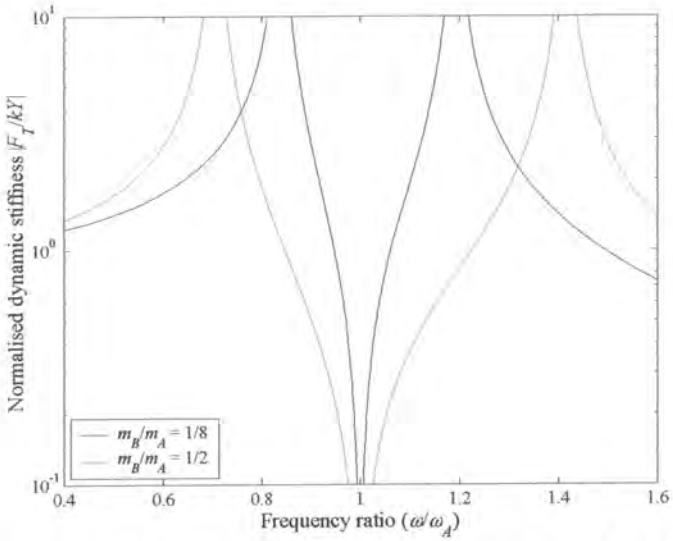

Figure 1.24: Normalised dynamic stiffness of a vibration-absorbing isolator as a function of mass ratio ($\eta = \eta_B = 0$ and $\omega_A = \omega_B$)

The bandwidth can be calculated by setting the normalised dynamic stiffness equal to 1 in Equation (1.15). There are four frequencies at which the undamped dynamic stiffness is equal to 1 as shown in Equation (1.16). Frequencies ω_2 and ω_3 define the bandwidth [Equations (A.30) and (A.32)].

$$\omega_1 = 0$$

$$\frac{\omega_2}{\omega_A} = \sqrt{\frac{1}{4}\mu_k + \left(\frac{\omega_B}{\omega_A}\right)^2} \tag{1.16}$$

$$\frac{\omega_3}{\omega_A}, \frac{\omega_4}{\omega_A} = \sqrt{\frac{\frac{1}{4}\mu_k + 2 + \left(\frac{\omega_B}{\omega_A}\right)^2 \mp \sqrt{\left[\frac{1}{4}\mu_k + 2 + \left(\frac{\omega_B}{\omega_A}\right)^2\right]^2 - 8\left(\frac{\omega_B}{\omega_A}\right)^2}}{2}}$$

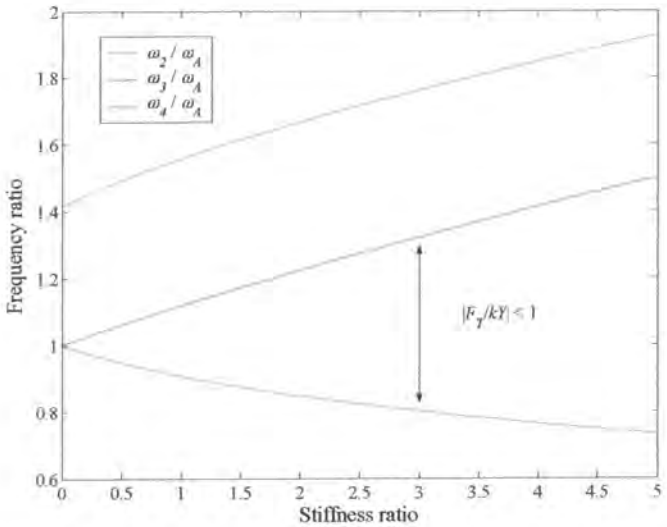

Figure 1.25: Frequencies at which the normalised dynamic stiffness is equal to 1 as a function of stiffness ratio (undamped, $\omega_B/\omega_A = 1$ and $\omega_1 = 0$)

The low stiffness bandwidth can be increased by attaching multiple vibration absorbers to the primary system as shown in Figure 1.26. The absorbers are tuned to a range of frequencies. It is possible to increase the suppression bandwidth by increasing the number of absorbers (Igusa & Xu, 1991 and Brennan, 1997a). Figure 1.27 shows a typical result for a system where the natural frequencies of a set of vibration absorbers are separated by η_q, the loss factor of the vibration absorbers. It is also clear from the figure that the resulting dynamic stiffness will be higher if the total mass of the absorbers is kept constant. The q^{th} natural frequency is:

$$\omega_q = \omega_A + (q-1)\eta_q \tag{1.17}$$

The q^{th} stiffness ratio is:

$$\frac{k_q}{k} = \frac{1}{N}\frac{\sum_{q=1}^{N} m_q}{m_A}\omega_q^2 \tag{1.18}$$

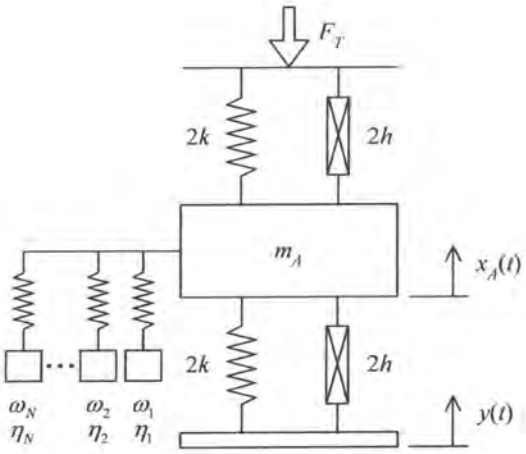

Figure 1.26: Mechanical model of a VAI with multiple vibration absorbers attached

The normalised dynamic stiffness for N absorbers can be written as [Equation (A.44)]:

$$\frac{F_T}{kY} = \frac{\left(1+i\eta_A\right)^2}{1+i\eta_A + \frac{1}{4}\sum_{q=1}^{N}\frac{k_q}{k}\left(1+i\eta_q\right) - \left(\frac{\omega}{\omega_A}\right)^2 - \frac{1}{4}\sum_{q=1}^{N}\frac{k_q}{k}\frac{\left(1+i\eta_q\right)^2}{1+i\eta_q - \left(\frac{\omega}{\omega_q}\right)^2}} \tag{1.19}$$

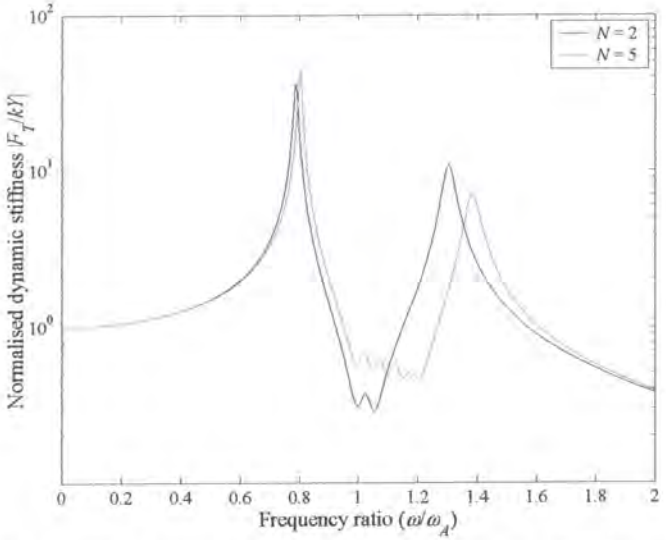

Figure 1.27: Normalised dynamic stiffness for a set of 2 and 5 vibration absorbers of equal total mass with natural frequencies separated by η_q starting at $\omega_A = 1$ ($\eta_1..\eta_q = 0.05$, $\eta = 0$ and $\Sigma m_q/m_A = 1$)

It has been shown that non-linear softening springs can be used to double the suppression bandwidth of a linear vibration absorber (Hunt & Nissen, 1981). For Duffing type non-linearity the spring restoring force (f_s) is given by:

$$f_s = k_B\left(x_A - x_B\right) + \alpha k_B\left(x_A - x_B\right)^3 \tag{1.20}$$

where α controls the degree of non-linearity. The normalised dynamic stiffness can be calculated by solving the following set of equations (Appendix A.3.3):

$$\begin{aligned}
&\ddot{x}_A + \frac{1}{2}\frac{k_B}{k}\frac{\zeta_B}{\omega_B}\omega_A^2(\dot{x}_A - \dot{x}_B) + \omega_A^2 x_A + \frac{1}{4}\frac{k_B}{k}\omega_A^2\left[x_A - x_B + \alpha(x_A - x_B)^3\right] = \frac{1}{2}\omega_A^2 y \\
&\ddot{x}_B - 2\zeta_B\omega_B(\dot{x}_A - \dot{x}_B) - \omega_B^2\left[x_A - x_B - \alpha(x_A - x_B)^3\right] = 0 \\
&\frac{f_T}{k} = 2x_A \\
&\text{where: } \zeta_B = \frac{c_B}{2m_B\omega_B},\quad \omega_A = \sqrt{\frac{4k}{m_A}},\quad \omega_B = \sqrt{\frac{k_B}{m_B}}
\end{aligned} \tag{1.21}$$

The normalised dynamic stiffness is shown in Figure 1.28 for various degrees of non-linearity.

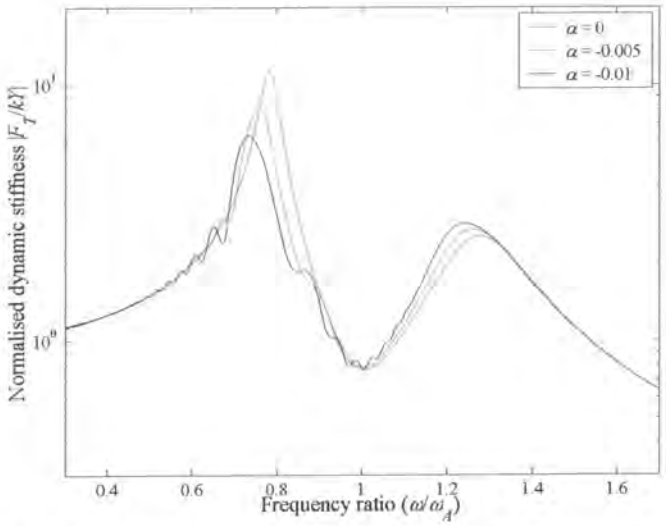

Figure 1.28: Normalised dynamic stiffness of a VAI with a non-linear absorber ($\zeta = 0.1$, $Y = 1$ and $\omega_A = \omega_B = k_B/k = 1$)

This section showed that it is possible to realise a device with a frequency range for which the dynamic stiffness is much less than one, even zero, in the ideal undamped configuration. It was also shown that the low stiffness bandwidth could be increased in a number of ways, each having its own disadvantage, notably addition of mass and added complexity. The adaptive vibration-absorbing isolator will address these problems, albeit with its own disadvantages, as will be shown next.

1.3.2 Adaptive vibration-absorbing isolators

Adaptive or tuneable vibration-absorbing isolators are devices that will automatically change their isolation frequency by changing either the absorber mass or stiffness. The advantage of tuning the absorber is that a low damping device can be used without the mass penalty normally required to increase the bandwidth. From Equation (1.15) it can be seen that the isolation frequency (ω_B) is equally sensitive to the absorber mass and stiffness. Practical implementations favour devices that changed stiffness, because it is easier to implement rather than attempting to change the absorber

mass. The technologies available to effect a change in stiffness are extensive, each with its own drawbacks and advantages. Methods that are available to vary stiffness can be categorised as follows:

1. Variable spring geometry:
    a. Compression of non-linear springs (Desanghere & Vansevenant, 1994).
    b. Moving a collar on a helical spring to control the number of active coils (Franchek *et al.*, 1995).
    c. Changing the moment of inertia of a beam or plate assembly (Walsh & Lamancusa, 1992 and Jensen, 1999).
    d. Varying spring displacement by changing its kinematics. Margolis (1992) used a variable fulcrum position for this purpose. Ribakov and Gluck (1998) changed the angle between the working direction and a set of angled helical springs to change their effective stiffness.
2. Variable physical property:
    a. Changing air spring pressure (Brennan, 1997b).
    b. Shape memory alloy Young's modulus modification, (Williams *et al.*, 2000).
    c. Using the magnetostrictive effect to vary the Young's modulus of a terfenol-D rod (Flatau *et al.*, 1998).
    d. Exploiting the temperature dependence of an elastomer's Young's modulus (Ketema, 1998).
    e. Magnetorheological elastomers under the influence of a magnetic field (Jolly *et al.*, 1996).
3. Electromagnets used to de-stiffen mechanical springs (Waterman, 1988).

Several variable damping methods have been published. Since variable damping is not useful for decreasing the low stiffness bandwidth it will not be discussed here. The model of an adaptive VAI with variable stiffness is shown in Figure 1.29.

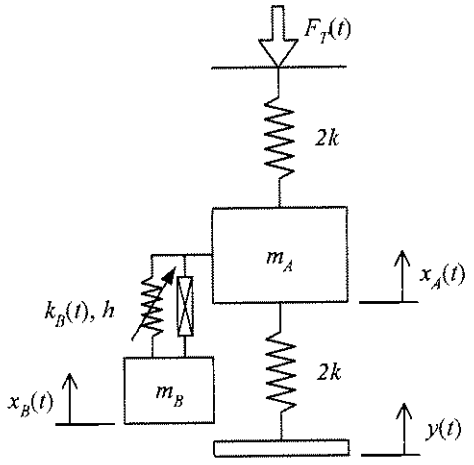

Figure 1.29: Mechanical model of an adaptive VAI

The normalised dynamic stiffness for the model shown in Figure 1.29 can be solved in the time domain using numerical integration. Such an analysis requires that the hysteretic damper be replaced by a viscous damper.

To calculate the transient behaviour the following set of equations must be solved [Equations (A.52) and (A.55)]:

$$\begin{aligned}
&\ddot{x}_A + \sqrt{\mu_m}\bar{\zeta}_B\omega_A\left(\dot{x}_A - \dot{x}_B\right) + \omega_A^2 x_A + \frac{1}{4}\mu_k(t)\,\omega_A^2\left(x_A - x_B\right) = \frac{1}{2}\omega_A^2 y \\
&\ddot{x}_B - \frac{\bar{\zeta}_B}{\sqrt{\mu_m}}\omega_A\left(\dot{x}_A - \dot{x}_B\right) - \frac{1}{4}\frac{\mu_k(t)}{\mu_m}\omega_A^2\left(x_A - x_B\right) = 0 \\
&\frac{f_T}{k} = 2x_A
\end{aligned} \tag{1.22}$$

where μ_k is the stiffness ratio k_B/k and μ_m is the mass ratio m_B/m_A. A simulation of the response of a system with an initial excitation frequency of 2π is shown in Figure 1.30. The excitation frequency is instantaneously doubled at 100 s and the stiffness is changed at 200 s such that the absorber is tuned to the new excitation frequency. In practice, there will be various delays associated with tuning and these will be discussed in more detail in §1.4.2. After tuning, some transient behaviour can be observed which must be controlled by the addition of damping.

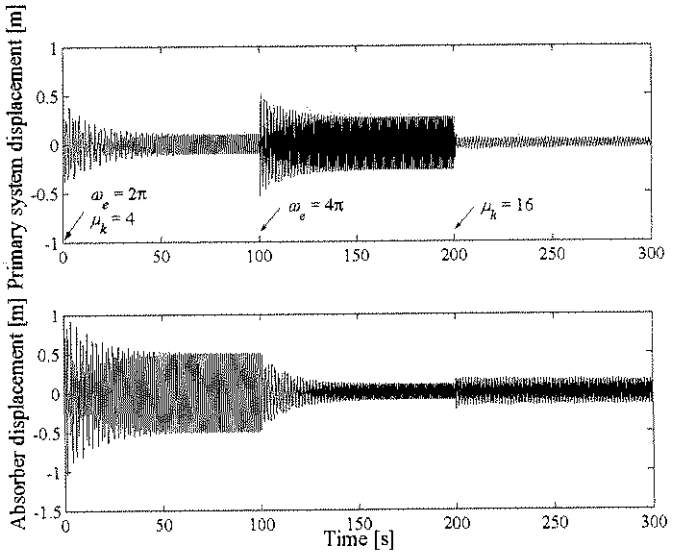

Figure 1.30: Transient response of a VAI ($\omega_A = 2\pi$, $\bar{\zeta}_B = 0.2$ and $Y = 1$)

If the assumption is made that the frequency changes will only occur occasionally and will be separated by long periods of steady state operation, it will be useful to derive the normalised dynamic stiffness. It is possible to find the normalised dynamic stiffness as a function of the intermediate mass natural frequency (ω_A) and the mass and stiffness ratios by rewriting Equation (1.15) [Equation (A.58)]:

$$\frac{F_T}{kY} = \frac{1 + i\eta_B - 4\dfrac{\mu_m}{\mu_k}\left(\dfrac{\omega}{\omega_A}\right)^2}{\left[1 + i\eta + \dfrac{1}{4}\mu_k\left(1 + i\eta_B\right) - \left(\dfrac{\omega}{\omega_A}\right)^2\right]\left[1 + i\eta_B - 4\dfrac{\mu_m}{\mu_k}\left(\dfrac{\omega}{\omega_A}\right)^2\right] - \dfrac{1}{4}\mu_k\left(1 + i\eta_B\right)} \tag{1.23}$$

where: $\mu_m = \dfrac{m_B}{m_A}$, $\mu_k = \dfrac{k_B}{k}$

This is a convenient equation with which to study the effect of absorber stiffness change on the dynamic stiffness of the VAI. The undamped frequency of minimum dynamic stiffness can be found by equating this equation to zero and will be termed the isolation frequency. The numerator can then be rewritten to yield the frequency ratio [Equation (A.56)]:

$$\frac{\omega_B}{\omega_A} = \frac{1}{2}\sqrt{\frac{\mu_k}{\mu_m}} \tag{1.24}$$

where ω_B is the isolation frequency. Figure 1.31 illustrates the effect when the stiffness ratio is changed from 2 to 6. At a stiffness ratio of 4 the isolation frequency is equal to the natural frequency of the intermediate mass (ω_A). To double the isolation frequency the stiffness ratio must be four times larger.

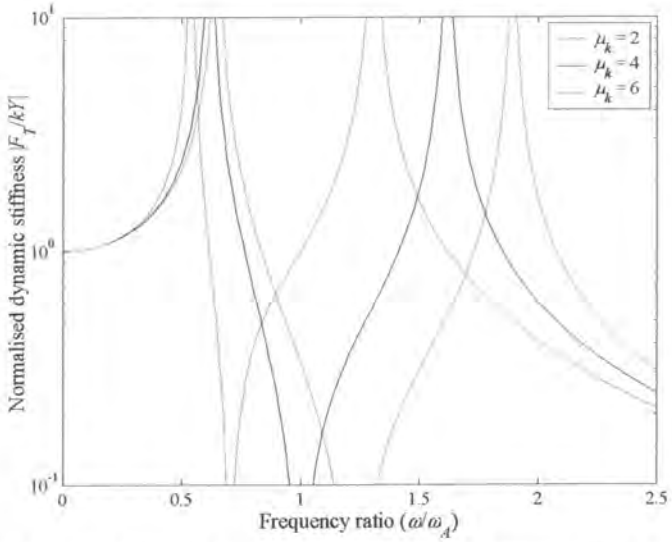

Figure 1.31: Effect of stiffness ratio on the normalised dynamic stiffness ($\mu_m = 1$, $\omega_A = 1$ and $\eta = \eta_B = 0$)

Figure 1.32 shows clearly that the adaptive VAI will be the most sensitive at low stiffness and mass ratios. At low mass ratios the adaptive VAI sensitivity increases, which strengthens the argument for tuning since for large mass ratios tuning will not be necessary.

Although it appears as if the adaptive VAI will be very sensitive at low stiffness ratios, its usefulness in this region will be limited by the proximity of the first frequency of large dynamic stiffness as illustrated in Figure 1.33 by the proximity of the black and blue lines for stiffness ratios less than 1. Depending on the application it could be decided that the separation is adequate above a stiffness ratio of, for instance, 1. If the stiffness change method chosen could vary the stiffness ratio from 1 to 6 the frequency ratio achievable will range from ~0.5 to ~1. Because of the proximity of the first frequency of large dynamic stiffness to the isolation frequency the full range of frequency ratios from 0 to ~1 is therefore not useful in practice. The frequencies of maximum dynamic stiffness are given by [Equation (A.61)]:

$$\frac{\Omega_1}{\omega_A}, \frac{\Omega_2}{\omega_A} = \sqrt{\frac{1+\frac{1}{4}\mu_k + \frac{1}{4}\frac{\mu_k}{\mu_m} \mp \sqrt{\left(1+\frac{1}{4}\mu_k + \frac{1}{4}\frac{\mu_k}{\mu_m}\right)^2 - \frac{\mu_k}{\mu_m}}}{2}} \tag{1.25}$$

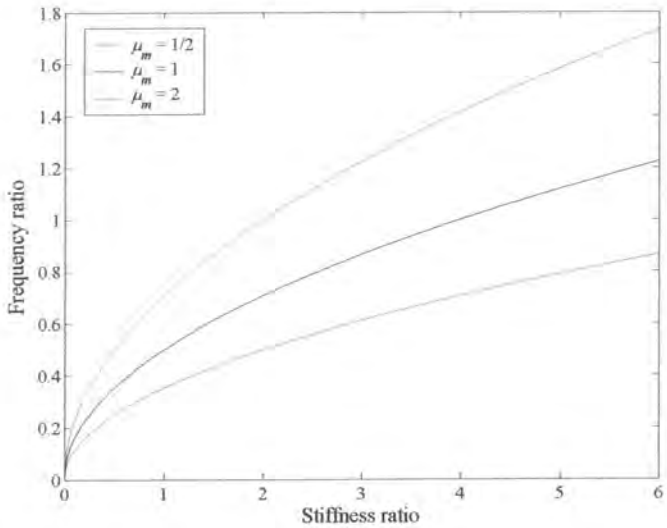

Figure 1.32: Undamped frequency ratio (ω_B/ω_A) *vs.* stiffness ratio for various mass ratios

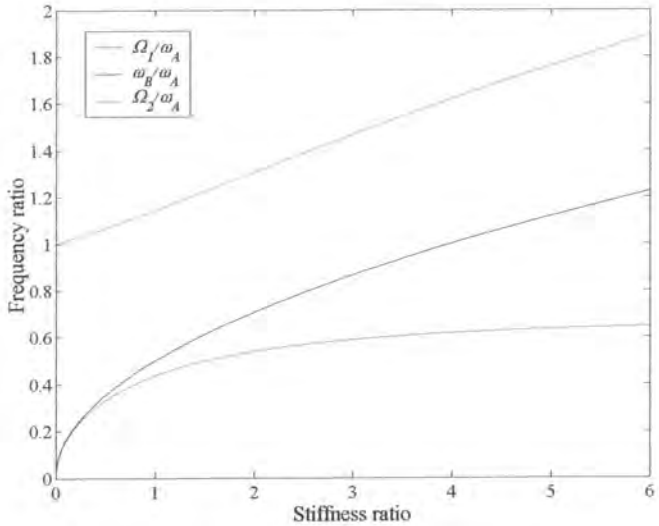

Figure 1.33: Undamped frequencies of maximum and minimum dynamic stiffness as a function of stiffness ratio ($\mu_m = 1$)

The envelope of the normalised dynamic stiffness can be calculated by finding the minimum stiffness at each frequency when changing the stiffness ratio from 0 to 6 and is shown in Figure 1.34. The normalised dynamic stiffness is less than 1 for a wide range of frequencies, but all frequencies will not be useful in a practical system because of the proximity of the first frequency of large dynamic stiffness at low stiffness ratios as discussed above.

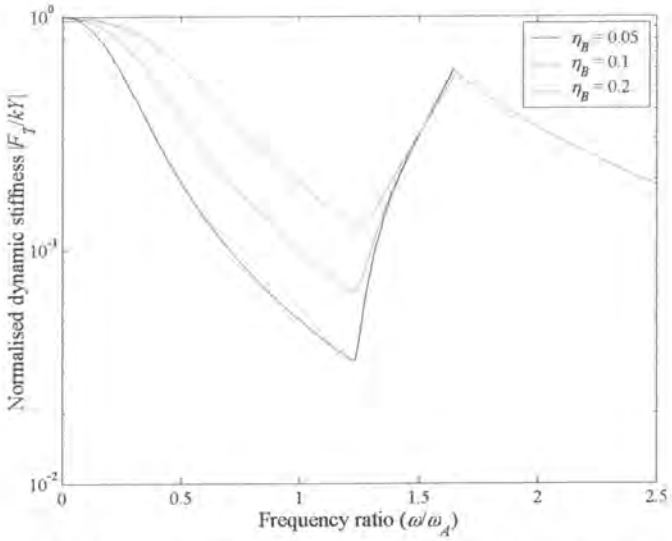

Figure 1.34: The normalised dynamic stiffness envelope *vs.* frequency ratio when changing the stiffness ratio (μ_k) from 0 to 6 ($\mu_m = 1$)

1.3.3 Active vibration-absorbing isolators

Active vibration absorbers consist of an actuator, most commonly in parallel with the passive spring supporting the absorber mass, as shown in Figure 1.35.

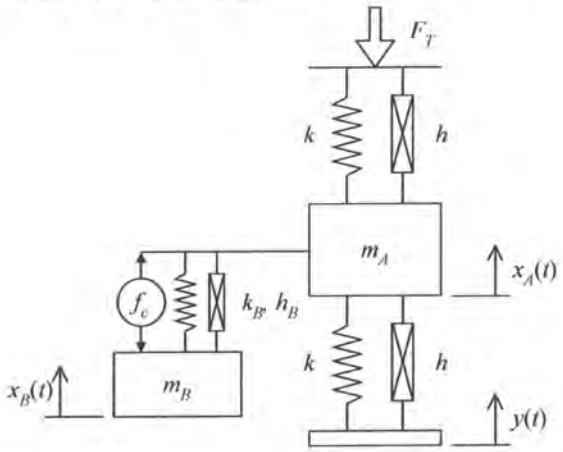

Figure 1.35: Mechanical model of an active vibration-absorbing isolator

The actuator provides a force acting on the absorber mass and must be controlled suitably. A wide variety of control methods have been used ranging from classic methods to fuzzy logic and neural networks. One possible method is to use acceleration, velocity and displacement feedback (Cunha & Rade, 2002). A shown before, the isolation frequency is a function of stiffness and mass and velocity feedback can therefore not be used to tune the device. Velocity feedback can be used to reduce damping and that will improve the isolation performance. Such a case will be considered later in this paragraph.

For tuning purposes the following control force can be used to change the effective stiffness and mass of the absorber:

$$f_c(t) = \alpha(\ddot{x}_B - \ddot{x}_A) + \gamma(x_B - x_A) \tag{1.26}$$

The advantages of using absolute instead of relative velocity feedback will be discussed later in this paragraph.

The dynamic stiffness for the undamped case is [Equation (A.70)]:

$$\frac{F_T}{kY} = \frac{1-\left(\frac{\omega}{\omega_B'}\right)^2}{\left[1+\frac{1}{4}\frac{k_B}{k}\left(1+\frac{\gamma}{k_B}\right)-\left(\frac{\omega}{\omega_A}\right)^2\right]\left[1-\left(\frac{\omega}{\omega_B'}\right)^2\right]-\frac{1}{4}\frac{k_B}{k}\left(1+\frac{\gamma}{k_B}\right)} \tag{1.27}$$

where: $\omega_A = \sqrt{\frac{4k}{m_A+\alpha}}$ $\omega_B' = \omega_B\sqrt{\frac{1+\frac{\gamma}{k_B}}{1+\frac{\alpha}{m_B}}}$

The following inequalities must be satisfied by the respective gains in order to satisfy the Routh-Hurwitz stability criterion [Equation (A.72)]:

$$\alpha > -\frac{m_B m_A}{m_A + m_B}$$
$$\frac{\gamma}{k_B} > -1 \tag{1.28}$$

It is also possible to reduce the response in the low-stiffness region by actively reducing damping as was shown by Kidner and Brennan (1999) for a vibration absorber. This can be done quite simply by using relative velocity feedback for the control force:

$$f_c(t) = \beta(\dot{x}_B - \dot{x}_A) \tag{1.29}$$

The dynamic stiffness then becomes [Equation (A.81)]:

$$\frac{F_T}{kY} = \frac{\left(1+i2\frac{\omega}{\omega_A}\zeta\right)^2\left[1+i2\frac{\omega}{\omega_B}\zeta_B-\left(\frac{\omega}{\omega_B}\right)^2\right]}{\left[1+\frac{1}{4}\frac{k_B}{k}+i2\left(\frac{\omega}{\omega_A}\zeta+\frac{1}{4}\frac{\omega}{\omega_B}\frac{k_B}{k}\zeta_B\right)-\left(\frac{\omega}{\omega_A}\right)^2\right]\left[1+i2\frac{\omega}{\omega_B}\zeta_B-\left(\frac{\omega}{\omega_B}\right)^2\right]-\frac{1}{4}\frac{k_B}{k}\left(1+i2\frac{\omega}{\omega_B}\zeta_B\right)^2} \tag{1.30}$$

where: $\zeta = \frac{c}{2m_A\omega_A}$, $\zeta_B = \frac{c_B}{2m_B\omega_B}\left(1+\frac{\beta}{c_B}\right)$

The absorber damping needs to be minimised, but as before, the gain (β) must comply with the Routh-Hurwitz criterion for stability [Equation (A.85)]:

$$\frac{\beta}{c_B} > -1 \tag{1.31}$$

From Equation (1.30) it can be seen that setting the velocity gain equal to the negative of the absorber viscous damping coefficient will result in zero absorber damping. This is favourable in the low stiffness region, but will also reduce damping at resonance, causing infinite stiffness (this was illustrated for the VAI in Figure 1.23 with $\eta_B = 0$). There is also the possibility of instability if the net damping becomes smaller than zero. Kidner and Brennan (1999) showed that it is possible to remove damping at isolation while keepings its benefits at resonance by using absolute velocity feedback:

$$f_c(t) = \beta \dot{x}_B \tag{1.32}$$

The normalised dynamic stiffness is now [Equation (A.93)]:

$$\frac{F_T}{kY} = \frac{\left(1+i2\zeta\frac{\omega}{\omega_A}\right)^2\left[1+i2\frac{\omega}{\omega_B}\zeta_B\left(1+\frac{\beta}{c_B}\right)-\left(\frac{\omega}{\omega_B}\right)^2\right]}{\left[1+\frac{1}{4}\frac{k_B}{k}+i2\left(\frac{\omega}{\omega_A}\zeta+\frac{1}{4}\frac{k_B}{k}\frac{\omega}{\omega_B}\zeta_B\right)-\left(\frac{\omega}{\omega_A}\right)^2\right]\left[1+i2\frac{\omega}{\omega_B}\zeta_B\left(1+\frac{\beta}{c_B}\right)-\left(\frac{\omega}{\omega_B}\right)^2\right]-\frac{1}{4}\frac{k_B}{k}\left[1+i2\frac{\omega}{\omega_B}\zeta_B\left(1+\frac{\beta}{c_B}\right)\right]\left(1+i2\frac{\omega}{\omega_B}\zeta_B\right)} \tag{1.33}$$

where: $\zeta_B = \frac{c_B}{2m_B\omega_B}$, $\zeta = \frac{c}{2m_A\omega_A}$

The stability is again given by Equation (1.31). Figure 1.36 shows that it will be most beneficial to have a system with high damping, but the trade-off is the cost of the power required to remove the damping:

$$p = \beta \dot{x}_B^2 \tag{1.34}$$

Importantly, the addition of primary system damping does not increase the stiffness at the isolation frequency, but will increase the high frequency roll-off and decrease the bandwidth and should therefore be minimised. Additional practical considerations include the maximum force output of the actuator and the large gain and damping needed.

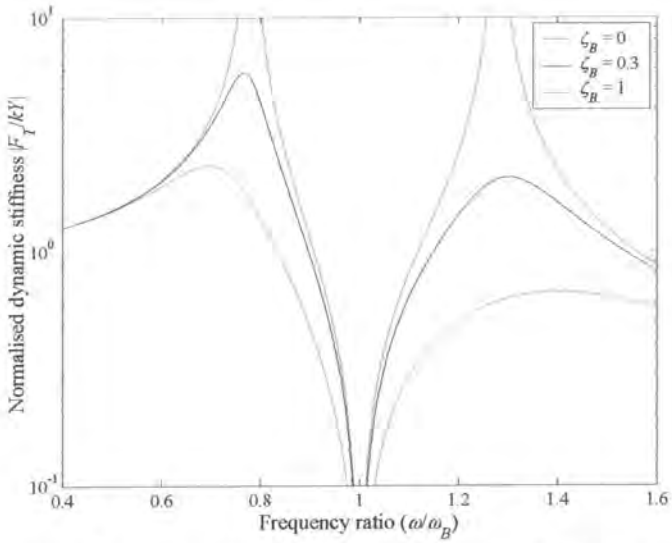

Figure 1.36 Normalised dynamic stiffness using absolute velocity feedback ($k_B/k = 1$ and $\zeta = 0$)

Other control methods have also been demonstrated. Sommerfeldt and Tichy (1990) describe a least-mean-squares (LMS) based control method for a two-stage vibration isolation mount that essentially is an active vibration absorber fitted in the load path. The advantage of the LMS algorithm control

method is that it will compensate for changes in the system and therefore control will be optimal at all times. This technique is similar to the method proposed in this work where physical properties are adapted to maintain optimal isolator stiffness at the excitation frequency. Other control methods have been suggested, specifically when applied to vibration absorbers and these might have benefits for vibration-absorbing isolators as well, although this was not investigated. These methods include an active dynamic vibration absorber incorporating a simple electromagnet arrangement used to enact a force on a pendulum (Mizuno & Araki, 1993). The control system used the theory of output regulation and could reduce the vibration to a low level over a wide range of frequencies, forcing it to zero at several specified frequencies. Burdisso and Heilmann (1998) found that a dual mass absorber with an active element inserted between the masses that are elastically coupled to the structure could have the same effectiveness as a single absorber, but with half the control effort. Filipović and Schröder (1998) demonstrated that a feedback compensator can be used to suppress a wide-band of frequencies. Olgac & Holm-Hansen (1993) introduced a delayed resonator where an actuator fitted between the primary and secondary masses is tuned using time delay and gaiu. They demonstrated that the delayed resonator could reduce the primary system response to zero.

1.4 Amplified vibration-absorbing isolators

1.4.1 Passive amplified vibration-absorbing isolators

The third distinction that will be made relate to devices that use absorber mass amplification. These are termed Amplified Vibration-Absorbing Isolators (AVAI) and the characteristics are in many respects similar to the VAI. The first important distinction that can be made is that the absorber mass is amplified using a lever mechanism, often termed a pendulum in literature (Braun, 1980). This makes it possible to reduce the mass of the device, but also amplifies damping associated with its movement. Interestingly it is not possible to increase the low stiffness bandwidth by having a large absorber mass. It is also important to note that the device has only one degree of freedom, the same as a simple isolator. A variety of physical implementations exist, as will be shown at the end of this paragraph, but all of them can be represented by an equivalent pendulum as shown in Figure 1.37.

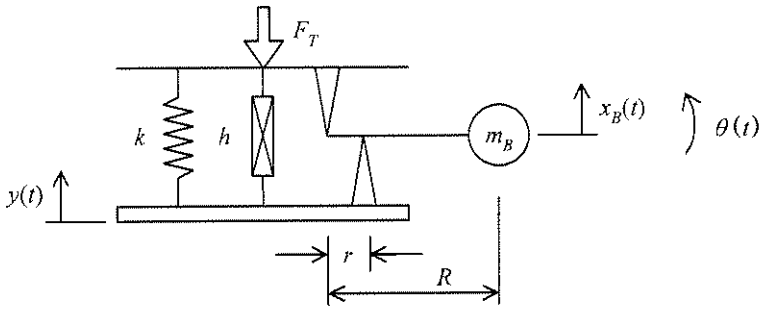

Figure 1.37: Mechanical model of a pendulum AVAI

The normalised dynamic stiffness for a pendulum type AVAI is given by [Equation (A.112)]:

$$\frac{F_T}{kY} = 1 + i\eta - \left(\frac{\omega}{\omega_i}\right)^2$$
$$\text{where:} \quad \omega_i = \sqrt{\frac{k}{m_B\left(\frac{R}{r}-1\right)\frac{R}{r} + \frac{I_G}{r^2}}} \tag{1.35}$$

where I_G is the moment of inertia about the mass centre of m_B. The characteristic of the AVAI is to reduce the dynamic stiffness over a limited frequency band as shown in Figure 1.38.

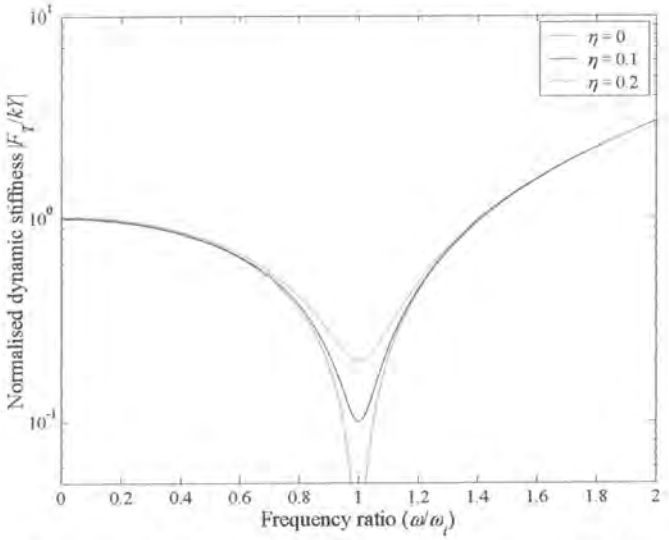

Figure 1.38: The normalised dynamic stiffness of an AVAI

The dynamic stiffness is less than one for:

$$0 < \omega < \sqrt{2}\omega_i \tag{1.36}$$

At high frequencies the AVAI will be very stiff. These properties make the AVAI ideal for narrow-band low-frequency excitation, which is often the most problematic case since it requires isolators with large static deflections. As for the VAI it would be beneficial if the low stiffness bandwidth could be increased. The low stiffness bandwidth is only slightly influenced by damping. However, it will be beneficial to have low damping at the isolation frequency.

Ideally the AVAI will be used when the excitation is tonal and time invariant. In such a case the parameters that determine the isolation frequency can be used for its design. A typical design procedure will be subject to certain size, mass and static deflection constraints while simultaneously trying to reduce the velocity of the absorber mass since this will increase damping in practical devices.

The dynamic stiffness is useful for comparison with other isolation methods, but it becomes important to study the transmissibility in order to get a more detailed description of AVAI behaviour, specifically, the response that must be evaluated using the set criteria. Adding a mass to be isolated to Figure 1.37 with degree of freedom $x(t)$ results in the model shown in Figure 1.40.

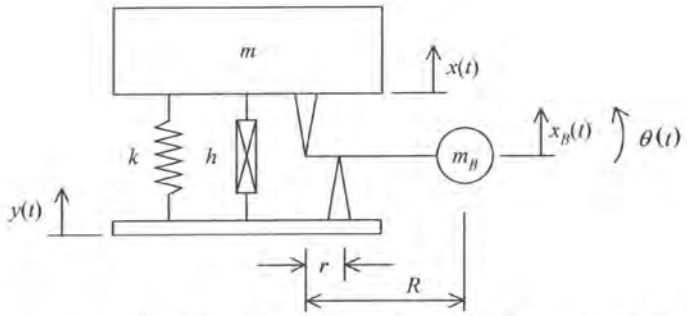

Figure 1.39: Mechanical model of a pendulum AVAI with the isolated mass included

The transmissibility is [Equation (A.108)]:

$$\frac{X}{Y}=\frac{1+i2\dfrac{\omega}{\omega_n}\zeta-\left(\dfrac{\omega}{\omega_i}\right)^2}{1+i2\dfrac{\omega}{\omega_n}\zeta-\left(\dfrac{\omega}{\omega_n}\right)^2} \tag{1.37}$$

$$\text{where: } \omega_n=\sqrt{\frac{k}{m+m_B\left(\dfrac{R}{r}-1\right)^2+\dfrac{I_G}{r^2}}}$$

The transmissibility is shown in Figure 1.40. The invariant point (A) is given by [Equation (A.109)]:

$$\frac{\omega_A}{\omega_i}=\sqrt{\frac{2}{1+\left(\dfrac{\omega_i}{\omega_n}\right)^2}} \tag{1.38}$$

Point B is where the benefit of the AVAI ends and is the same as was indicated before by Equation (1.36). Figure 1.40 clearly shows the benefit of the AVAI over a conventional isolator.

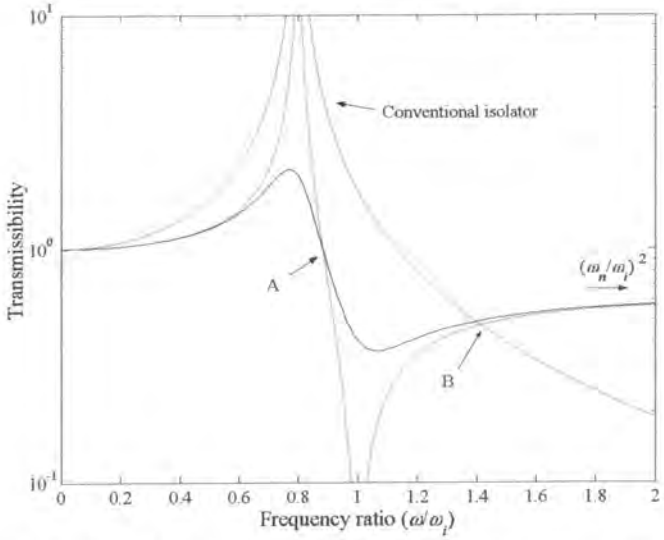

Figure 1.40: Damped (black) and undamped (red) AVAI transmissibility compared to a conventional isolator. A is the invariant point and B the cross over point ($\omega_n = 0.8$ and $\omega_i = 1$)

The high frequency transmissibility is given by the frequency ratio:

$$\left.\frac{X}{Y}\right|_{\omega\to\infty} = \left(\frac{\omega_n}{\omega_i}\right)^2 = \frac{m_B\left(\frac{R}{r}-1\right)\frac{R}{r}+\frac{I_G}{r^2}}{m+m_B\left(\frac{R}{r}-1\right)^2+\frac{I_G}{r^2}} \tag{1.39}$$

The only way to ensure that the high frequency transmissibility is low is to make certain that the effective absorber mass is much smaller than the mass of the system being isolated as shown by the above equation. At the isolation frequency the transmissibility is:

$$\left.\frac{X}{Y}\right|_{\omega=\omega_i} = \frac{i2\frac{\omega_i}{\omega_n}\zeta}{1-\left(\frac{\omega_i}{\omega_n}\right)^2+i2\frac{\omega_i}{\omega_n}\zeta} = \frac{1}{\frac{1-\left(\frac{\omega_i}{\omega_n}\right)^2}{i2\frac{\omega_i}{\omega_n}\zeta}+1} \approx \frac{i2\frac{\omega_i}{\omega_n}\zeta}{1-\left(\frac{\omega_i}{\omega_n}\right)^2} \approx i2\zeta\frac{\omega_n}{\omega_i} \tag{1.40}$$

The approximation shown in Equation (1.40) is not accurate at low values of the frequency ratio (ω_i/ω_n) as shown in Figure 1.41, but it aids in understanding the dependency of transmissibility on the parameters. It is obvious from Equation (1.40) that the natural frequency must be small in relation to the isolation frequency and that the damping ratio must be small to minimise the transmissibility.

The damped isolation frequency can be found by differentiating the absolute value of Equation (1.37) with respect to frequency [Equation (A.109)]:

$$\frac{\Omega_n}{\omega_n},\frac{\Omega_i}{\omega_n} = \sqrt{\frac{-\left(\frac{\omega_n}{\omega_i}\right)^2-1\pm\sqrt{\left[\left(\frac{\omega_n}{\omega_i}\right)^2-1\right]^2+8\zeta^2\left[\left(\frac{\omega_n}{\omega_i}\right)^2+1\right]}}{4\zeta^2+4\zeta^2\left(\frac{\omega_n}{\omega_i}\right)^2-2\left(\frac{\omega_n}{\omega_i}\right)^2}} \tag{1.41}$$

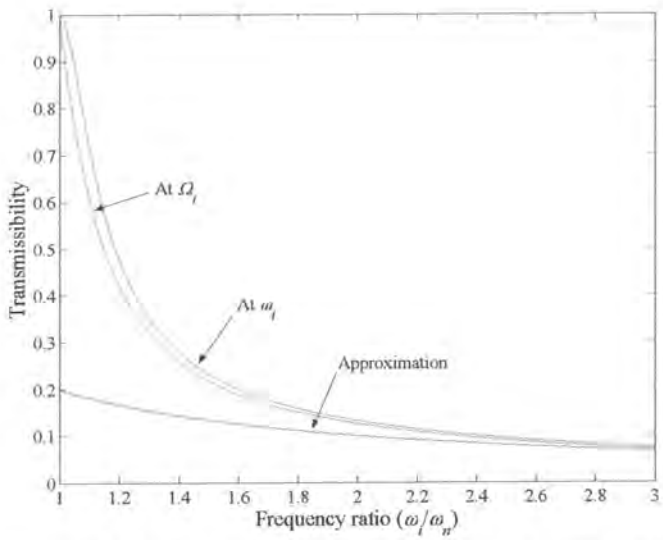

Figure 1.41: Approximation of the transmissibility at the isolation frequency (Equation (1.40)) as a function of frequency ratio ($\zeta = 0.1$)

For large values of frequency ratio (ω_i/ω_n) and damping the damped isolation frequency may not be defined as can be seen in Figure 1.42.

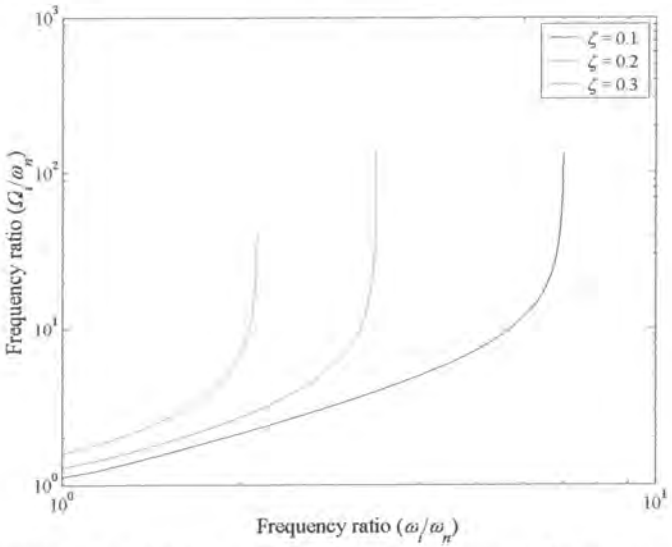

Figure 1.42: Damped frequency ratio *vs.* undamped frequency ratio

Adding pendulums in parallel will not have the same effect as was shown for the VAI in §1.3.1; in fact it is possible to reduce parallel pendulums to one equivalent pendulum. A number of discrete frequencies can, however, be suppressed if the pendulum absorber is extended by adding absorbers to the pendulum mass as shown in Figure 1.43 (Desjardins & Hooper, 1976).

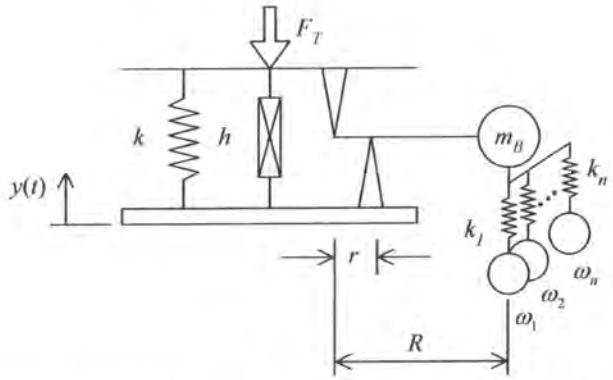

Figure 1.43: Mechanical model of an AVAI with multiple absorbers fitted to a pendulum

For a case with n absorbers attached to the pendulum mass the dynamic stiffness is [Equation (A.121)]:

$$\frac{F_T}{kY} = 1 + i\eta + \left(\frac{R}{r} - 1\right)\frac{R}{r}\sum_{q=1}^{n}\frac{k_q}{k}\left(1 + i\eta_q\right) - \left(\frac{\omega}{\omega_i}\right)^2 - \frac{R}{r}\left(\frac{R}{r} - 1\right)\sum_{q=1}^{n}\frac{k_q}{k}\frac{\left(1 + i\eta_q\right)^2}{1 + i\eta_q - \left(\frac{\omega}{\omega_q}\right)^2} \tag{1.42}$$

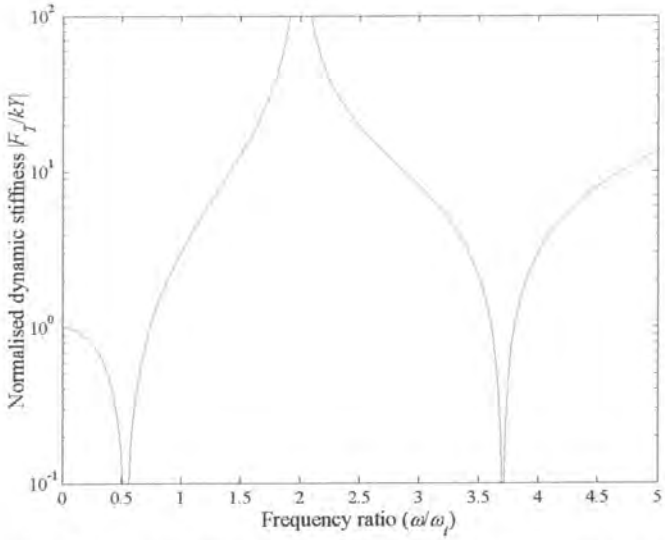

Figure 1.44: Normalised dynamic stiffness of a multi-frequency isolator with one absorber attached ($\omega_i = 1$, $\omega_1 = 2$, $R/r = 10$, $\eta = \eta_1 = 0$, $k_1/k = 0.1$)

The undamped frequencies of zero dynamic stiffness can be found by setting the normalised dynamic stiffness equal to zero. For one absorber these frequencies will be given by Equation (1.43) [Equation (A.120)]. This equation can be solved to find the system parameters that will give the required zero dynamic stiffness frequencies.

$$\frac{\omega'_{i1}}{\omega_i}, \frac{\omega'_{i2}}{\omega_i} = \sqrt{\frac{1+\left(\frac{R}{r}-1\right)\frac{R}{r}\frac{k_1}{k}+\left(\frac{\omega_1}{\omega_i}\right)^2 \mp \sqrt{\left[1+\left(\frac{R}{r}-1\right)\frac{R}{r}\frac{k_1}{k}+\left(\frac{\omega_1}{\omega_i}\right)^2\right]^2 - 4\left(\frac{\omega_1}{\omega_i}\right)^2}}{2}} \tag{1.43}$$

Figure 1.45 shows the effect of the absorber natural frequency on the isolation frequencies for two stiffness ratios.

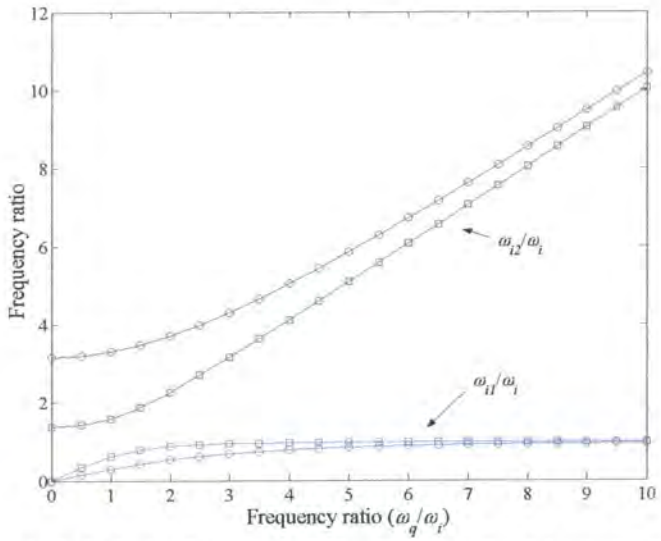

Figure 1.45: Isolation frequency ($k_1/k = 0.01$ □, $k_1/k = 0.1$ ○ and $R/r = 10$)

Softening non-linear springs can be used to increase the low stiffness bandwidth. Non-linear effects cannot be explained by using the dynamic stiffness and therefore the transmissibility will be calculated. This can be done by solving the equation of motion in the time domain using the Runge-Kutta algorithm and then calculating the transfer function using the H_1 estimator.

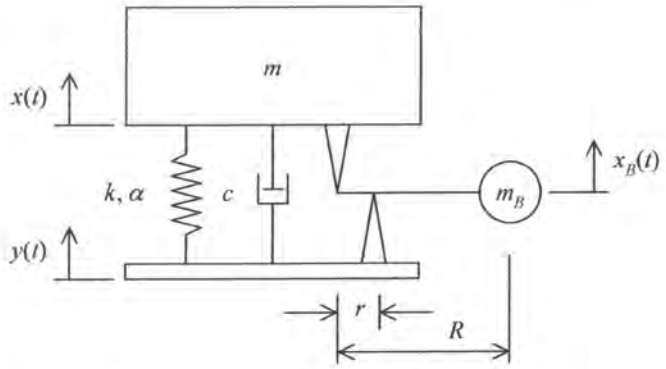

Figure 1.46: Mechanical model of an AVAI with non-linear spring

The equation of motion for a system with Duffing type non-linearity is [Equation (A.124)]:

$$\ddot{x}-\left(\frac{\omega_n}{\omega_i}\right)^2 \ddot{y}+2\zeta\omega_n\left(\dot{x}-\dot{y}\right)+\omega_n^2\left[\left(x-y\right)+\alpha\left(x-y\right)^3\right]=0 \tag{1.44}$$

Figure 1.47 shows the transmissibility of a softening system when excited by sine sweep excitation. It is clear that softening non-linearity increases the suppression bandwidth. A hardening spring will result in a decrease of the suppression bandwidth. Since this effect is highly dependent on the properties of the AVAI and the excitation amplitude it will be of limited use in most practical situations.

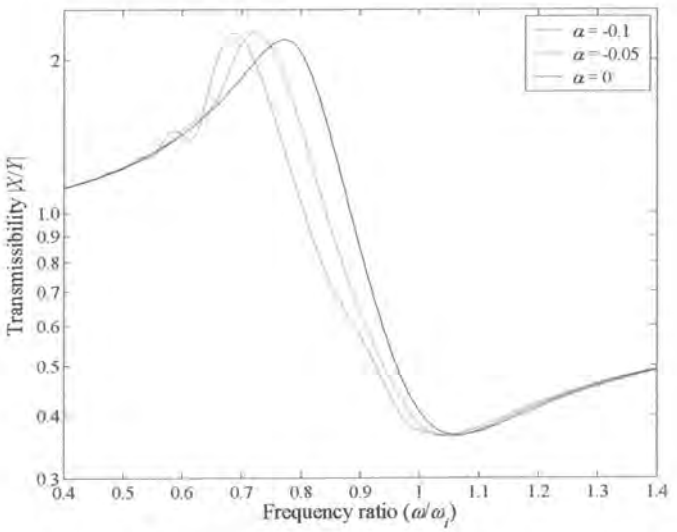

Figure 1.47: Effect of a softening spring on the transmissibility of an AVAI ($\zeta = 0.1$, $\omega_n = 0.8$, $\omega_i = 1$ and $Y = 1$)

AVAI can have a variety of physical realisations. These include nodal beams, mechanical pendulums, lead screw arrangements and various hydraulic devices. Some of these are shown in Figure 1.48. Figures (a) through (c) show schematic drawings of typical devices. Figures (d) through (f) show models of the major classes of devices and their isolation frequencies. Their relationship with Equation (1.35) is immediately apparent. Since all of these devices can realise the same low stiffness region, the final choice will include economic considerations.

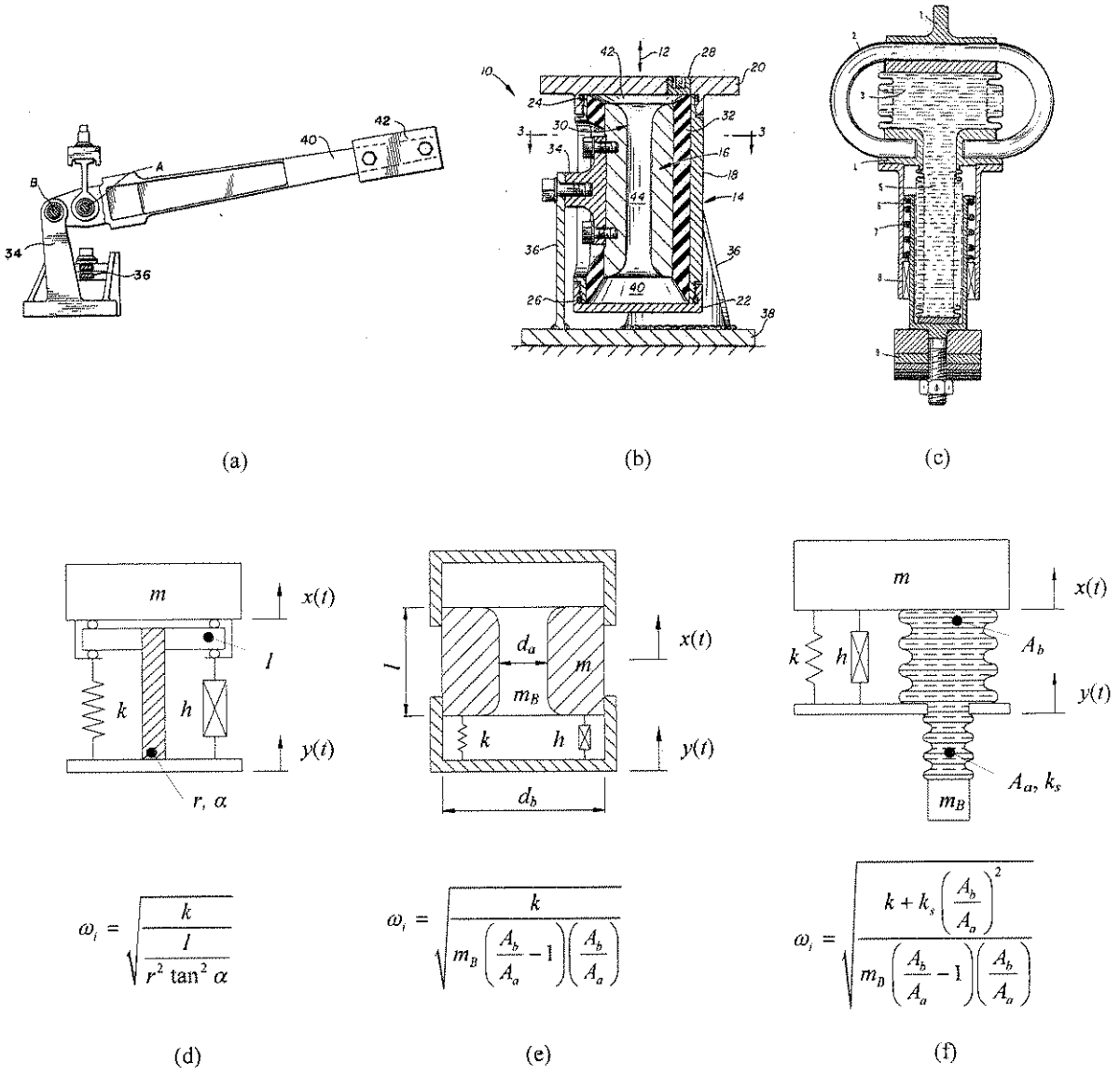

Figure 1.48: Practical implementations of the AVAI (a) pendulum type (Dejardins & Sankewitsch, 1982), (b and e) LIVE (Halwes & Simmons, 1980), (c and f) hydraulic amplification (Braun, 1980) and (d) motion transformation system (Rivin, 2001)

Hydraulic amplification isolators are also called fluid mounts and can be designed to have a static stiffness of 1.5 to 2 times that of an elastomeric isolator with a 10 times (20 dB) improvement in

isolation at the excitation frequency (Miller *et al.*, 1995). Fluid mounts are in use in cars, trucks and buses and more recently in aircraft as engine mounts and helicopter pylon isolators.

1.4.2 Adaptive amplified vibration-absorbing isolators

If the input excitation is tonal and time-varying it will be possible to adjust the AVAI such that the region of lowest stiffness coincides with the excitation frequency. The effect of varying the isolation frequency is illustrated in Figure 1.49. One advantage of the AVAI over the VAI is that the frequency ratio at which the normalised dynamic stiffness becomes more than 1 stays constant ($\omega_c/\omega_i = \sqrt{2}$). This significantly reduces the risk of tuning.

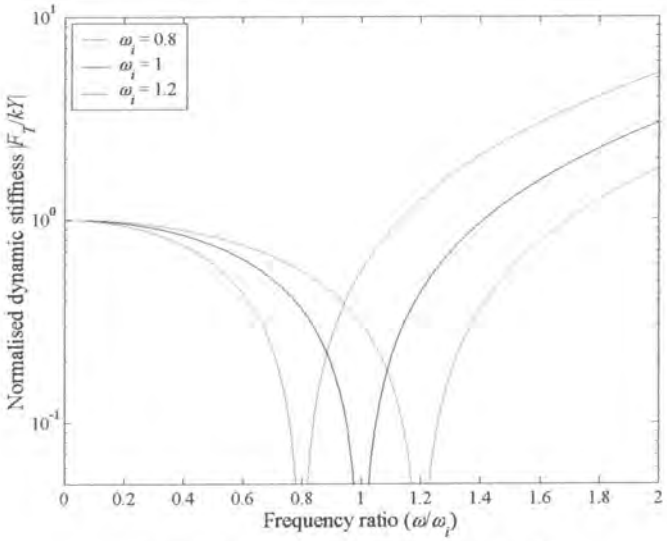

Figure 1.49: Effect of tuning the AVAI

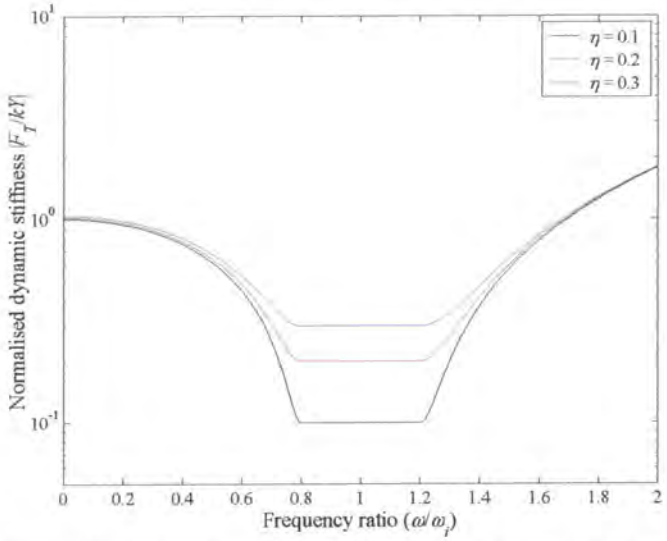

Figure 1.50: Envelope of minimum normalised dynamic stiffness for $0.8 < \omega/\omega_i < 1.2$

The objective of tuning is illustrated more clearly in Figure 1.50, which shows the envelope of normalised dynamic stiffness curves when changing the frequency ratio from 0.8 to 1.2. The effect of tuning is to increase the effective low stiffness bandwidth for this very specific class of excitation.

Another important advantage of the AVAI is that geometric variables are available for tuning, which increases the number of applicable technologies. In order to choose the best parameter to adjust, it is necessary to investigate the sensitivity of the isolation frequency to the variation of parameters shown in Equation (1.35). It is assumed that the moment of inertia is zero and that the mechanical advantage is much larger than 1. These assumptions lead to the following equation and the related sensitivities:

$$\omega_i \approx \sqrt{\frac{k}{m_B\left(\frac{R}{r}\right)^2}}, \qquad \omega_i \propto \sqrt{k}, \qquad \omega_i \propto \frac{1}{\sqrt{m_B}}, \qquad \omega_i \propto \frac{1}{\frac{R}{r}} \tag{1.45}$$

Equation (1.45) shows that the isolation frequency will be most sensitive to the mechanical advantage. This is also illustrated in Figure 1.51, which is a plot of Equation (1.46).

$$\frac{\omega_i}{\omega_i'} = \sqrt{\frac{k}{k'}\frac{m_B'}{m_B}}\left(\frac{\frac{R'}{r'}}{\frac{R}{r}}\right) \tag{1.46}$$

where the prime indicates the initial value.

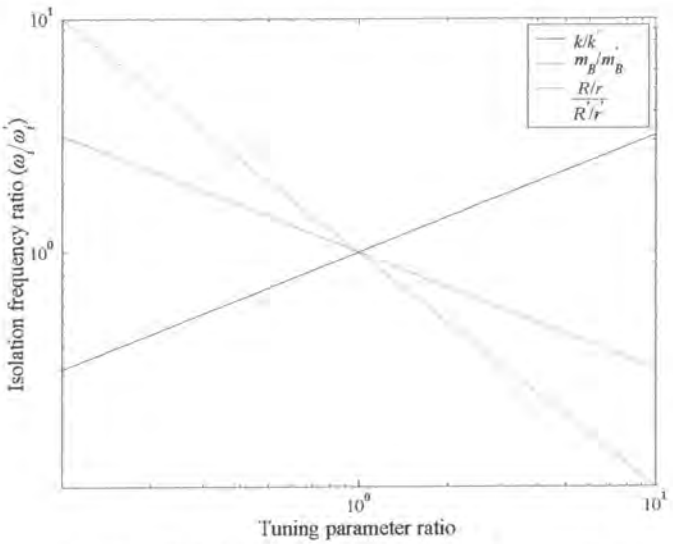

Figure 1.51: Sensitivity of the isolation frequency

Although Figure 1.51 shows a change in parameter ratio of 2 orders of magnitude, the amount achieved in practice will depend on the capability of the technology used. Also important are other constraints put on the system, for instance, there might be limited space available to lengthen the mechanical advantage or the change in static position by changing the stiffness, absorber mass or mechanical advantage may be undesirable. As with the VAI, changing the mass will be difficult while changing the mechanical advantage can be achieved easily through, for instance, a lead screw arrangement. Methods for changing the stiffness have been discussed before (§1.3.2).

Considering a Liquid Inertia Vibration Eliminator (LIVE) type AVAI it can be seen that the absorber mass is also a function of geometry as well as density:

$$\omega_i \approx \sqrt{\frac{kd_a^2}{\frac{\pi}{4}\rho l d_b^4}}, \qquad \omega_i \propto \sqrt{k}, \qquad \omega_i \propto d_a, \qquad \omega_i \propto \frac{1}{d_b^2}, \qquad \omega_i \propto \frac{1}{\sqrt{\rho}}, \qquad \omega_i \propto \frac{1}{\sqrt{l}} \tag{1.47}$$

The isolation frequency is very sensitive to the reservoir diameter, but changing it will be very difficult, if at all possible. The sensitivity to all the parameters is shown in Figure 1.52.

$$\frac{\omega_i}{\omega_i'} = \sqrt{\frac{k}{k'}\frac{\rho'}{\rho}\frac{l'}{l}\frac{d_a}{d_a'}\left(\frac{d_b'}{d_b}\right)^2} \tag{1.48}$$

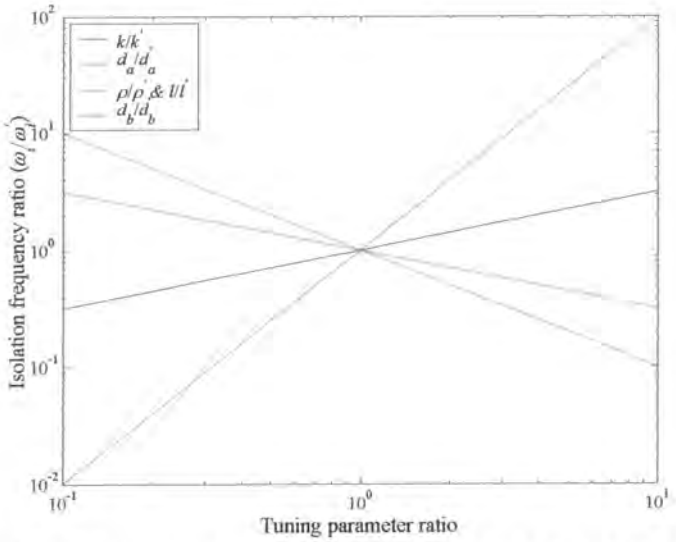

Figure 1.52: Sensitivity of the isolation frequency for a LIVE type AVAI

Figure 1.53(a) shows a proposed system to vary the port length of a LIVE type AVAI. Such a system needs careful design to minimise flow induced damping at the port inlet and outlet. Figure 1.53(b) shows a system that suggests that the port area can be changed by stretching a flexible member. It should be kept in mind that the fluid is incompressible and some compensating mechanism must be provided. In this case the fluid occupies the space between the flexible member and the port such that the total fluid volume remains constant. It has also been suggested that a chamber pressurised by nitrogen and connected by a small orifice to the reservoir to act as a volume compensator be used, specifically for heat expansion of the fluid (Ahmadian & Ahn, 1999).

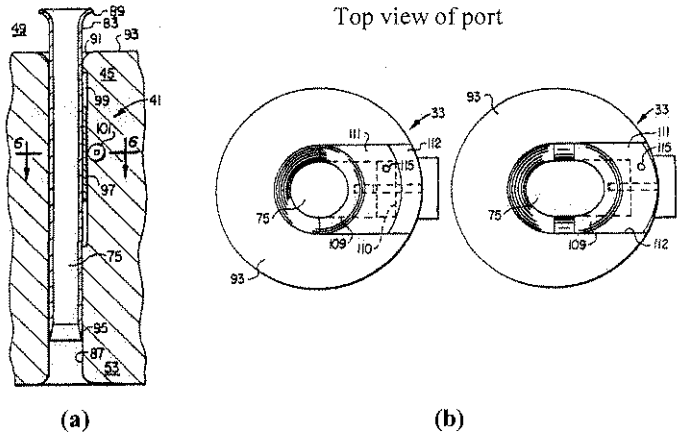

Figure 1.53: Adjustable (a) port length and (b) port area (Smith & Stamps, 1998)

Duclos *et al.* (1988) demonstrated a system using an electro-rheological fluid with a number of parallel ports, each with a valve that can be selectively switched so that the isolator can be tuned at a number of discrete frequencies. One problematic aspect with regards to tuning is that for some of the parameters the transmissibility at the isolation frequency is a function of the tuning parameter. Tuning could therefore increase the transmissibility at the isolation frequency so much that no benefit results.

It can be anticipated that an instantaneous change in excitation frequency or stiffness will result in impulsive loading of the system. This can be studied in the time domain by solving the equation of motion for the AVAI (Equation (1.44) with $\alpha = 0$):

$$\ddot{x} + 2\zeta\omega_n(t)\dot{x} + \omega_n^2(t)x = \left[\frac{\omega_n(t)}{\omega_i(t)}\right]^2 \ddot{y} + 2\zeta\omega_n(t)\dot{y} + \omega_n^2(t)y \tag{1.49}$$

When the stiffness is used as the tuning parameter the current isolation and natural frequencies can be expressed in terms of the initial values (using Equation (1.48) for the isolation frequency, the natural frequency follows similarly):

$$\omega_i = \sqrt{\frac{k}{k'}}\omega_i', \qquad \omega_n = \sqrt{\frac{k}{k'}}\omega_n' \tag{1.50}$$

The effect is illustrated in Figure 1.54. The AVAI is initially tuned to the excitation frequency. After a short transient the displacement settles. At 10 seconds the excitation frequency is doubled when the displacement passes through zero, exciting the system. In any practical system some delay between the change in excitation frequency and subsequent tuning is inevitable. Von Flotow (1994) identified three delays:

1. Logic delay: Associated with the time needed for data acquisition and to estimate if and how much mistuning has occurred.
2. Actuation delay: Changing any of the parameters needed to adapt the isolation frequency cannot happen instantaneously. In fact, instantaneous adaptation will excite the system impulsively, which could result in unacceptably large response.

3. Dynamic delay: The time taken by the system to reach steady-state conditions which can be found in terms of the exponential time constant as the number of periods before the system has settled:

$$T = \frac{1}{2\pi\zeta} \tag{1.51}$$

Clearly damping can be used to control the transient.

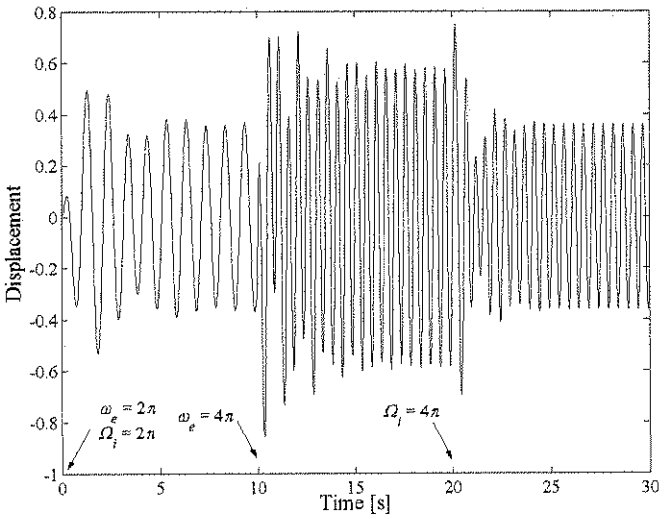

Figure 1.54: Transient response of an AVAI (initially tuned), subjected to an instantaneous frequency change at $t = 10$ and retnned at $t = 20$ s ($\omega_n/\omega_i = 0.8$, $\zeta = 0.1$ and $Y = 1$)

It is possible to extend the model of the AVAI by considering the effect of a flexible fulcrum as shown in Figure 1.55. At first glance it might seem superfluous, but it will be shown in Chapter 2 that such a configuration can be a reasonable compromise between constructability and tuning performance.

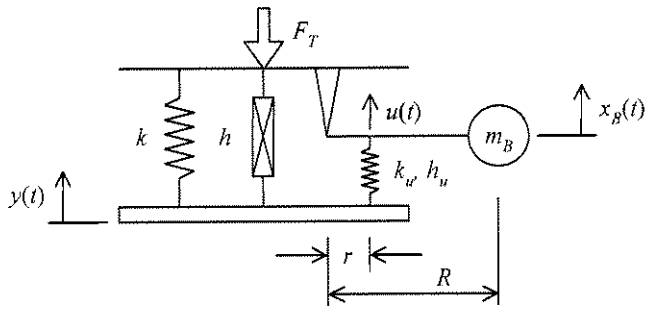

Figure 1.55: Mechanical model of an AVAI with flexible fulcrum

The system now has a degree of freedom which can be accounted for by the natural frequency of the pendulum mass (ω_u) [Equation (A.143)]:

$$\frac{F_T}{kY} = 1 + i\eta - \frac{\left(\frac{\omega}{\omega_l}\right)^2 (1 + i\eta_u)}{1 + i\eta_u - \left(\frac{\omega}{\omega_u}\right)^2} \tag{1.52}$$

$$\text{where: } \omega_l = \sqrt{\frac{k}{m_B\left(\frac{R}{r} - 1\right)\frac{R}{r} + \frac{I_G}{r^2}}}, \quad \omega_u = \sqrt{\frac{k_u}{m_B\left(\frac{R}{r}\right)^2 + \frac{I_G}{r^2}}}$$

The effect of adding the flexible fulcrum is shown in Figure 1.56.

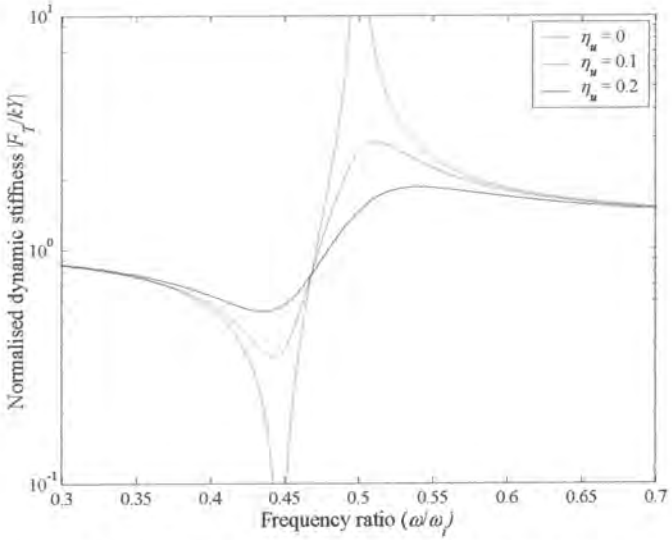

Figure 1.56: Normalised dynamic stiffness of the AVAI with flexible fulcrum ($\omega_u = 0.5$ and $\omega_l = 1$)

Equation (1.52) can be rewritten to show the effect of changing the fulcrum stiffness [Equation (A.144)]:

$$\frac{F_T}{kY} = 1 + i\eta - \frac{\left(\frac{\omega}{\omega_l}\right)^2 (1 + i\eta_u)}{1 + i\eta_u - \frac{k}{k_u}\left(\frac{\frac{R}{r}}{\frac{R}{r} - 1}\right)\left(\frac{\omega}{\omega_l}\right)^2} \tag{1.53}$$

As the stiffness ratio (k_u/k) increases, Equation (1.53) approaches that of the AVAI. Figure 1.57 shows that the low stiffness frequency range is a function of the stiffness ratio and therefore the risk of tuning is greater than in the case of the AVAI. The normalised dynamic stiffness is less than 1 when:

$$0 < \omega < \sqrt{\frac{2}{1 + 2\frac{k}{k_u}\left(\frac{\frac{R}{r}}{\frac{R}{r} - 1}\right)}}\,\omega_l \tag{1.54}$$

There is also the advantage that the high-frequency stiffness is finite for low stiffness ratios:

$$\left.\frac{F_T}{kY}\right|_{\omega\to\infty} = \frac{k_u}{k}\frac{1+i\eta_u}{\dfrac{\dfrac{R}{r}}{\dfrac{R}{r}-1}} \tag{1.55}$$

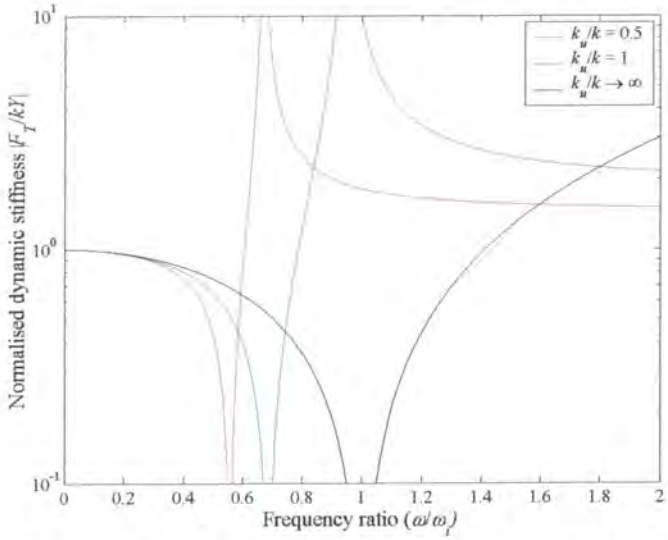

Figure 1.57: Effect of tuning the AVAI with flexible fulcrum ($R/r = 10$, $\omega_i = 1$ and $\eta = \eta_u = 0$)

Since the equation describing the actual isolation frequency as a function of stiffness ratio becomes unwieldy it is proposed that the system should be designed graphically as shown in Figure 1.58. This graph is, of course, dependent on several parameters and must be recreated for each specific case. For instance, the acceptable margin will be application specific and the range of stiffness change that can be achieved will depend on the method chosen for this purpose.

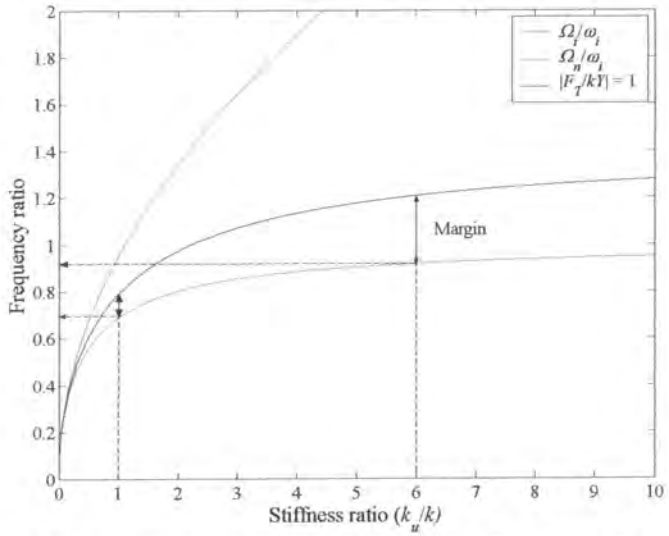

Figure 1.58 Design graph for the AVAI with flexible fulcrum with Ω_i the actual isolation frequency and Ω_n the frequency of maximum dynamic stiffness ($\eta = 0.1$, $\eta_u = 0$ and $R/r = 10$)

1.4.3 Active amplified vibration-absorbing isolators

As for the VAI it will be possible to apply various active control forces to the AVAI. Miller and Ahmadian (1992) noted that both traditional feedback and adaptive feedforward including LMS have been implemented to reject tonal disturbances. They further state that neural network based controllers will be essential when considering broadband vibration inputs. When considering traditional feedback control three cases will be identified. Firstly, tuning can be effected by using acceleration and displacement feedback. Secondly, damping can be removed by using relative velocity feedback. Thirdly, absolute velocity feedback can be used to add a "skyhook" damper to the system, reducing the transmissibility at both the natural and isolation frequencies.

The mechanical model describing the force transmitted for an active system is shown in Figure 1.59. The control force using input acceleration and displacement feedback to facilitate tuning is:

$$f_c = \alpha \ddot{y} + \gamma y \tag{1.56}$$

It will also be possible to use the acceleration and displacement of the pendulum mass x_B.

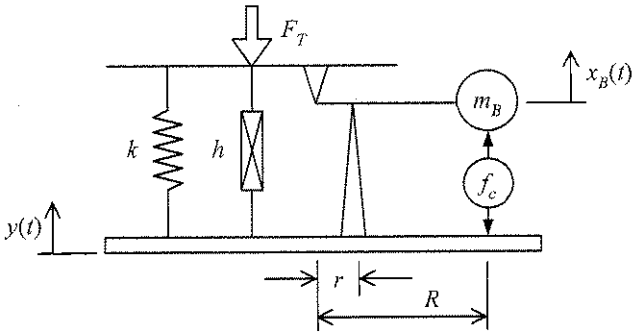

Figure 1.59: Mechanical model of an active AVAI for dynamic stiffness

The normalised dynamic stiffness of the active AVAI is [Equation (A.149)]:

$$\frac{F_T}{\left[k-\gamma\left(\frac{R}{r}-1\right)\right]Y} = 1+i\frac{\eta}{1-\frac{\gamma}{k}\left(\frac{R}{r}-1\right)}-\left(\frac{\omega}{\omega_i'}\right)^2$$

$$\omega_i' = \sqrt{\frac{k-\gamma\left(\frac{R}{r}-1\right)}{m_B\left(\frac{R}{r}-1\right)\frac{R}{r}+\frac{I_G}{r^2}-\alpha\left(\frac{R}{r}-1\right)}} \tag{1.57}$$

The above equation is similar to Equation (1.14). However, it has the advantage that the feedback gains are amplified by the mechanical advantage.

In practice it is difficult to build a device with low enough damping. As shown for the active VAI it is possible to use relative velocity feedback to reduce the damping (§1.3.3). The effect of velocity feedback must necessarily include a viscous damping model and will therefore be explained by considering the transmissibility of the system shown in Figure 1.60.

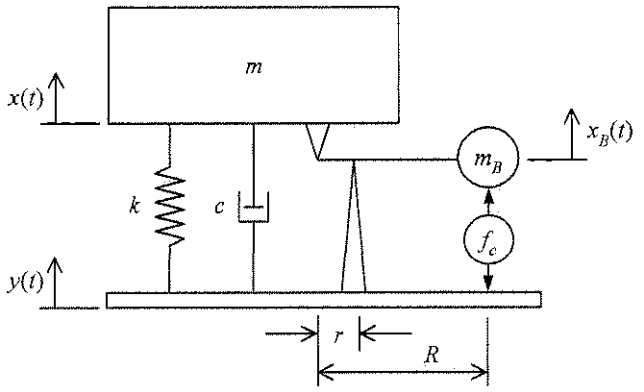

Figure 1.60: Mechanical model of an active AVAI for transmissibility

The control force is:

$$f_c = \beta(\dot{x} - \dot{y}) \tag{1.58}$$

The transmissibility is [Equation (A.155)]:

$$\frac{X}{Y} = \frac{1 + i2\frac{\omega}{\omega_n}\left[\zeta + \zeta_\beta\left(\frac{R}{r} - 1\right)\right] - \left(\frac{\omega}{\omega_i}\right)^2}{1 + i2\frac{\omega}{\omega_n}\left[\zeta + \zeta_\beta\left(\frac{R}{r} - 1\right)\right] - \left(\frac{\omega}{\omega_n}\right)^2} \tag{1.59}$$

where: $\zeta_\beta = \dfrac{\beta}{2\left[m + m_B\left(\frac{R}{r} - 1\right)^2 + \frac{I_G}{r^2}\right]\omega_n}$

From the above equation it can be deduced that if negative relative velocity feedback is used it will be possible to reduce the damping in the system to zero when [Equation (A.158)]:

$$\zeta_\beta = -\frac{\zeta}{\frac{R}{r} - 1} \tag{1.60}$$

If larger negative feedback is used the system will be unstable.

There are several advantages when using an active AVAI. The control force needed is less than that for the VAI because of the mechanical advantage of the pendulum. The tuning speed will be faster than that for an adaptive system and it should be possible to attain a larger range of isolation frequencies. McKeown *et al.* (1995) patented the active AVAI shown in Figure 1.61. This design used acceleration feedback to shift the isolation frequency up by 10% and down by 25% while consuming a maximum of 600 W. The system also used negative velocity feedback to reduce the damping such that the isolation approached 100%.

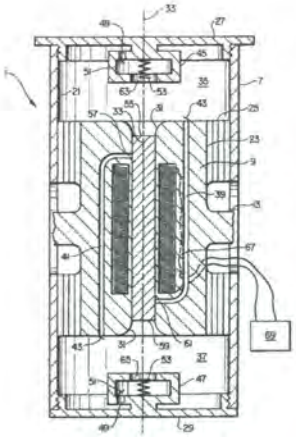

Figure 1.61: Cross section of a proposed active AVAI (McKeown *et al.*, 1995)

If absolute velocity feedback is used the control force is:

$$f_c(t) = \beta \dot{x} \tag{1.61}$$

The transmissibility is given by [Equation (A.163)]:

$$\frac{X}{Y} = \frac{1 + i2\dfrac{\omega}{\omega_n}\zeta - \left(\dfrac{\omega}{\omega_i}\right)^2}{1 + i2\dfrac{\omega}{\omega_n}\left[\zeta + \zeta_\beta\left(\dfrac{R}{r} - 1\right)\right] - \left(\dfrac{\omega}{\omega_n}\right)^2} \tag{1.62}$$

The effect of the damping added by the actuator is shown in Figure 1.62. It is interesting to note that the addition of damping is advantageous at the isolation frequency. Additionally, since damping is added and not removed the system is unconditionally stable.

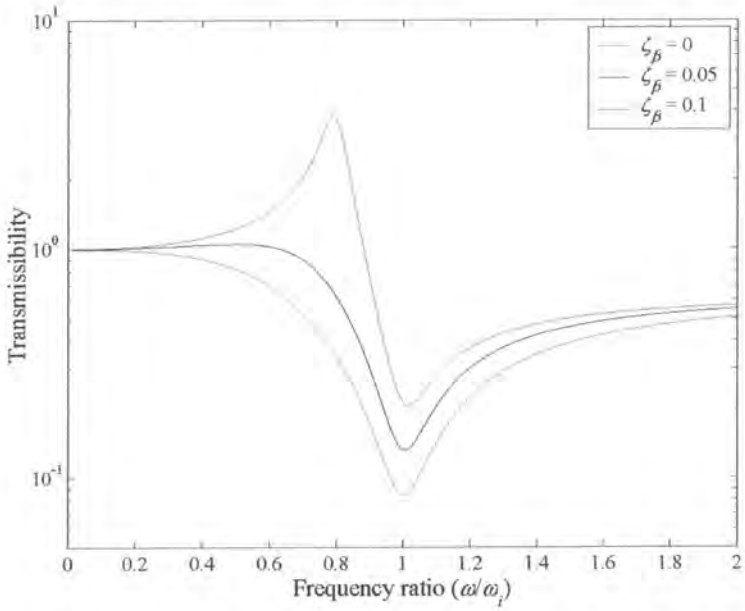

Figure 1.62: Transmissibility of an AVAI with absolute positive velocity feedback ($R/r = 10$, $\omega_n = 0.8$, $\omega_i = 1$ and $\zeta = 0.1$)

1.5 Thesis objectives

This chapter served as in introduction to methods that can be used to reduce the low stiffness bandwidth of isolators. It relied heavily on vibration absorber literature because these devices are related and very little has been published regarding their use as isolators. It introduced the normalised dynamic stiffness as a convenient and intuitive method to compare these devices. In most cases it was necessary to derive the equations because no references exist. This overview lays the foundation for the contribution of the thesis.

The focus of this work is the broadening of the effective low-stiffness bandwidth of amplified vibration-absorbing isolators (AVAIs) by adapting system parameters. The objectives are to:

1. Compare various isolator concepts using the transfer dynamic stiffness.
2. Develop mathematical models for two novel adaptive AVAIs.
3. Show how these devices can be controlled effectively using optimisation techniques.
4. Establish a design methodology for adaptive AVAIs for a pneumatic rock drill handle application.
5. Verify the mathematical models through experiment.

In order to achieve the above objectives, the following were done:

Comparison of isolators using the transfer dynamic stiffness

- Classify isolators according to their mechanical layout as either isolators, vibration-absorbing isolators or amplified vibration-absorbing isolators and according to their degree of autonomy as passive, adaptive or active.
- Define the blocked transfer dynamic stiffness as a measure of the suitability of an isolator for a specific excitation type.
- Compare isolators using the blocked transfer dynamic stiffness, specifically concentrating on various techniques to broaden the low stiffness bandwidth. For this purpose techniques established in the fields of isolators and vibration absorbers will be applied to the AVAI to show the benefits that can be obtained.
- Introduce the concept of adapting isolator properties to minimise the objective of the isolator. For the case of hand-transmitted vibration the objective is defined as the weighted equivalent acceleration given by ISO 5349.
- Study current techniques of adapting stiffness of springs as a foundation for applying such a technique to an adaptive AVAI.

Mathematical models for novel adaptive AVAIs

- Derive and verify the mathematical models of two novel adaptive AVAI designs. Here the emphasis will be on calculating the response of the devices and for this purpose the dynamic stiffness is abandoned in favour of the transmissibility properties of the AVAIs.
- Show that the first AVAI offers low construction cost, simplicity and robustness. Three cases will be investigated. The first option consists of flexible reservoir walls covering the full wall area, the second shows the effect of reducing the flexible section of the reservoir wall and the third considers a single flexible wall.

- Confirm that the second AVAI offers low mass at the expense of robustness. Three refinements to this design will be investigated. The first refinement derives the non-linear equation for a system with impact stops. The second investigates the effect of leakage on the transmissibility and the third explores a system utilising diaphragm seals to eliminate leakage.
- Develop general design methodologies for passive and adaptive damped and undamped devices using optimisation techniques.

Effective control of these devices using optimisation techniques

- Demonstrate that the adaptive AVAI can be controlled to ensure optimal transmissibility.
- Show that the objective function exhibits local minima, which must be handled appropriately to ensure convergence. Also compare different methods of estimating the objective function.
- Compare some common optimisation algorithms' ability to solve various excitation scenarios.

Design methodology for adaptive AVAIs for a pneumatic rock drill handle application

- Investigate current methods of vibration reduction for hand-operated tool handles.
- Present measurements of the Boart Longyear S215 rock drill vibration and analyse these as prescribed in ISO 5349.
- Qualitatively demonstrate the suitability of the both AVAIs for excitation containing broadband noise and narrowband tonal excitation.
- Develop a design methodology for the adaptive AVAI with specific application to a pneumatic rock drill. As part of this design methodology the effect of leakage on the stiffness, loss factor and tuning speed will be investigated through time domain simulation. Additionally, techniques for estimating the stiffness of rubber components for various loadings will be compared.
- Show that a rock drill handle can be set up in such a way that tuning is achieved through direct coupling with the supply line, making the use of a control system unnecessary.
- Compare the following: Tuning through air spring coupling to the supply line, an optimisation based control system and open-loop tuning to the frequency of maximum excitation through simulation using the measured vibration data.

Experimental verification of the mathematical models

- Experimentally verify and improve the mathematical models used to design the AVAIs.
- Estimate the system parameters by fitting the mathematical models to the experimental data.
- Show through experimentation that an optimisation control system can adapt the stiffness of the type I AVAI to find the optimal transmissibility.

It is believed that achieving the above objectives will extend and contribute to the current knowledge on these devices.

1.6 Thesis description

Chapter 2 will introduce the two innovative AVAIs that will be studied in this thesis. Mathematical models are derived in non-dimensional form and manipulated to clearly show their properties and

specifically the effects of tuning. This is done in a general way without considering application-specific issues. Chapter 3 will discuss possible control strategies. It will include numerical simulations that show which methods could be problematic and under which circumstances problems can occur. Chapter 4 will detail the design methodology for the pneumatic rock drill. An introduction to hand-arm vibration is given, specifically considering the diseases caused by vibration as well as the ISO specification used to assess the severity of tool vibration. A large set of measurements of a pneumatic drill commonly used in South-African gold mining industry is shown, which illustrate its operational behaviour. In this chapter application-specific issues will be addressed and the design methodology for each device will be applied. Chapter 5 will highlight experimental results obtained from the two devices. The experiments will show where assumptions made led to inaccurate modelling and how these can be improved. For the first prototype a control system will be implemented which will demonstrate that it can tune the device accurately. Chapter 6 will cover the conclusions.

2 Novel adaptive amplified vibration-absorbing isolators

The two novel types of adaptive AVAI that will be studied are shown in Figure 2.1, with the tuneable stiffness elements indicated. The type I modifies the continuity through the port using flexible reservoir walls. The primary spring stiffness (k in Figure 2.1(a)) remains constant. The main advantage of the addition of a degree of freedom to the LIVE isolator is that it simplifies the construction of the AVAI. The addition of the degree of freedom (u) to aid tuning is considered to be unique. The type II exploits the high density of a heavy metal slug in replacement of the fluid in the port. The main advantage of this approach is the reduced size of the device. As far as could be established the concepts for changing the stiffness of the springs in these ways for both the type I and type II AVAI are unique and innovative.

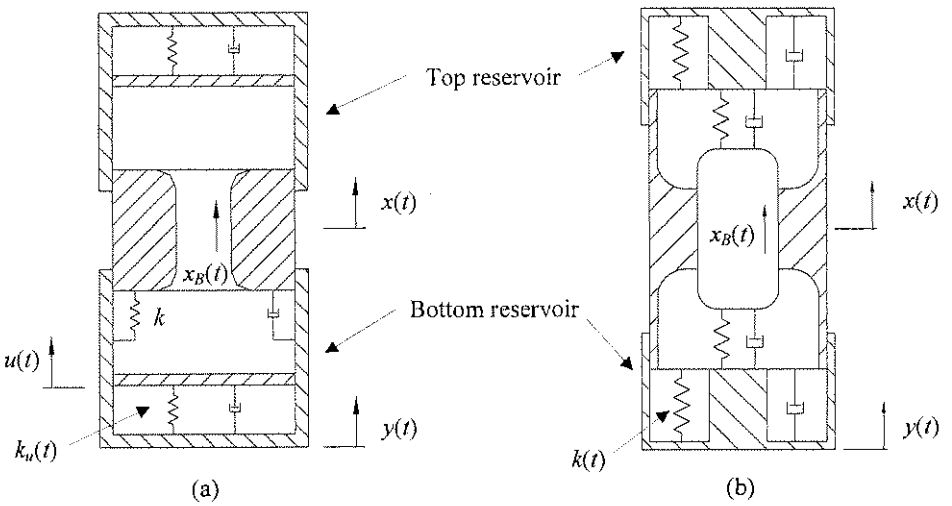

Figure 2.1: Adaptive AVAI (a) Type I: with adaptive reservoir wall stiffness (b) Type II: with adaptive stiffness and slug (moveable rigid bodies are hatched, flexible elements are indicated by springs and the top and bottom reservoirs are rigidly connected)

Chapter 1 showed the relationship between various isolator concepts using the blocked transfer dynamic stiffness. This method worked well for frequency domain comparison since the equations could be normalised easily in terms of non-dimensional parameters commonly used in the field of vibration. The dynamic stiffness was the best quantity to use for this evaluation because it focused on the isolator while disregarding the role of the equipment being isolated since it was assumed to be present in all cases. For this purpose the method proved to be both simple and intuitive.

Since it has already been established that there are advantages when using AVAI the need for the dynamic stiffness has passed. In this chapter the main consideration is the response of the equipment, simply finding the best isolator is not enough, the exact response is needed to assess if a design is feasible. As was shown in Chapter 1 the transmissibility cannot be calculated directly from the blocked transfer dynamic stiffness and it will therefore be derived from the equations of motion for each concept. The response must then be evaluated against a set of criteria to establish which isolator should be used as was shown in Figure 1.1. The specific characteristics of these devices will therefore

be considered using transmissibility and time domain integration. The main properties of the two AVAIs will be shown in this chapter with complete derivations shown in Appendix B.

2.1 Adaptive AVAI with variable reservoir wall flexibility (Type I)

The pendulum equivalent of this class of AVAI was discussed in §1.3.2 (Figure 1.55). Three devices will be discussed according to the type of flexibility added to the system:

1. Flexibility covering the full reservoir wall.
2. Flexibility covering a reduced area of the reservoir wall.
3. A single flexible wall.

The first device is more advantageous than the second and will be presented in detail. The second shows the effect of reducing the area of the flexible part of the reservoir wall. Such a device is less attractive than the first, but can be used to represent a real system more accurately. The single flexible wall device differs fundamentally from the first two in its principle of operation but has physical similarities that will be discussed.

2.1.1 Reservoir flexibility covering full wall

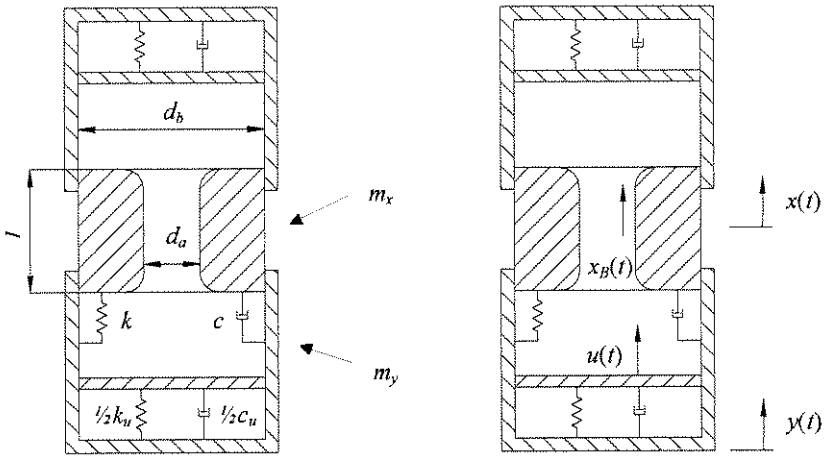

Figure 2.2: Mechanical model of an adaptive AVAI with flexibility covering the complete reservoir wall ($m_B = \rho A_a l$, $A_a = \pi d_a^2/4$ and $A_b = \pi d_b^2/4$)

In Figure 2.2 the u degree of freedom represents the displacement of the reservoir wall. Since the fluid is incompressible the fluid continuity through the port is [Equation (B.1)]:

$$x_B = \left(1 - \frac{A_b}{A_a}\right)x + \frac{A_b}{A_a}u \tag{2.1}$$

where A_b is the reservoir area and A_a the port area. Excitation can occur at the x or the y degree of freedom. In this chapter excitation will be assumed to be at the x degree of freedom because it has practical advantages for the experimental device that will be presented later. Equations for excitation

at the y degree of freedom are shown in Appendix B. If it is assumed that no external forces are acting on the system the equation of motion is [Equation (B.14)]:

$$\begin{bmatrix} m_y & 0 \\ 0 & m_B\left(\frac{A_b}{A_a}\right)^2 \end{bmatrix}\begin{bmatrix} \ddot{y} \\ \ddot{u} \end{bmatrix}+\begin{bmatrix} c+c_u & -c_u \\ -c_u & c_u \end{bmatrix}\begin{bmatrix} \dot{y} \\ \dot{u} \end{bmatrix}+\begin{bmatrix} k+k_u & -k_u \\ -k_u & k_u \end{bmatrix}\begin{bmatrix} y \\ u \end{bmatrix}=\begin{bmatrix} c\dot{x}+kx \\ -m_B\left(1-\frac{A_b}{A_a}\right)\frac{A_b}{A_a}\ddot{x} \end{bmatrix} \tag{2.2}$$

where m_y is the mass associated with y degree of freedom, m_B is the absorber mass, c and k denote the primary spring properties and c_u and k_u the reservoir spring properties. The above equation can be transformed to the frequency domain by assuming harmonic excitation:

$$\begin{bmatrix} -\omega^2 m_y + i\omega(c+c_u)+k+k_u & -(i\omega c_u + k_u) \\ -(i\omega c_u + k_u) & -\omega^2 m_B\left(\frac{A_b}{A_a}\right)^2 + i\omega c_u + k_u \end{bmatrix}\begin{bmatrix} Y \\ U \end{bmatrix}=\begin{bmatrix} i\omega c + k \\ \omega^2 m_B\left(1-\frac{A_b}{A_a}\right)\frac{A_b}{A_a} \end{bmatrix}X \tag{2.3}$$

Using the second equation in the set defined above it is possible to eliminate the U degree of freedom and to find the transmissibility between the input and the response [Equation (B.17)]:

$$\frac{Y}{X}=\frac{(k+i\omega c)\left[k_u+i\omega c_u-\omega^2 m_B\left(\frac{A_b}{A_a}\right)^2\right]-(k_u+i\omega c_u)\omega^2 m_B\left(\frac{A_b}{A_a}-1\right)\frac{A_b}{A_a}}{\left[k+k_u+i\omega(c+c_u)-\omega^2 m_y\right]\left[k_u+i\omega c_u-\omega^2 m_B\left(\frac{A_b}{A_a}\right)^2\right]-(k_u+i\omega c_u)^2} \tag{2.4}$$

Equation (2.4) can be non-dimensionalised by introducing the stiffness ratio and the frequencies ω_1, ω_2 and $\bar{\omega}_i$ [Equation (B.18)]:

$$\frac{Y}{X}=\frac{1-\left(\frac{\omega}{\omega_2}\right)^2-\left(\frac{\omega}{\bar{\omega}_i}\right)^2}{\left[1+\frac{k_u}{k}-\left(\frac{\omega}{\omega_1}\right)^2\right]\left[1-\left(\frac{\omega}{\omega_2}\right)^2\right]-\frac{k_u}{k}} \tag{2.5}$$

where: $\omega_1^2=\frac{k}{m_y}$, $\omega_2^2=\frac{k_u}{m_B\left(\frac{A_b}{A_a}\right)^2}$, $\bar{\omega}_i^2=\frac{k}{m_B\left(\frac{A_b}{A_a}-1\right)\frac{A_b}{A_a}}$

The defined frequencies have physical significance. The frequency ω_1 is the natural frequency of the primary system without the fluid. As was shown in Chapter 1 this frequency should be as low as possible, requiring a low primary stiffness (k). The second frequency is the natural frequency of the column of fluid in the port suspended by the membrane. This frequency is a function of the membrane stiffness, but it will be beneficial for explaining tuning to rewrite it in terms of a constant frequency (i.e. $\bar{\omega}_2 \neq f(k_u)$) and the stiffness ratio ($\mu_k = k_u/k$):

$$\omega_2^2=\frac{k_u}{k}\frac{k}{m_B\left(\frac{A_b}{A_a}\right)^2}=\mu_k\bar{\omega}_2^2 \tag{2.6}$$

The frequency $\bar{\omega}_i$ is the isolation frequency at infinite stiffness ratio and is the same as for a LIVE type AVAI. If the area ratio is large then the relationship between ω_2 and $\bar{\omega}_i$ is:

$$\omega_2^2 = \mu_k \frac{k}{m_B\left(\frac{A_b}{A_a}\right)^2} = \mu_k \bar{\omega}_2^2 \approx \mu_k \bar{\omega}_i^2 \tag{2.7}$$

The actual isolation frequency will be designated ω_i. The isolation frequency can be found by equating the numerator of Equation (2.5) to zero:

$$\left(\frac{\omega_i}{\omega_1}\right)^2 = \frac{1}{\left(\frac{\omega_1}{\bar{\omega}_i}\right)^2 + \frac{1}{\mu_k}\left(\frac{\omega_1}{\bar{\omega}_2}\right)^2} \tag{2.8}$$

By introducing the isolation frequency Equation (2.5) can be generalised:

$$\frac{Y}{X} = \frac{1-\left(\frac{\omega}{\omega_i}\right)^2}{\left[1+\mu_k-\left(\frac{\omega}{\omega_1}\right)^2\right]\left[1-\left(\frac{\omega}{\omega_2}\right)^2\right]-\mu_k} \tag{2.9}$$

Notably Equation (2.9) is similar to the equation describing the amplitude of a vibration absorber (Rao, 1990).

Vibration absorber theory generally identifies two distinct cases (Brennan, 1997b). Firstly, a resonance of the primary structure is excited and the absorber is used to add damping to the structure at frequencies in the region of the natural frequency. Such a device is often called a tuned damper. A second case occurs when a large force excites the system and in such a case the absorber is tuned to excitation frequency. Here only the second case will be considered since operation at resonance for an isolated system is unlikely. An important difference between a vibration absorber and the type I AVAI is that the isolation frequency (ω_i) for the present device is not equal to the absorber natural frequency (ω_2). The two frequencies are, however, related through their dependence on the mass and area ratios. This can be shown by considering the frequency ratios $\omega_1/\bar{\omega}_2$ and $\omega_1/\bar{\omega}_i$ [Equations (B.21) and (B.22)]:

$$\left(\frac{\omega_1}{\bar{\omega}_2}\right)^2 = \frac{m_B}{m_y}\left(\frac{A_b}{A_a}\right)^2 \tag{2.10}$$

$$\left(\frac{\omega_1}{\bar{\omega}_i}\right)^2 = \frac{m_B}{m_y}\left(\frac{A_b}{A_a}-1\right)\frac{A_b}{A_a} \tag{2.11}$$

The transmissibility can now be rewritten as:

$$\frac{Y}{X} = \frac{1-\frac{1}{\mu_k}\left(\frac{\omega_1}{\bar{\omega}_2}\right)^2\left(\frac{\omega}{\omega_1}\right)^2-\left(\frac{\omega_1}{\bar{\omega}_i}\right)^2\left(\frac{\omega}{\omega_1}\right)^2}{\left[1+\mu_k-\left(\frac{\omega}{\omega_1}\right)^2\right]\left[1-\frac{1}{\mu_k}\left(\frac{\omega_1}{\bar{\omega}_2}\right)^2\left(\frac{\omega}{\omega_1}\right)^2\right]-\mu_k} \tag{2.12}$$

A typical plot of Equation (2.12) is shown in Figure 2.3. It can be seen from the equation that the system will approach the transmissibility of the LIVE isolator as the stiffness ratio approaches infinity, since $1/\mu_k$ approaches zero.

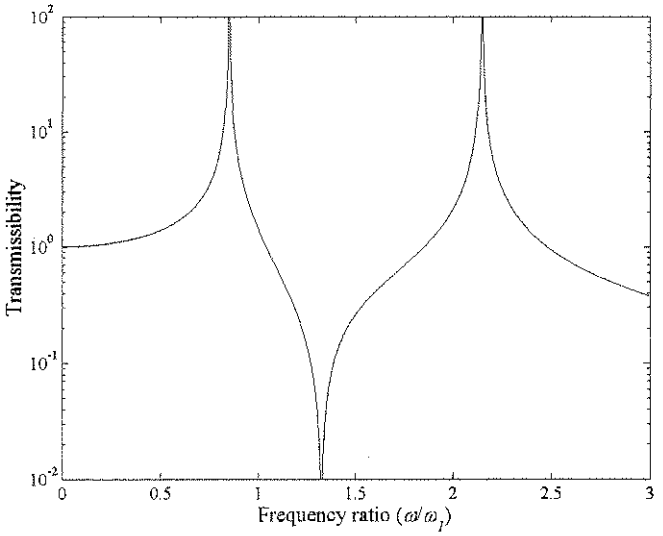

Figure 2.3: Undamped transmissibility curve ($m_B/m_y = 0.003$, $A_b/A_a = 10$ and $\mu_k = 1$ in Equation (2.12))

The objective of the design is for the excitation and isolation frequencies to coincide. The isolation frequency can be calculated by setting the numerator of Equation (2.12) to zero. Replacing the frequency ratios in the resulting equation with the ratios defined in Equation (2.10) and Equation (2.11) yields:

$$\frac{1}{\frac{m_B}{m_y}\left(\frac{A_b}{A_a}-1\right)\frac{A_b}{A_a}+\frac{1}{\mu_k}\frac{m_B}{m_y}\left(\frac{A_b}{A_a}\right)^2}=\left(\frac{\omega_i}{\omega_1}\right)^2 \tag{2.13}$$

Clearly there are multiple solutions for Equation (2.13), but all the ratios will have physical constraints in practice. Some constraints may even be discrete if standard parts are used, for instance, to achieve a certain area ratio. Since the primary natural frequency must be chosen as low as feasible the only parameters available for tuning are the mass, area and stiffness ratios. To find an appropriate choice it is necessary to investigate their effect on the frequencies of maximum transmissibility. The undamped frequencies of maximum transmissibility can be found by equating the denominator of Equation (2.12) to zero [Equation (B.24)]:

$$\left(\frac{\Omega_1}{\omega_1}\right)^2,\left(\frac{\Omega_2}{\omega_1}\right)^2=\frac{\frac{1+\mu_k}{\mu_k}\left(\frac{\omega_1}{\bar{\omega}_2}\right)^2+1\mp\sqrt{\left[\frac{1+\mu_k}{\mu_k}\left(\frac{\omega_1}{\bar{\omega}_2}\right)^2+1\right]^2-\frac{4}{\mu_k}\left(\frac{\omega_1}{\bar{\omega}_2}\right)^2}}{\frac{2}{\mu_k}\left(\frac{\omega_1}{\bar{\omega}_2}\right)^2} \tag{2.14}$$

Figure 2.4 and Figure 2.5 illustrate the effect of mass and stiffness ratios on the frequencies of maximum transmissibility as well as the isolation frequency. At low stiffness ratios and large mass ratios the isolation frequency approaches the first frequency of maximum transmissibility. It will be

beneficial if the isolation frequency is separated from the frequencies of maximum transmissibility, but in doing so the isolation frequency is increased. Since a low isolation frequency is normally required the primary system natural frequency must be as low as feasible to ensure coincidence. The effect of the area ratio will be similar to that of the mass ratio.

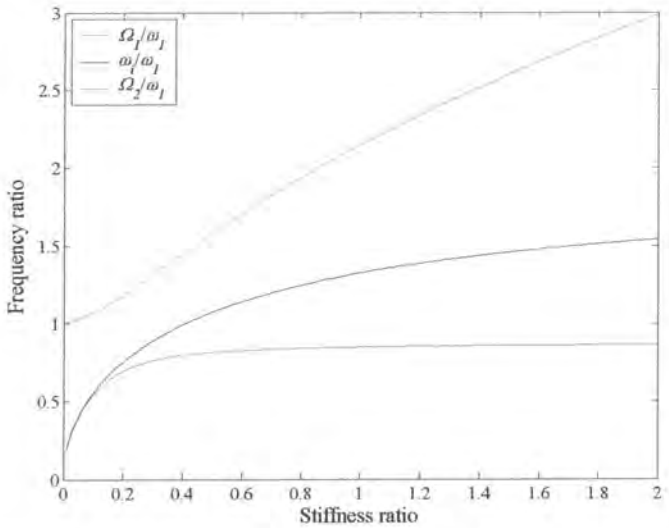

Figure 2.4: Frequencies of maximum and minimum transmissibility *vs.* stiffness ratio (μ_k) (m_B/m_y = 0.003 and A_b/A_a= 10)

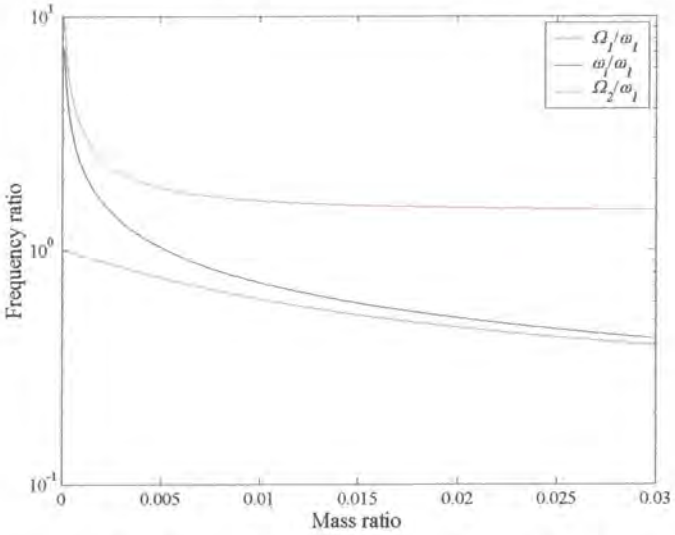

Figure 2.5: Frequencies of maximum and minimum transmissibility *vs.* mass ratio (m_B/m_y) (A_b/A_a= 10 and μ_k = 1)

The frequencies of maximum transmissibility can now be used to guide a more appropriate choice of parameter ratios to satisfy Equation (2.13). One method would be to require equal spacing between the isolation frequency and the two frequencies of maximum transmissibility. Mathematically this requirement can be expressed as:

$$\left(\frac{\omega_i}{\omega_1}\right)^2 - \left(\frac{\Omega_1}{\omega_1}\right)^2 = \left(\frac{\Omega_2}{\omega_1}\right)^2 - \left(\frac{\omega_i}{\omega_1}\right)^2 \tag{2.15}$$

Each of the above ratios can be written in terms of the parameter ratios as shown before in Equations (2.13) and (2.14), although not explicitly. It is necessary to solve the parameter ratios using a numerical method and for this purpose the equations are rewritten as follows:

$$\left(\frac{\Omega_1}{\omega_1}\right)^2 \frac{2\mu_m\mu_A^2}{\mu_k} - \frac{1+\mu_k}{\mu_k}\mu_m\mu_A^2 - 1 + \sqrt{\left[\frac{1+\mu_k}{\mu_k}\mu_m\mu_A^2 + 1\right]^2 - \frac{4\mu_m\mu_A^2}{\mu_k}} = 0$$

$$\left(\frac{\Omega_2}{\omega_1}\right)^2 \frac{2\mu_m\mu_A^2}{\mu_k} - \frac{1+\mu_k}{\mu_k}\mu_m\mu_A^2 - 1 - \sqrt{\left[\frac{1+\mu_k}{\mu_k}\mu_m\mu_A^2 + 1\right]^2 - \frac{4\mu_m\mu_A^2}{\mu_k}} = 0$$

$$\left(\frac{\omega_i}{\omega_1}\right)^2 \left[\mu_m(\mu_A - 1)\mu_A + \frac{\mu_m\mu_A^2}{\mu_k}\right] - 1 = 0 \qquad (2.16)$$

$$2\left(\frac{\omega_i}{\omega_1}\right)^2 - \left(\frac{\Omega_1}{\omega_1}\right)^2 - \left(\frac{\Omega_2}{\omega_1}\right)^2 = 0$$

where: $\mu_A = \frac{A_b}{A_a}$, $\mu_m = \frac{m_B}{m_y}$

In this set of equations there are 5 unknowns (μ_k, μ_A, μ_m, Ω_2/ω_1 and Ω_1/ω_1) and four equations, which requires that one parameter be prescribed. A typical design might prescribe the area ratio (μ_A) and calculate the required mass and stiffness ratios. The result for a design requiring an isolation frequency ratio ω_i/ω_1 = 1.5 and area ratio (μ_A) of 10 is shown in Figure 2.6. Clearly the frequency ratios of maximum transmissibility are equidistant from the isolation frequency ratio. The calculated values for the mass and stiffness ratios are μ_m = 0.00182 and μ_k = 0.65 respectively.

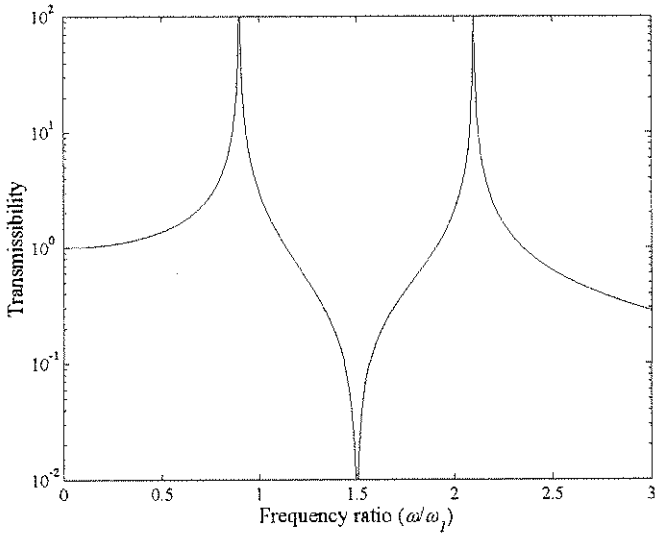

Figure 2.6: Design result for ω_i/ω_1 = 1.5

It is also possible for other requirements to exist such as limits on the stiffness, mass and area ratios as well as on the primary system natural frequency, in which case an optimisation approach can be used to find suitable parameters.

The approach described above is suitable for an undamped device. Although unwanted in most cases, damping will always be present in practical devices, and can influence the design substantially. The effect of damping will be considered next.

For the damped case the transmissibility can be non-dimensionalised by introducing the frequencies defined before and the damping ratios in Equation (2.4) [Equation (B.28)]:

$$\frac{Y}{X}=\frac{\left(1+i2\frac{\omega}{\omega_1}\zeta_1\right)\left[1+i2\frac{\omega}{\omega_2}\zeta_2-\left(\frac{\omega}{\omega_2}\right)^2\right]-\left(1+i2\frac{\omega}{\omega_2}\zeta_2\right)\left(\frac{\omega}{\overline{\omega}_i}\right)^2}{\left[1+\mu_k+i2\left(\frac{\omega}{\omega_1}\zeta_1+\mu_k\frac{\omega}{\omega_2}\zeta_2\right)-\left(\frac{\omega}{\omega_1}\right)^2\right]\left[1+i2\frac{\omega}{\omega_2}\zeta_2-\left(\frac{\omega}{\omega_2}\right)^2\right]-\mu_k\left(1+i2\frac{\omega}{\omega_2}\zeta_2\right)^2} \tag{2.17}$$

where: $\zeta_1=\dfrac{c}{2m_y\omega_1}$, $\zeta_2=\dfrac{c_u}{2m_B\left(\frac{A_b}{A_a}\right)^2\omega_2}$

The second damping ratio can be written in terms of the stiffness ratio:

$$\zeta_2=\frac{1}{\sqrt{\mu_k}}\frac{c_u}{2m_B\left(\frac{A_b}{A_a}\right)^2\overline{\omega}_2}=\frac{1}{\sqrt{\mu_k}}\overline{\zeta}_2 \tag{2.18}$$

It is convenient to rearrange Equation (2.17) in terms of the frequency ratio (ω/ω_1) and the stiffness ratio (μ_k) [Equation (B.29)]:

$$\frac{Y}{X}=\frac{\left(1+i2\frac{\omega}{\omega_1}\zeta_1\right)\left[1+i\frac{2}{\mu_k}\frac{\omega_1}{\overline{\omega}_2}\frac{\omega}{\omega_1}\overline{\zeta}_2-\frac{1}{\mu_k}\left(\frac{\omega_1}{\overline{\omega}_2}\right)^2\left(\frac{\omega}{\omega_1}\right)^2\right]-\left(1+i\frac{2}{\mu_k}\frac{\omega_1}{\overline{\omega}_2}\frac{\omega}{\omega_1}\overline{\zeta}_2\right)\left(\frac{\omega_1}{\overline{\omega}_i}\right)^2\left(\frac{\omega}{\omega_1}\right)^2}{\left[1+\mu_k+i2\frac{\omega}{\omega_1}\left(\zeta_1+\frac{\omega_1}{\overline{\omega}_2}\overline{\zeta}_2\right)-\left(\frac{\omega}{\omega_1}\right)^2\right]\left[1+i\frac{2}{\mu_k}\frac{\omega_1}{\overline{\omega}_2}\frac{\omega}{\omega_1}\overline{\zeta}_2-\frac{1}{\mu_k}\left(\frac{\omega_1}{\overline{\omega}_2}\right)^2\left(\frac{\omega}{\omega_1}\right)^2\right]-\mu_k\left(1+i\frac{2}{\mu_k}\frac{\omega_1}{\overline{\omega}_2}\frac{\omega}{\omega_1}\overline{\zeta}_2\right)^2} \tag{2.19}$$

The effect of damping on the transmissibility is illustrated in Figure 2.7 and Figure 2.8. The damping ratio ζ_1 is associated with the primary system before the addition of the absorber fluid. The source of this damping is the primary spring. For the combined system the primary spring damping will influence the response at all the frequencies of maximum and minimum transmissibility. The damping ratio ζ_2 is associated with the membrane and the fluid and will only influence the transmissibility at the second frequency of maximum transmissibility and the frequency of minimum transmissibility. The effect on the transmissibility at the isolation frequency is less than for the primary damping ratio ζ_1. It is also important to note that the addition of damping will have a significant effect on the isolation frequency. Normally this effect will not influence the design, since the AVAI is designed to have little damping. In a case where some damping is required it must clearly be accounted for to ensure optimal tuning.

In some cases high frequency transmissibility can enter the design requirements, for instance, to limit noise generation. It has already been shown for the single degree of freedom AVAI that the high frequency transmissibility is related to the ratio of natural to isolation frequencies and is independent of frequency. For the AVAI with flexible reservoir wall the high frequency roll-off is -20 dB/decade when damped and -40 dB/decade when undamped, which is the same as for a normal isolator.

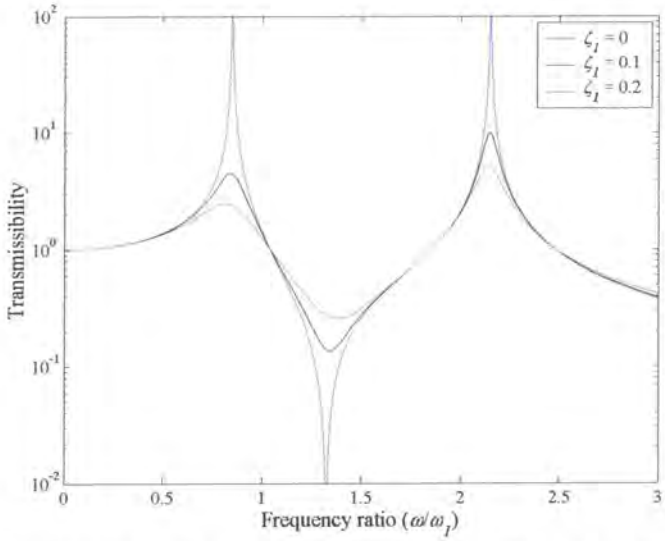

Figure 2.7: Transmissibility *vs.* damping ratio ζ_1 (m_B/m_y = 0.003, A_b/A_a= 10, ζ_2 = 0 and μ_k = 1)

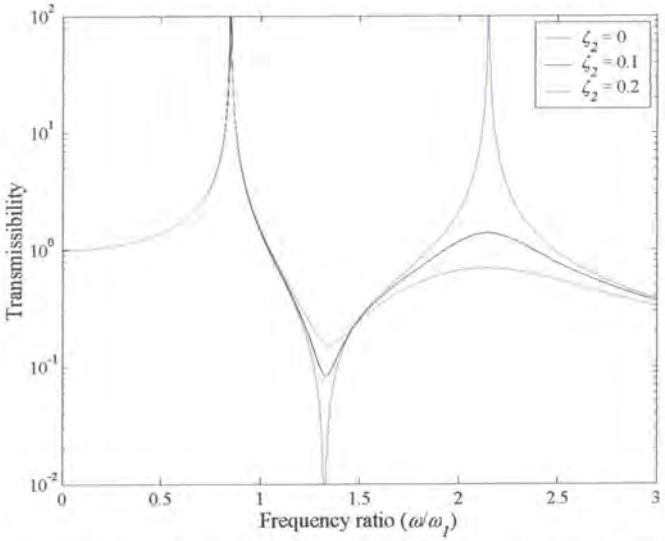

Figure 2.8: Transmissibility *vs.* damping ratio ζ_2 (m_B/m_y = 0.003, A_b/A_a= 10, ζ_1 = 0 and μ_k = 1)

It would be ideal to have a robust device that is insensitive to changes in excitation frequency. A high bandwidth device will fit this requirement. The bandwidth is defined as the normalised frequency range for which the transmissibility is within √2 of the minimum transmissibility at the isolation frequency:

$$B = \frac{\hat{\omega}_2 - \hat{\omega}_1}{\omega_t} \tag{2.20}$$

Analytical expressions for $\hat{\omega}_1$ and $\hat{\omega}_2$ can be found using Equation (2.19), but will be cluttered and will not be attempted. Instead the values will be obtained numerically. Figure 2.9 shows the effect of damping on the bandwidth, isolation frequency and frequencies of maximum transmissibility. It shows that for primary damping ratios of up to 0.1 the effect on the isolation frequency can be ignored for the

system considered. This might not be the case for other designs. As expected the bandwidth increases with damping.

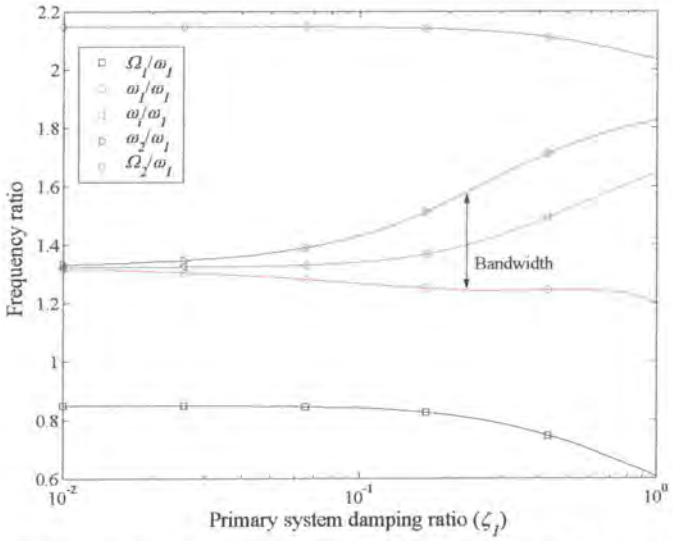

Figure 2.9: Frequency ratio *vs.* primary system damping ($m_B/m_y = 0.003$, $A_b/A_a = 10$, $\zeta_2 = 0$ and $\mu_k = 1$)

A device with large bandwidth only is, however, of little use if the isolation is not adequate, as will happen for a highly damped device. This is illustrated in Figure 2.10. Also shown is that use of the undamped isolation frequency will be adequate for designs with a damping ratio of less than 0.1.

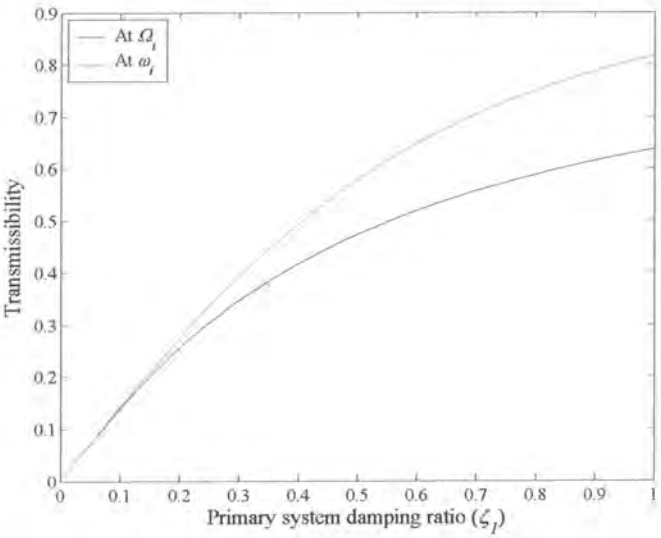

Figure 2.10: Transmissibility at the damped (Ω_i) and undamped (ω_i) isolation frequency as a function of primary system damping ($m_B/m_y = 0.003$, $A_b/A_a = 10$, $\zeta_2 = 0$ and $\mu_k = 1$)

To account for both the bandwidth and isolation in one parameter, Brennan (1997b) defined the robustness as the isolation bandwidth product:

$$R = B\left(1 - \left|\frac{Y}{X}\right|\right) \tag{2.21}$$

The robustness is shown in Figure 2.11.

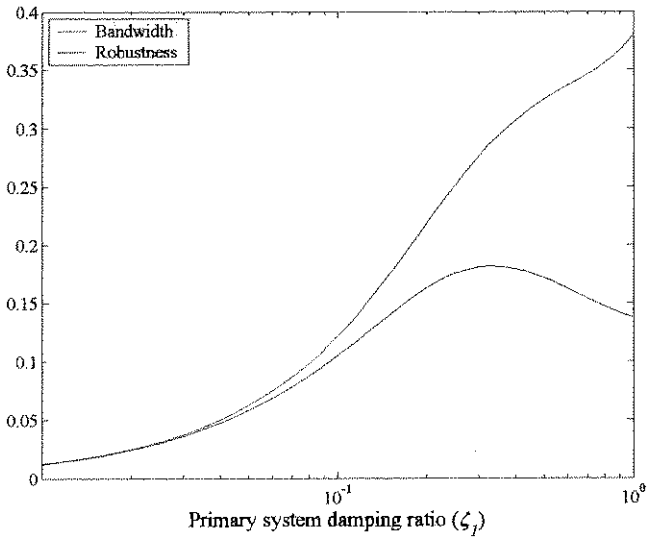

Figure 2.11: Bandwidth and robustness (m_B/m_y = 0.003, A_b/A_a= 10, ζ_2 = 0 and μ_k = 1)

Clearly an optimal value exist for this design, but practically a damping ratio of ~0.3 will not provide adequate isolation and a less robust design will be necessary. One way to increase both the bandwidth and the robustness is to increase the mass ratio as shown in Figure 2.12. This result should be interpreted with care, since it presupposes that a certain stiffness ratio can be realised. This might not be the case in practice, in which case an increase in mass ratio will result in inadequate separation between the isolation frequency and the first frequency of maximum transmissibility (Figure 2.5)

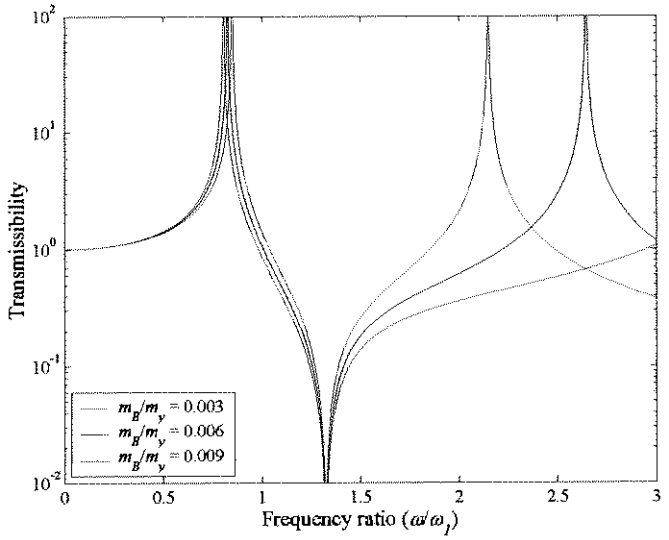

Figure 2.12: Transmissibility as a function of mass ratio ($\bar{\omega}_i/\omega_1$ = 1.3, A_b/A_a= 10 and $\zeta_1 = \zeta_2$ = 0)

Another constraint on the design is the membrane deflection. The transmissibility between the excitation and the membrane response is given by:

$$\frac{U}{X}=\frac{\left(1+i\frac{2}{\mu_k}\frac{\omega_1}{\bar{\omega}_2}\frac{\omega}{\omega_1}\bar{\zeta}_2\right)\left(1+i2\frac{\omega}{\omega_1}\zeta_1\right)-\left[1+\mu_k+i2\frac{\omega}{\omega_1}\left(\zeta_1+\frac{\omega_1}{\bar{\omega}_2}\bar{\zeta}_2\right)-\left(\frac{\omega}{\omega_1}\right)^2\right]\left(\frac{\omega_1}{\bar{\omega}_1}\right)^2\left(\frac{\omega}{\omega_1}\right)^2}{\left[1+\mu_k+i2\frac{\omega}{\omega_1}\left(\zeta_1+\frac{\omega_1}{\bar{\omega}_2}\bar{\zeta}_2\right)-\left(\frac{\omega}{\omega_1}\right)^2\right]\left[1+i\frac{2}{\mu_k}\frac{\omega_1}{\bar{\omega}_2}\frac{\omega}{\omega_1}\bar{\zeta}_2-\frac{1}{\mu_k}\left(\frac{\omega_1}{\bar{\omega}_2}\right)^2\left(\frac{\omega}{\omega_1}\right)^2\right]-\mu_k\left(1+i\frac{2}{\mu_k}\frac{\omega_1}{\bar{\omega}_2}\frac{\omega}{\omega_1}\bar{\zeta}_2\right)^2} \quad (2.22)$$

Figure 2.13 shows the transmissibility as a function of frequency ratio with the damped isolation frequency indicated. In this case the design must be able to pass through the first frequency of maximum transmissibility without damage to the membrane and must also be able to operate continuously with membrane deflections of similar size as the excitation. At low stiffness ratios the required deflection increases.

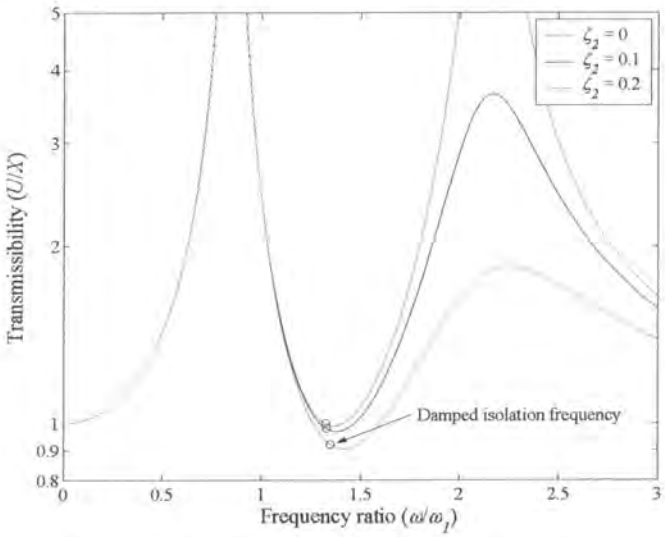

Figure 2.13: Transmissibility between the excitation and the membrane ($m_B/m_y = 0.003$, $A_b/A_a = 10$, $\zeta_1 = 0$ and $\mu_k = 1$)

When damping is included in the design it is possible to set bandwidth and transmissibility (or robustness) requirements for the design. One possible method for finding a suitable design will be discussed next. An optimisation approach will be used with the objective function defined as the transmissibility at a specified frequency. This will be done subject to some constraints. It is important to note that many other formulations can be used and these should be set up according to the design objectives. The constraints are listed in Table 2.1. The first two constraints will ensure proper separation of the frequencies of maximum transmissibility and the isolation frequency. The third constraint prescribes the required bandwidth.

Table 2.1: Definition of constraints

Parameter	Function	Constraint
First frequency of maximum transmissibility	$p_1(\bar{x})$	$< a\omega_i/\omega_1$
Second frequency of maximum transmissibility	$p_2(\bar{x})$	$> b\omega_i/\omega_1$
Bandwidth	$p_3(\bar{x})$	$> c$

The optimisation problem is shown in Equation (2.23). In this case five variables were used, but in practice it will be difficult to prescribe the damping terms. All of the variables were subjected to upper and lower bounds to ensure a realistic solution. It is also necessary to provide initial values that will ensure that the required prescribed isolation frequency is in-between the frequencies of minimum and maximum transmissibility. This can be guaranteed by solving the undamped design problem [Equation (2.16)] first.

$$f(\bar{x}) = \left| \frac{\left(1+i2\frac{\omega_i}{\omega_1}x_4\right)\left[1+i\frac{2\sqrt{x_1x_2^2}}{x_3}\frac{\omega_i}{\omega_1}x_5-\frac{x_1x_2^2}{x_3}\left(\frac{\omega_i}{\omega_1}\right)^2\right]-\left(1+i\frac{2\sqrt{x_1x_2^2}}{x_3}\frac{\omega_i}{\omega_1}x_5\right)x_1(x_2-1)x_2\left(\frac{\omega_i}{\omega_1}\right)^2}{\left[1+x_3+i2\frac{\omega_i}{\omega_1}\left(x_4+\sqrt{x_1x_2^2}x_5\right)-\left(\frac{\omega_i}{\omega_1}\right)^2\right]\left[1+i\frac{2\sqrt{x_1x_2^2}}{x_3}\frac{\omega_i}{\omega_1}x_5-\frac{x_1x_2^2}{x_3}\left(\frac{\omega_i}{\omega_1}\right)^2\right]-x_3\left(1+i\frac{2\sqrt{x_1x_2^2}}{x_3}\frac{\omega_i}{\omega_1}x_5\right)^2} \right|$$

$$g_1(\bar{x}) = p_1(\bar{x}) - a\frac{\omega_i}{\omega_1} \le 0$$

$$g_2(\bar{x}) = -p_2(\bar{x}) + b\frac{\omega_i}{\omega_1} \le 0 \qquad (2.23)$$

$$g_3(\bar{x}) = -p_3(\bar{x}) + c \le 0$$

$$x_1 = \frac{m_h}{m_y}, \quad x_2 = \frac{A_h}{A_a}, \quad x_3 = \frac{k_u}{k}, \quad x_4 = \zeta_1, \quad x_5 = \zeta_2$$

The optimal solution was found using the Matlab function `fmincon.m` and is shown in Figure 2.14 and Table 2.2. The choice of constraints must be realistic since it is easy to overconstrain the problem, which will then have no feasible solution. In this case the ratio of the first frequency of maximum transmissibility (Ω_1/ω_1) was chosen to be less than 70% of the isolation frequency ratio and the second frequency of maximum transmissibility (Ω_2/ω_1) was chosen to be more than 130% of the isolation frequency ratio. The frequencies of maximum transmissibility are found by calculating the maxima of the transmissibility equation (Equation (2.17)) defined by the solution of the optimisation problem (Equation (2.23)). The bandwidth is 6% of the isolation frequency and is also calculated using the transmissibility equation. These would be typical values used in an actual design. Since the calculated parameters are dimensionless, the result can easily be scaled to the actual desired isolation frequency.

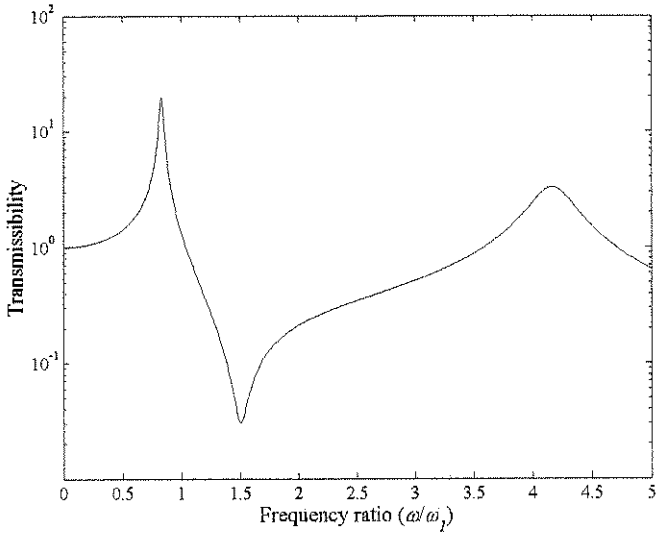

Figure 2.14: Optimal damped transmissibility curve

Table 2.2: Defined constants and solved parameter values

Constants	Parameter	Value
Ratio of first frequency of maximum transmissibility	a	0.7
Ratio of second frequency of maximum transmissibility	b	1.3
Bandwidth	c	0.06
Isolation frequency	ω_i/ω_1	1.5
Variables	Initial value (x_0)	Solution (x^*)
Mass ratio	0.0018	0.0069
Area ratio	10	7.739
Stiffness ratio	0.065	5
Primary damping ratio	0.05	0.02
Absorber damping ratio	0.05	0.078

If an increase in mass ratio is impractical and the excitation frequency is tonal time-varying, an adaptive device can be considered as a method for increasing the effective isolation bandwidth. The effect of changing the stiffness ratio for an undamped device is illustrated in Figure 2.15.

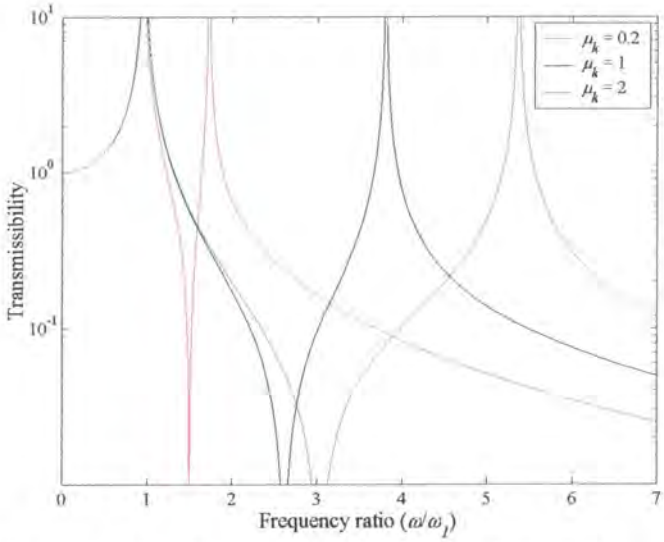

Figure 2.15: Effect of changing the stiffness ratio on the transmissibility (A_b/A_a= 16 and m_B/m_y = 0.00029)

At low stiffness ratios the bandwidth is low, but since the device can adapt to changes in frequency this will only be a problem if rapid frequency changes are expected. In order to design a device the excitation frequency range and the range of stiffness ratios that can be achieved must be known. The device is now designed for the lowest frequency ratio that must be achieved [Equation (B.23)]:

$$\mu_m = \frac{1}{\left(\frac{\omega_i}{\omega_1}\right)^2_{\min}\left[\left(\mu_A - 1\right)\mu_A + \frac{\mu_A^2}{\mu_k|_{\min}}\right]} \tag{2.24}$$

recalling that $\mu_m = m_B/m_y$, $\mu_A = A_b/A_a$ and $\mu_k = k_u/k$. Using the data from the undamped design with an isolation frequency ratio of $\omega_i/\omega_1 = 1.5$, $\mu_A = 16$ and $\mu_k|_{\min} = 0.2$ the mass ratio needed is $\mu_m = 0.00029$.

The highest frequency that can be achieved can now be calculated using Equation (2.13). If it is assumed to be $\mu_k|_{max} = 2$, then the maximum frequency ratio is $\omega_i/\omega_l = 3.05$. If the highest frequency cannot be attained the stiffness ratio must be increased, keeping in mind that there is an upper limit to the isolation frequency ratio [Equation (B.21)]:

$$\left(\frac{\bar{\omega}_i}{\omega_1}\right)^2 = \frac{1}{\mu_m(\mu_A - 1)\mu_A} \tag{2.25}$$

If it is impossible to increase the stiffness ratio or when the above limit has been reached the area ratio must be decreased. As the area ratio is decreased the calculated mass ratio will increase to maintain the isolation frequency ratio in Equation (2.24) and the upper limit of the isolation frequency ratio will increase as illustrated in Figure 2.16. The trade-off in the design is the size and mass of the device and to a lesser extent the bandwidth (for a constant stiffness ratio the bandwidth will decrease as the area ratio is decreased and the mass ratio increased).

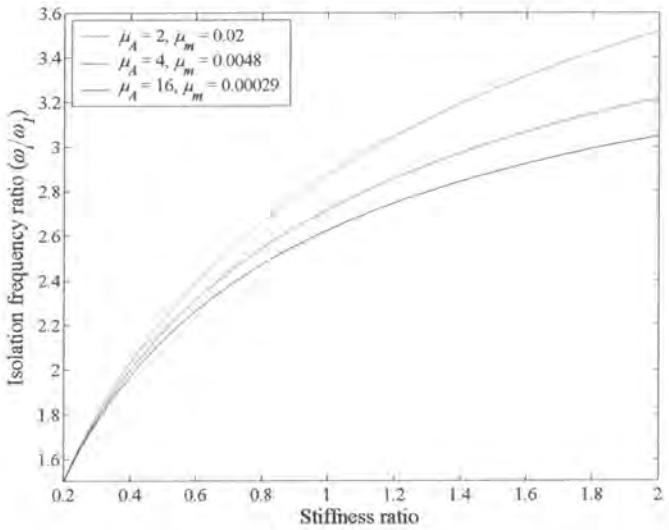

Figure 2.16: Range for various area ratios

Clearly the design method described above is iterative, but has the advantage that the designer can keep in touch with the values of mass ratio and area ratio required and those that can be achieved practically. Alternatively, the following set of equations can be solved numerically for the mass and area ratios [Equation (B.23)]:

$$\left(\frac{\omega_i}{\omega_1}\right)^2_{min} = \frac{1}{\mu_m\left[(\mu_A - 1)\mu_A + \frac{\mu_A^2}{\mu_k|_{min}}\right]}$$
$$\left(\frac{\omega_i}{\omega_1}\right)^2_{max} = \frac{1}{\mu_m\left[(\mu_A - 1)\mu_A + \frac{\mu_A^2}{\mu_k|_{max}}\right]} \tag{2.26}$$

It must, however, be kept in mind that there may not be a solution for the above equations if a too large frequency range is requested. Constraints similar to the single frequency design can also enter the design process, in which case optimisation can be used to find the best solution.

When damping is considered, it becomes clear that the transmissibility will be a function of the stiffness ratio, as illustrated in Figure 2.17. This phenomenon is a major disadvantage of the type I device as opposed to the type II AVAI.

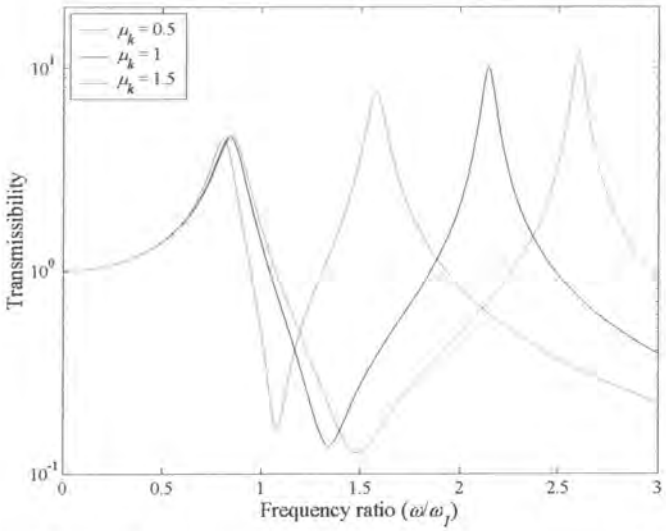

Figure 2.17: Effect of primary system damping on the transmissibility (A_b/A_a= 10, m_B/m_y = 0.003, ζ_1 = 0.1 and ζ_2 = 0)

The choice of area and mass ratios will be based on minimising the transmissibility at the isolation frequencies. The optimisation problem for the minimum isolation frequency ratio can be stated as:

$$f(x_1)=\left|\frac{\left(1+i2\frac{\omega_i}{\omega_1}\Big|_{\min}\zeta_1\right)\left[1+i\frac{2\mu_A\sqrt{x_1}}{\mu_k|_{\min}}\frac{\omega_i}{\omega_1}\Big|_{\min}\bar{\zeta}_2-\frac{x_1\mu_A^2}{\mu_k|_{\min}}\left(\frac{\omega_i}{\omega_1}\right)^2_{\min}\right]-\left(1+i\frac{2\mu_A\sqrt{x_1}}{\mu_k|_{\min}}\frac{\omega_i}{\omega_1}\Big|_{\min}\bar{\zeta}_2\right)x_1\left(\mu_A^2-1\right)\mu_{il}^2\left(\frac{\omega_i}{\omega_1}\right)^2_{\min}}{\left[1+\mu_k|_{\min}+i2\frac{\omega_i}{\omega_1}\Big|_{\min}\left(\zeta_1+\mu_A\sqrt{x_1}\bar{\zeta}_2\right)-\left(\frac{\omega_i}{\omega_1}\right)^2_{\min}\right]\left[1+i\frac{2\mu_A\sqrt{x_1}}{\mu_k|_{\min}}\frac{\omega_i}{\omega_1}\Big|_{\min}\bar{\zeta}_2-\frac{x_1\mu_A^2}{\mu_k|_{\min}}\left(\frac{\omega_i}{\omega_1}\right)^2_{\min}\right]-\mu_k|_{\min}\left(1+i\frac{2\mu_A\sqrt{x_1}}{\mu_k|_{\min}}\frac{\omega_i}{\omega_1}\Big|_{\min}\bar{\zeta}_2\right)^2}\right| \tag{2.27}$$

where x_1 is the mass ratio and the only design variable. At the maximum isolation frequency ratio a similar problem can be defined. For the problem shown above it is impossible to minimise both the transmissibility at the maximum and the minimum stiffness ratios simultaneously as the following example illustrates (Table 2.3). When the transmissibility at the minimum isolation frequency is minimised the result is that the transmissibility at the maximum isolation frequency is more than the optimal value possible. It would however make sense to tune it to the minimum value since the transmissibility decreases as the stiffness ratio is increased.

Table 2.3: Design results with $\mu_A = 16$

	Mass ratio (μ_m)	Minimum transmissibility	Maximum transmissibility
Tuned to minimum isolation frequency ratio ($\omega_i/\omega_1 = 1.5$)	0.000312	0.127139	0.064893
Tuned to maximum isolation frequency ratio ($\omega_i/\omega_1 = 3.05$)	0.000318	0.141605	0.064800

The effect of the area ratio at the minimum isolation frequency is shown in Figure 2.18. It is clear from this figure that the transmissibility at the isolation frequency can be improved noticeably by using a lower area ratio. However, the trade-off as discussed before remains.

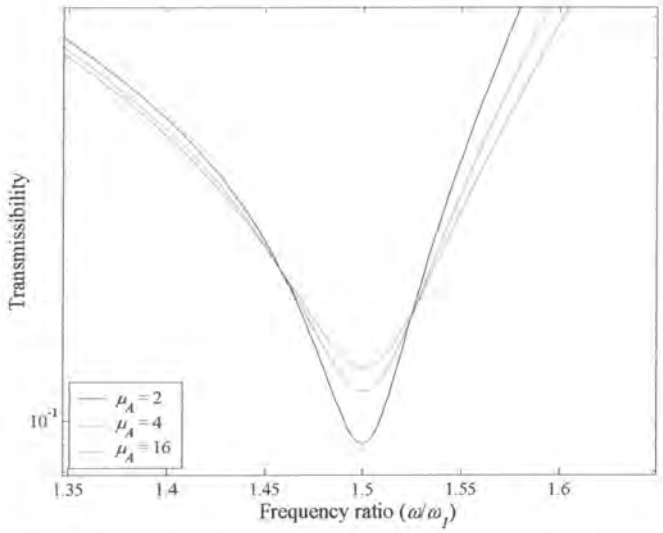

Figure 2.18: Transmissibility at the minimum isolation frequency

The envelopes for two designs are shown in Figure 2.19. The transmissibility is improved over the entire range of frequencies as the area ratio is decreased. The tuning range is also larger for a lower mass ratio, as was the case for the undamped design. Since the range is larger than that specified, the device can either be designed so that a lower minimum isolation frequency ratio or a higher maximum isolation frequency ratio can be achieved. At low stiffness ratios the isolation frequency ratio is more sensitive to the stiffness ratio and tuning will therefore be quicker. The device will also be slightly lighter. The lowest transmissibility that can be reached at a specific isolation frequency ratio will not be affected, but it will occur at a different stiffness ratio. The optimal design will therefore start at the minimum isolation frequency ratio and then minimise the area ratio within the mass and size constraints required by the application. It is also possible to set bandwidth or robustness requirements as for the fixed frequency design.

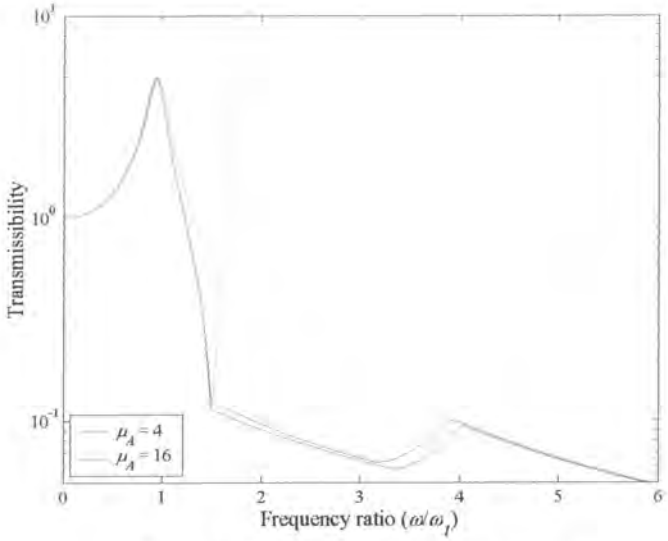

Figure 2.19: Transmissibility envelopes

For any of the above designs the physical parameters can be calculated from the various non-dimensional ratios. If the isolated mass is known the absorber mass can be calculated using the mass ratio. The absorber mass is also:

$$m_B = \rho A_a l \tag{2.28}$$

Once the fluid is chosen the size of the device can be calculated using the above equation and the area ratio. The design methods described in this section were mainly aimed at understanding the type I AVAI. In chapter 4 a more practical methodology will be described where the design starts at the maximum size and then calculates the performance that can be achieved, which can be evaluated against the performance requirements.

2.1.2 Reduced-area reservoir wall flexibility

This section will show what the effect will be if the membrane covers an area that is smaller than the reservoir wall as shown in Figure 2.20. There is no advantage to this arrangement in terms of transmissibility or frequency range over the previous case, but since it can better approximate actual system behaviour it will be discussed briefly. The fluid continuity is [Equation (B.32)]:

$$x_B = \left(1 - \frac{A_b}{A_a}\right)x + \frac{A_b - A_c}{A_a}y + \frac{A_c}{A_a}u \tag{2.29}$$

The damped transmissibility is [Equation (B.37)]:

$$\frac{Y}{X} = \frac{\left[k + i\omega c - \omega^2 m_B\left(\frac{A_b}{A_a} - 1\right)\left(\frac{A_b - A_c}{A_a}\right)\right]\left[k_w + i\omega c_w - \omega^2 m_B\left(\frac{A_c}{A_a}\right)^2\right] - \omega^2 m_B\left(\frac{A_b}{A_a} - 1\right)\frac{A_c}{A_a}\left[k_w + i\omega c_w + \omega^2 m_B\left(\frac{A_b - A_c}{A_a}\right)\frac{A_c}{A_a}\right]}{\left\{k + k_w + i\omega(c + c_w) - \omega^2\left[m_y + m_B\left(\frac{A_b - A_c}{A_a}\right)^2\right]\right\}\left[k_w + i\omega c_w - \omega^2 m_B\left(\frac{A_c}{A_a}\right)^2\right] - \left[k_w + i\omega c_w + \omega^2 m_B\left(\frac{A_b - A_c}{A_a}\right)\frac{A_c}{A_a}\right]^2} \tag{2.30}$$

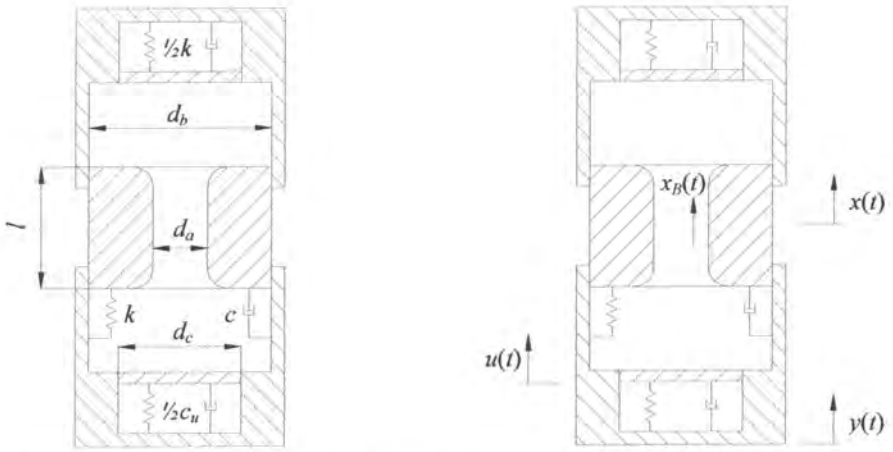

Figure 2.20: Mechanical model of an AVAI with reduced-area reservoir wall stiffness

The undamped non-dimensional transmissibility is [Equation (B.37)]:

$$\frac{Y}{X}=\frac{\left[1-(1-\lambda)\left(\frac{\omega}{\bar{\omega}_i}\right)^2\right]\left[1-\lambda^2\left(\frac{\omega}{\omega_2}\right)^2\right]-\lambda\left(\frac{\omega}{\bar{\omega}_i}\right)^2\left[1+(1-\lambda)\lambda\left(\frac{\omega}{\omega_2}\right)^2\right]}{\left[1+\mu_k-\left(\frac{\omega}{\omega_1}\right)^2-(1-\lambda)^2\mu_k\left(\frac{\omega}{\omega_2}\right)^2\right]\left[1-\lambda^2\left(\frac{\omega}{\omega_2}\right)^2\right]-\mu_k\left[1+(1-\lambda)\lambda\left(\frac{\omega}{\omega_2}\right)^2\right]^2} \tag{2.31}$$

where: $\lambda=\frac{A_c}{A_b}$, $\left(\frac{\omega_1}{\omega_2}\right)^2=\frac{1}{\sqrt{\mu_k}}\frac{m_B}{m_y}\left(\frac{A_b}{A_a}\right)^2$, $\left(\frac{\omega_1}{\bar{\omega}_i}\right)^2=\frac{m_B}{m_y}\left(\frac{A_b}{A_a}-1\right)\frac{A_b}{A_a}$

Equation (2.31) is equal to the transmissibility with full wall reservoir stiffness when $\lambda = 1$ (refer to Equation (2.5)). The equation for the damped transmissibility is shown in Appendix B.

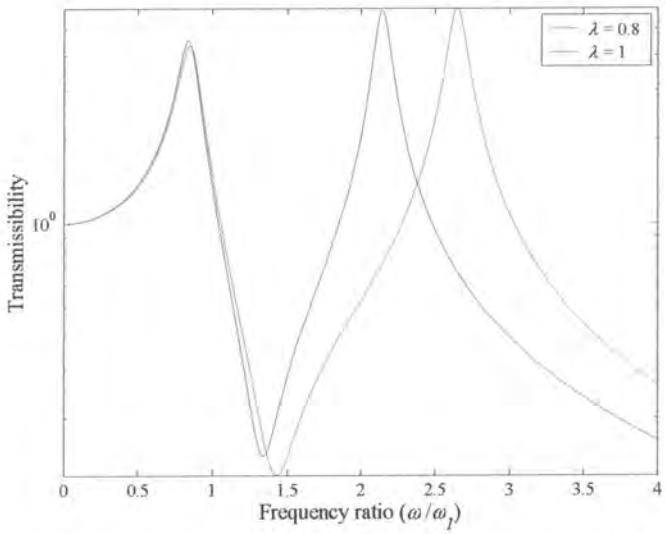

Figure 2.21: Transmissibility comparison ($\mu_k = 1$, $A_b/A_a = 10$, $m_B/m_y = 0.003$, $\zeta_1 = 0.1$ and $\zeta_2 = 0.01$ in Equation (B.38))

Figure 2.21 shows the effect of the reduced area ratio (λ) on the transmissibility. It appears as if the transmissibility is improved, but the comparison is biased since the isolation frequency is higher.

When plotting the minimum transmissibility against the isolation frequency as shown in Figure 2.22 the trend is clearer. Only at high stiffness ratios there is a slight improvement of the transmissibility at the same isolation frequency. At low stiffness ratios the disadvantage of having an area ratio of less than 1 is apparent. The effect on the isolation frequency is shown in Figure 2.23.

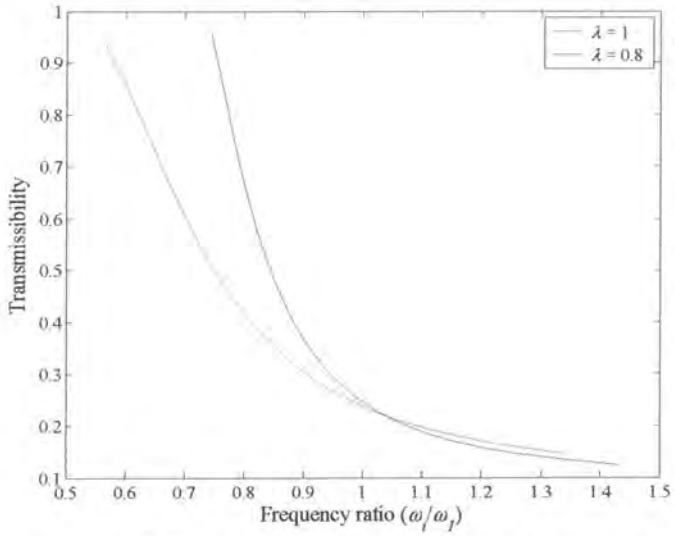

Figure 2.22: Minimum transmissibility *vs.* isolation frequency for stiffness ratios ranging from $\mu_k = 0.1$ to 1 ($A_b/A_a = 10$, $m_B/m_y = 0.003$, $\zeta_1 = 0.1$ and $\bar{\zeta}_2 = 0.01$)

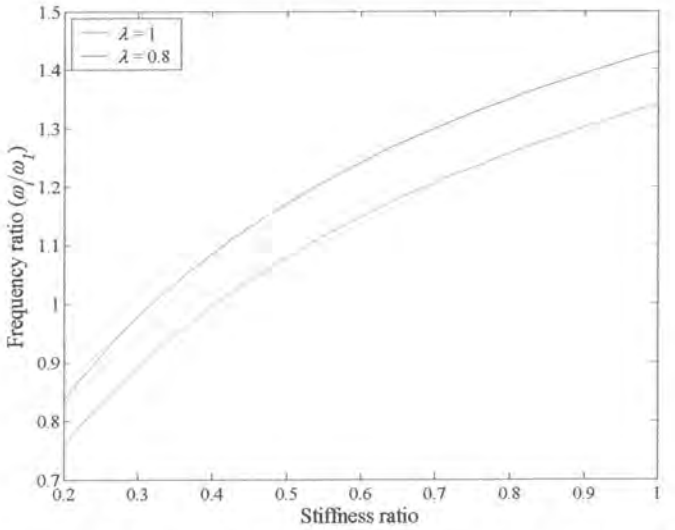

Figure 2.23: Isolation frequency *vs.* stiffness ratio for stiffness ratios ranging from $\mu_k = 0.1$ to 1 ($A_b/A_a = 10$, $m_B/m_y = 0.003$, $\zeta_1 = 0.1$ and $\bar{\zeta}_2 = 0.01$)

2.1.3 Single flexible wall

A special case occurs when only one flexible wall is used. Such a device is presently available from the Lord Corporation (Figure 2.24).

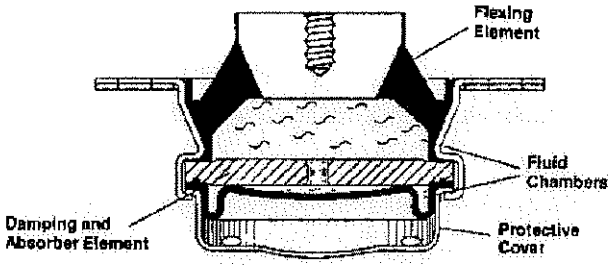

Figure 2.24: Sectional view of the fluidlastic® mount (Lord Corporation)

Several tuneable configurations have been patented. One used an adjustable length inertia track (Hodgson & Duclos, 1990) while another used variable compliance of an air filled chamber (Miller, 1987) as shown in Figure 2.25.

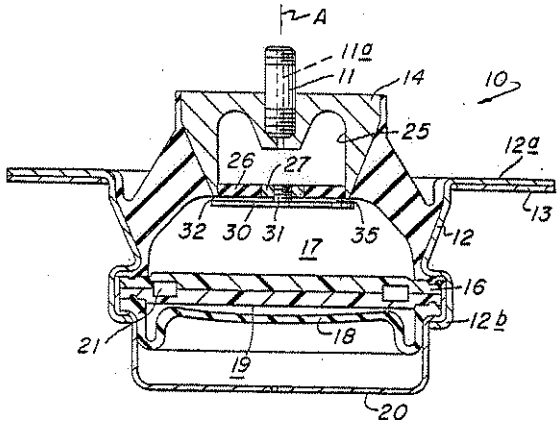

Figure 2.25: Variable compliance tuneable AVAI (Miller, 1987)

Strydom (2000) showed that this AVAI could also be made tuneable by charging the bottom chamber with air pressure. The model describing this device is shown in Figure 2.26.

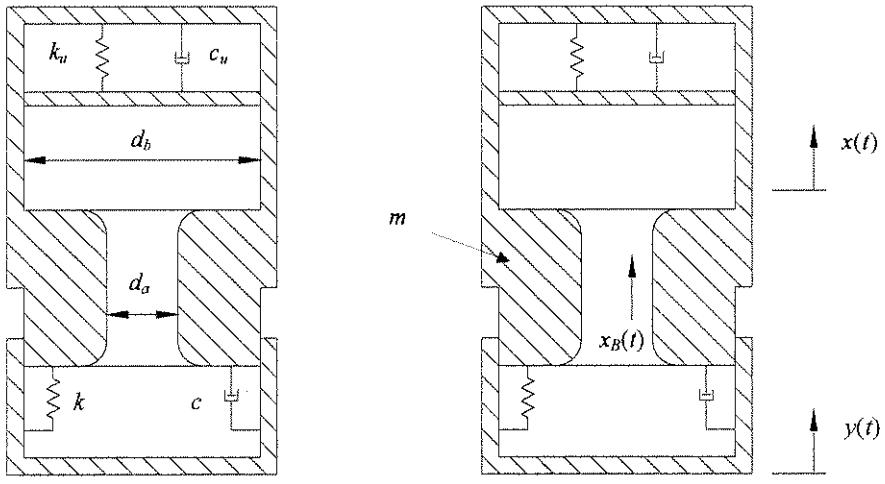

Figure 2.26: Mechanical model of one-sided stiffness

The continuity is not influenced by the membrane stiffness, as was the case before. It is simply:

$$x_B = \left(1 - \frac{A_b}{A_a}\right)x + \frac{A_b}{A_a}y \tag{2.32}$$

Incompressibility requires the membrane displacement to be equal to x. Incompressibility also requires that the effort required to change the distance between the x and y degrees of freedom will depend on the membrane stiffness.

The transmissibility is therefore the same as for the LIVE absorber [Equation (A.108)]:

$$\frac{X}{Y} = \frac{1 + i2\frac{\omega}{\omega_n}\zeta - \left(\frac{\omega}{\omega_i}\right)^2}{1 + i2\frac{\omega}{\omega_n}\zeta - \left(\frac{\omega}{\omega_n}\right)^2} \tag{2.33}$$

where: $\omega_i = \sqrt{\dfrac{k + k_u}{m_B\left(\frac{A_b}{A_a} - 1\right)\frac{A_b}{A_a}}}$, $\omega_n = \sqrt{\dfrac{k + k_u}{m + m_B\left(\frac{A_b}{A_a} - 1\right)^2}}$, $\zeta = \dfrac{c}{2\left[m + m_B\left(\frac{A_b}{A_a} - 1\right)^2\right]\omega_n}$

Although the construction of this device is different to the type II it is mathematically equivalent and its properties will be discussed in more detail in the following paragraphs. It does, however, have some practical properties that need some clarification. The main advantage is its simplicity of construction since it does not require a cylinder that can move axially inside another. One disadvantage is that it is difficult to transfer any moment that might be applied to the device with a soft spring that is only situated on one side of the device. The moment can, of course, be transferred through a bearing as long as it adds little damping. This will, however, result in loss of some of the advantage gained by its simple construction. If pressure is used to change the stiffness of the membrane, large static displacement will result which could be a problem in a practical device. The static displacement will be:

$$\delta_{st} = \frac{pA_b}{k} \tag{2.34}$$

2.2 Adaptive AVAI with slug (Type II)

The absorber mass and area ratio determine the overall size of the AVAI. A low area ratio minimizes the flow-induced losses through entrance, exit and friction effects. Achieving a large absorber mass is difficult using fluids due to the toxicity of heavy liquids. For these reasons it was decided to investigate a device that uses a heavy metal slug instead of a liquid. The use of a slug is not new, in fact the very first LIVE type isolators used slugs, which were later replaced by liquids (Halwes, 1981b). These designs were not adaptive. There are several problems with the use of slugs. Firstly the amplitude is limited, which puts a limit on the area ratio that can be used. In applications where the input is not known exactly provision must be made for over travel. A second problem with slug type devices is ensuring that the slug is centred vertically (Figure 2.27). Two methods will be described. The first uses slug springs to create a differential pressure on the top and bottom reservoirs, thereby

encouraging leakage to reach equilibrium. The second method uses rubber stops that will create a restoring force when the slug comes into contact with the stop.

2.2.1 Slug springs

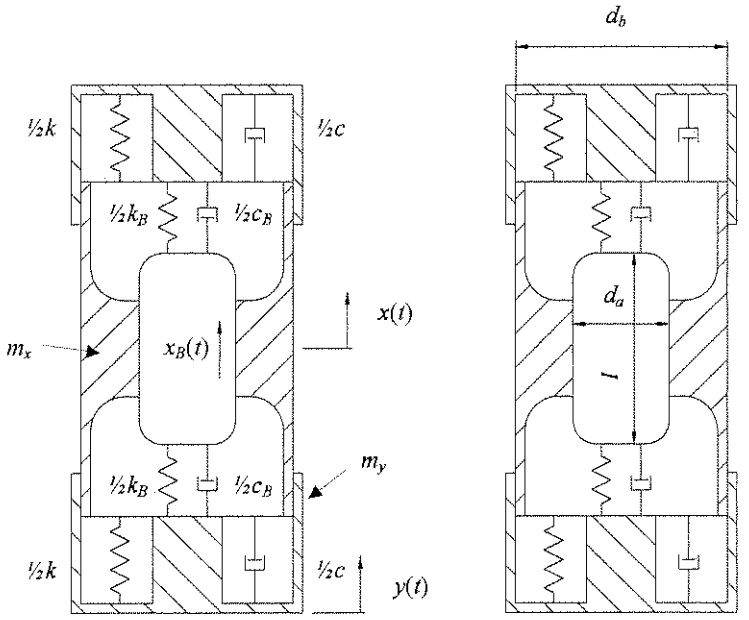

Figure 2.27: Mechanical model of an adaptive AVAI with a slug defined by length l and diameter d_a and slug spring properties defined by k_B and c_B

The continuity through the port (occupied by the slug) is [Equation (B.39)]:

$$x_B = \left(1 - \frac{A_b}{A_a}\right)x + \frac{A_b}{A_a}y \tag{2.35}$$

The equation of motion when assuming excitation at the y degree of freedom, is [Equation (B.46)]:

$$\ddot{x} + 2\zeta\omega_n x + \omega_n^2 x = \left(\frac{\omega_n}{\omega_i}\right)^2 \ddot{y} + 2\zeta\omega_n \dot{y} + \omega_n^2 y$$

$$\text{where: } \omega_i = \sqrt{\frac{k + k_B\left(\frac{A_b}{A_a} - 1\right)^2}{m_B\left(\frac{A_b}{A_a} - 1\right)\frac{A_b}{A_a}}}, \quad \omega_n = \sqrt{\frac{k + k_B\left(\frac{A_b}{A_a} - 1\right)^2}{m_x + m_B\left(\frac{A_b}{A_a} - 1\right)^2}}, \quad \zeta = \frac{c + c_B\left(\frac{A_b}{A_a} - 1\right)^2}{2\left[m_x + m_B\left(\frac{A_b}{A_a} - 1\right)^2\right]\omega_n} \tag{2.36}$$

Equation (2.36) shows the effect of the slug springs. Inclusion of such springs will increase the isolation (ω_i) and natural (ω_n) frequencies, which is undesirable since lowering the frequencies requires the addition of mass. The springs perform a necessary function of positioning the slug vertically and it should be possible to use low stiffness springs to achieve this goal. It will also be possible to use the slug spring for adapting the isolation frequency, especially since the isolation frequency will be very sensitive to this parameter. A practical device implementing such a concept

will, however, be a challenge because of space and low damping requirements. When using a slug spring additional care is necessary when a large area ratio is used to allow enough space for the spring in its compressed state.

If excitation occurs at the x degree of freedom the equation of motion is the same but the coordinates are swapped and the definition of the natural frequency and damping ratio is now given by [Equation (B.49)]:

$$\ddot{y}+2\zeta\omega_n\dot{y}+\omega_n^2 y=\left(\frac{\omega_n}{\omega_i}\right)^2\ddot{x}+2\zeta\omega_n\dot{x}+\omega_n^2 x$$

$$\text{where:}\quad \omega_n=\sqrt{\frac{k+k_B\left(\frac{A_b}{A_a}-1\right)^2}{m_y+m_B\left(\frac{A_b}{A_a}\right)^2}},\quad \zeta=\frac{c+c_B\left(\frac{A_b}{A_a}-1\right)^2}{2\left[m_y+m_B\left(\frac{A_b}{A_a}\right)^2\right]\omega_n} \tag{2.37}$$

The definition for the isolation frequency is the same as in Equation (2.36) for excitation at the y degree of freedom and the design will therefore remain unaffected. In the analysis that follows the ratio X/Y can therefore simply be inverted as long as the corresponding definition of the natural frequency and damping ratio is used. The transmissibility is (refer also to §1.4.1):

$$\frac{X}{Y}=\frac{1+i2\frac{\omega}{\omega_n}\zeta-\left(\frac{\omega}{\omega_i}\right)^2}{1+i2\frac{\omega}{\omega_n}\zeta-\left(\frac{\omega}{\omega_n}\right)^2} \tag{2.38}$$

The isolation frequency is clearly a function of damping as is shown in Figure 2.28.

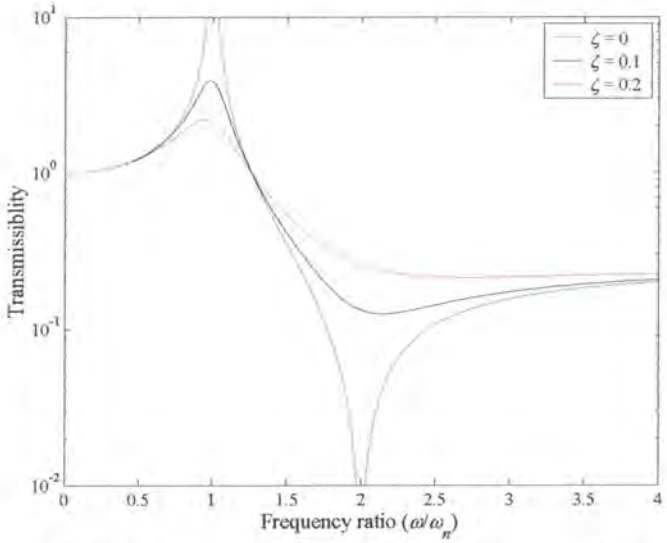

Figure 2.28: Effect of damping on the transmissibility ($\omega_n=1$ and $\omega_i=2$)

The frequency ratio is independent of stiffness and can be written for excitation at y as:

$$\left(\frac{\omega_n}{\omega_i}\right)^2 = \frac{m_B\left(\frac{A_b}{A_a}-1\right)\frac{A_b}{A_a}}{m_x + m_B\left(\frac{A_b}{A_a}-1\right)^2} = \frac{\frac{m_B}{m_x}\left(\frac{A_b}{A_a}-1\right)\frac{A_b}{A_a}}{1+\frac{m_B}{m_x}\left(\frac{A_b}{A_a}-1\right)^2} = \frac{\mu_m(\mu_A-1)\mu_A}{1+\mu_m(\mu_A-1)^2} \tag{2.39}$$

where: $\mu_m = \frac{m_B}{m_x}, \quad \mu_A = \frac{A_b}{A_a}$

and for excitation at x:

$$\left(\frac{\omega_n}{\omega_i}\right)^2 = \frac{m_B\left(\frac{A_b}{A_a}-1\right)\frac{A_b}{A_a}}{m_y + m_B\left(\frac{A_b}{A_a}\right)^2} = \frac{\frac{m_B}{m_y}\left(\frac{A_b}{A_a}-1\right)\frac{A_b}{A_a}}{1+\frac{m_B}{m_y}\left(\frac{A_b}{A_a}\right)^2} = \frac{\mu_m(\mu_A-1)\mu_A}{1+\mu_m\mu_A^2} \tag{2.40}$$

where: $\mu_m = \frac{m_B}{m_y}, \quad \mu_A = \frac{A_b}{A_a}$

Using the above relation the transmissibility can be rewritten in terms of the isolation frequency [Equation (B.50)]:

$$\frac{X}{Y} = \frac{1+i2\frac{\omega_i}{\omega_n}\frac{\omega}{\omega_i}\zeta - \left(\frac{\omega}{\omega_i}\right)^2}{1+i2\frac{\omega_i}{\omega_n}\frac{\omega}{\omega_i}\zeta - \left(\frac{\omega_i}{\omega_n}\right)^2\left(\frac{\omega}{\omega_i}\right)^2} \tag{2.41}$$

In §1.4.1 it was shown that a low frequency ratio (ω_n/ω_i) would minimise the transmissibility at the isolation frequency. This concept is reinforced by Figure 2.29. A design with a low frequency ratio can be realised when the mass ratio approaches zero or when the area ratio approaches 1. Implicit in this graph is the fact that the damping ratio is constant and not the viscous damping coefficient. This result is not unexpected and is similar to what was found for the type I AVAI. Of course, to ensure a low isolation frequency the exact opposite applies.

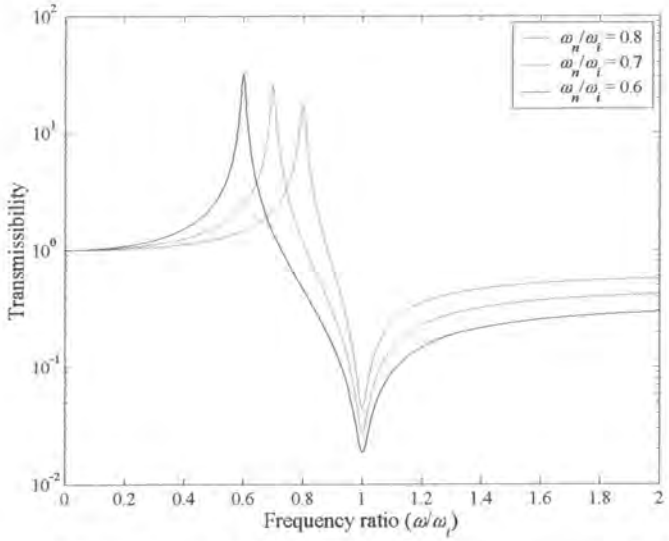

Figure 2.29: Transmissibility as a function frequency ratio ($\zeta = 0.01$)

The design for the type II device differs from the type I since it has an additional constraint on the slug travel. An equation will be set up that takes this constraint into account and can then be solved to yield the size of the device required. The absorber mass can be calculated as follows:

$$m_B = \rho A_a l = \frac{k + k_B\left(\frac{A_b}{A_a} - 1\right)^2}{\omega_i^2\left(\frac{A_b}{A_a} - 1\right)\frac{A_b}{A_a}} \tag{2.42}$$

where l is the length of the slug as shown in Figure 2.30. The excitation frequency is known and both the stiffness values must be as low as possible to decrease the absorber mass (m_B) and therefore the mass ratio. The area ratio is governed by the total length of the device. At isolation the amplitude of the isolated system (X) will be zero for an undamped device. The amplitude of the slug is:

$$X_B = \frac{A_b}{A_a} Y \tag{2.43}$$

If the slug amplitude is larger than the length of the slug protrusion (l_e) the slug will move into the port, which will create entrance losses and thereby increase damping. The compressed length of the slug spring can now be used to calculate the reservoir length:

$$l_r = l_c + 2l_e - Y \tag{2.44}$$

where l_c is the compressed length of the spring.

The port serves two purposes that will determine its length. When the AVAI is in a horizontal position the port length needs to be sufficient to ensure that the slug will not wedge when it is at its maximum displacement. Additionally, it offers some resistance to leak flow. A minimum port length must be specified to determine which designs are appropriate.

The total length of the AVAI can be found using Equations (2.43) and (2.44):

$$l_T = 2l_c + 2\left(\frac{A_b}{A_a} - 1\right)Y + l \tag{2.45}$$

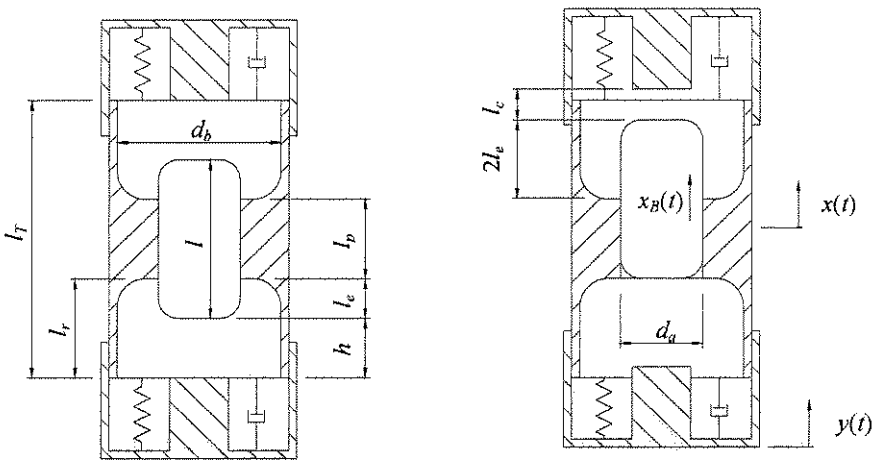

Figure 2.30: Definition of dimensions (length l_p and diameter d_a defines the port geometry)

One possible design approach would be to specify the overall device dimensions (l_T and d_b), excitation frequency (ω_e) and excitation amplitude (Y), spring stiffnesses (k and k_B), slug density (ρ), minimum port length and then to calculate the port diameter (d_a). Using Equation (2.44) and (2.42) the following design equation can be derived [Equation (B.62)]:

$$\begin{aligned}&\left(2l_c\omega_i^2 A_b\rho - 2Y\omega_i^2 A_b\rho - l_T\omega_i^2 A_b\rho - k - k_B\right)A_a^2 \\ &+\left(l_T\omega_i^2\rho A_b^2 - 2l_c\omega_i^2\rho A_b^2 + 4Y\omega_i^2 A_b^2\rho + 2k_B A_b\right)A_a - 2Y\omega_i^2\rho A_b^3 - k_B A_b^2 = 0\end{aligned} \tag{2.46}$$

It is evident that for a set of parameters four port diameters (d_a) will result from the solution of Equation (2.46), but some solutions might lack physical meaning since they result in complex or negative diameters or in port lengths shorter than the minimum required. The design approach will be explained using an example with a set of fixed parameters shown in Table 2.4. The set of parameters results in the two design spaces in terms of the overall size defined by length (l_T) and diameter (d_b) as shown in Figure 2.31 and Figure 2.32. In each figure design points are shown which are physically illustrated in Figure 2.33. The application will dictate which of the designs are the most appropriate in terms of geometry. The trade-off between two designs with identical outer dimensions lies in the total mass and area ratio. Large area ratios will result in high slug velocity (increasing damping) and low absorber mass. The absorber mass is shown in Figure 2.34 and Figure 2.35.

Table 2.4: Fixed design parameters

Parameter	Value
Frequency	10 Hz
Static deflection (δ_{st})	0.005 m
Isolated mass (m)	100 kg
Stiffness	mg/δ_{st}
Excitation amplitude	0.003 m
Slug spring (k_B)	$k/100$
Slug density	1000 kg/m^3
Spring compressed length (l_c)	0.01 m

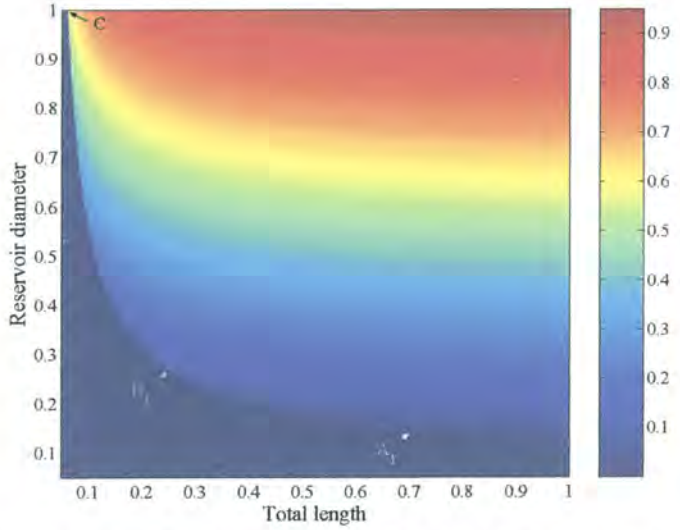

Figure 2.31: Port diameter for the first solution space ($l_p > 0$, $d_a = 0$ indicates complex or negative solution)

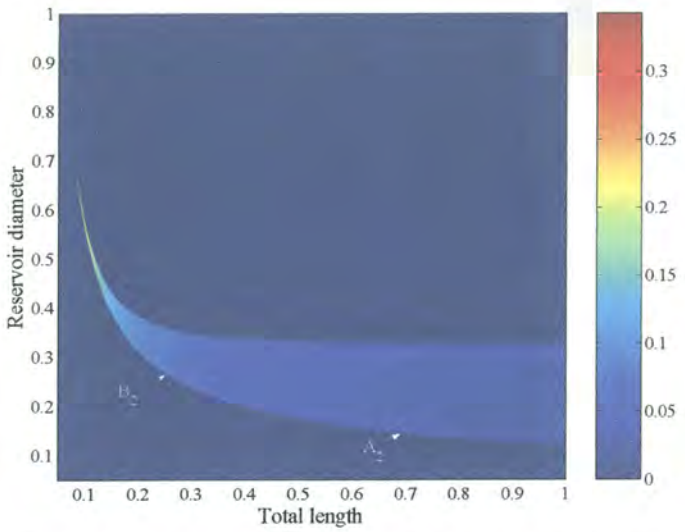

Figure 2.32: Port diameter for the second solution space ($l_p > 0$, $d_a = 0$ indicates complex or negative solution)

Table 2.5: Design parameters

	A_1	A_2	B_1	B_2	C
Total length (l_T)	0.700	0.700	0.260	0.260	0.100
Reservoir diameter (d_b)	0.150	0.150	0.260	0.260	1.000
Port diameter (d_a)	0.057	0.039	0.089	0.086	0.735
Slug length (l)	0.645	0.596	0.195	0.191	0.075
Slug protrusion (l_e)	0.021	0.045	0.026	0.027	0.006
Port length (l_p)	0.604	0.505	0.144	0.137	0.064
Area ratio (A_b/A_a)	6.9	15.1	8.5	9.1	1.9
Slug mass (m_B)	1.65	0.71	1.21	1.11	31.82

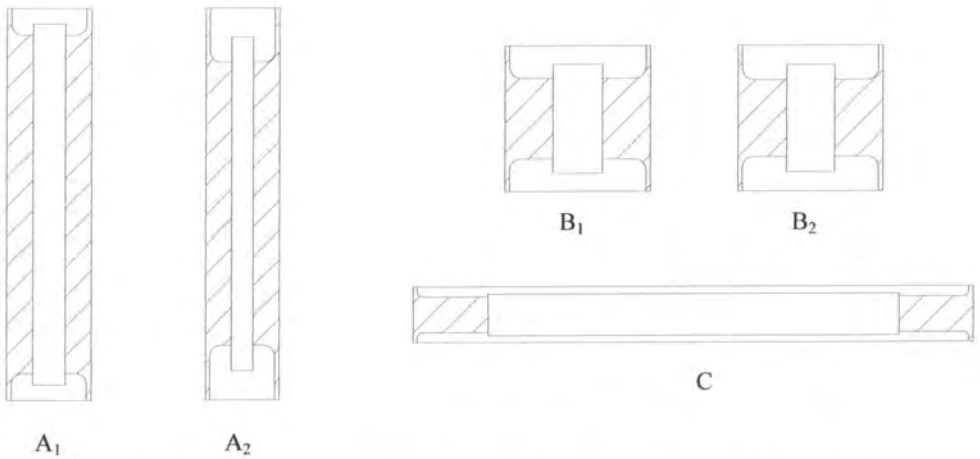

Figure 2.33: Five possible designs that fit the requirements of Table 2.4

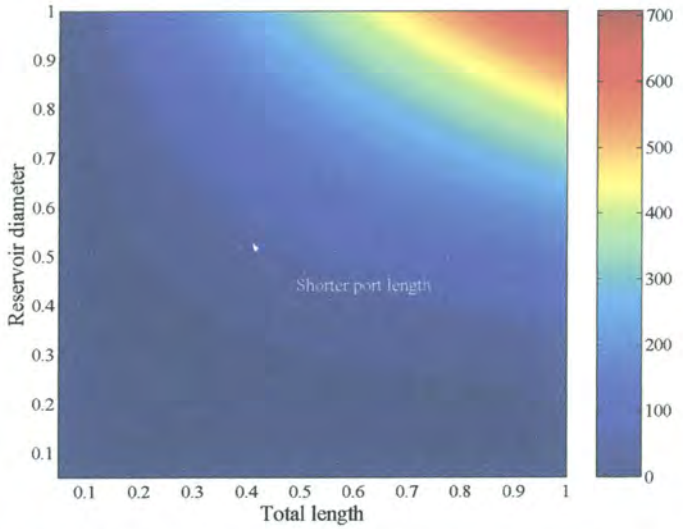

Figure 2.34: Absorber mass for the first solution space showing the direction in which the port length shortens ($l_p > 0$, $d_a = 0$ indicates complex or negative solution)

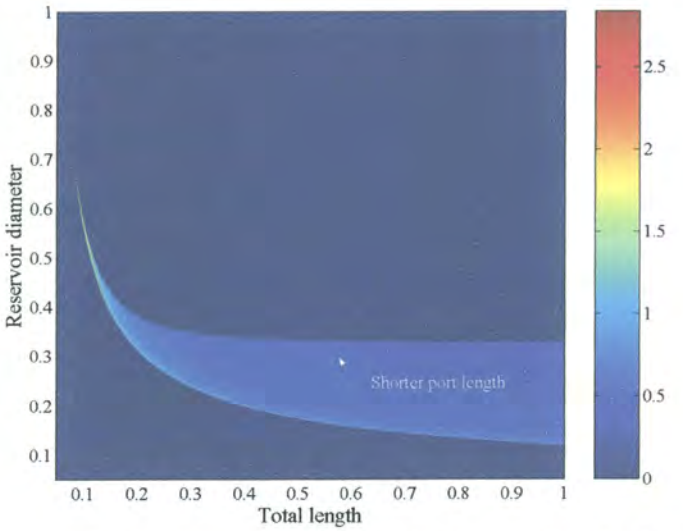

Figure 2.35: Absorber mass for the second solution space showing the direction in which the port length shortens ($l_p > 0$, $d_a = 0$ indicates complex or negative solution)

If a large amount of damping is present the damped isolation frequency must be set equal to the excitation frequency (Ω_i in Equation (2.47)). It is possible to use this equation to calculate the undamped isolation frequency, which can then be used in the same design procedure as shown before with the slug amplitude adapted to account for the fact that the motion of the mass is nonzero for a damped system.

$$\left(\frac{\Omega_i}{\omega_n}\right)^2 = \frac{-\left(\frac{\omega_n}{\omega_i}\right)^2 - 1 - \sqrt{\left[\left(\frac{\omega_n}{\omega_i}\right)^2 - 1\right]^2 + 8\zeta^2\left[\left(\frac{\omega_n}{\omega_i}\right)^2 + 1\right]}}{4\zeta^2 + 4\zeta^2\left(\frac{\omega_n}{\omega_i}\right)^2 - 2\left(\frac{\omega_n}{\omega_i}\right)^2} \tag{2.47}$$

To investigate the effects of changing the stiffness the transmissibility can conveniently be written in terms of the initial values (indicated by a prime) [Equation (B.55)]:

$$\frac{X}{Y}=\frac{1+i\frac{2}{\mu_k}\frac{\omega}{\omega_n'}\zeta'-\frac{1}{\mu_k}\left(\frac{\omega_n'}{\omega_i'}\right)^2\left(\frac{\omega}{\omega_n'}\right)^2}{1+i\frac{2}{\mu_k}\frac{\omega}{\omega_n'}\zeta'-\frac{1}{\mu_k}\left(\frac{\omega}{\omega_n'}\right)^2}$$

$$\text{where:}\quad \mu_k=\frac{k+k_B\left(\frac{A_b}{A_a}-1\right)^2}{k'+k_B'\left(\frac{A_b}{A_a}-1\right)^2},\quad \zeta'=\frac{c}{2\left[m_x+m_B\left(\frac{A_b}{A_a}-1\right)^2\right]\omega_n'},\tag{2.48}$$

$$\omega_i'=\sqrt{\frac{k'+k_B'\left(\frac{A_b}{A_a}-1\right)^2}{m_B\left(\frac{A_b}{A_a}-1\right)\frac{A_b}{A_a}}},\quad \omega_n'=\sqrt{\frac{k'+k_B'\left(\frac{A_b}{A_a}-1\right)^2}{m_x+m_B\left(\frac{A_b}{A_a}-1\right)^2}}$$

where k' is the initial value and k the current value. In the above equation it is assumed that the damping coefficient is constant. Figure 2.36 shows the effect of changing the stiffness ratio for an undamped device. From the figure it is clear that the natural frequency is a function of the stiffness change and consequently also the static deflection. This effect must be kept in mind, as it could be problematic in a practical device.

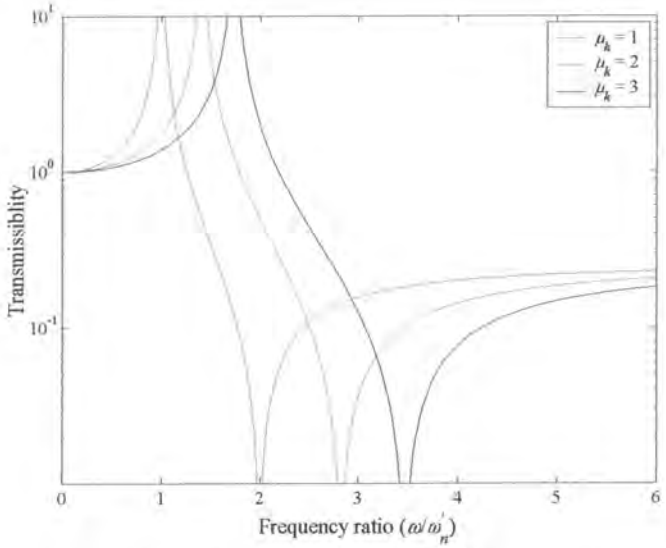

Figure 2.36: Transmissibility *vs.* frequency ratio for 3 stiffness ratios ($\omega_n'/\omega_i' = ½$ and $\zeta' = 0$)

Since it is difficult to design stable low stiffness springs it will be appropriate to use the passive design method to design the device for the lowest required frequency and then to calculate if the maximum frequency covers the required range. The isolation frequency ratio can be written in terms of the stiffness ratio (excitation at x) [Equation (B.63)]:

$$\left(\frac{\omega_i}{\omega_n'}\right)^2=\mu_k\left(\frac{\omega_i'}{\omega_n'}\right)^2=\mu_k\left(\frac{\omega_i}{\omega_n}\right)^2=\mu_k\frac{1+\mu_m\left(\mu_A-1\right)^2}{\mu_m\left(\mu_A-1\right)\mu_A}\tag{2.49}$$

The difference between the above equation and Equation (2.13) for the type I AVAI is that the mass and area ratios do not influence the tuning range. For the undamped case the only way to increase the tuning range is to increase the stiffness ratio.

The effect of changing the stiffness ratio for a damped design is shown in Figure 2.37. The provision is that the damping coefficient is independent of the stiffness ratio and frequency, which will not be the case in practice since the slug velocity will increase and the spring's loss factor can be frequency dependent.

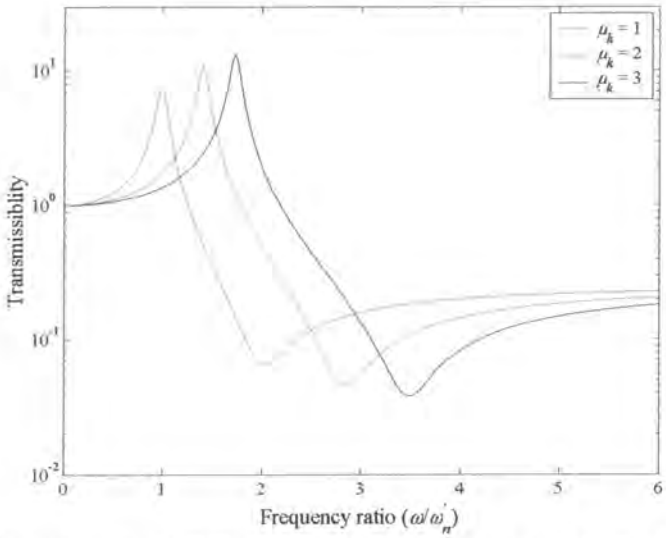

Figure 2.37: Damped transmissibility as a function of stiffness ratio ($\omega_n/\omega_i = ½$ and $\zeta' = 0.01$)

2.2.2 Slug stops

The use of flexible slug stops is one method of ensuring that the slug stays centred. When the slug hits the stop the pressure in the opposite chamber will increase, thereby forcing some fluid through he gap between the slug and the port. This action will tend to equalize the volume of fluid in the reservoirs, thereby centring the slug. Such a system will require a balancing act between a sufficient gap size to ensure adequate flow and one that will decrease the effectiveness of the device. Another method will be to construct channels with one-way valves that will open when the pressure rises to a certain level above that of normal operation. This will be at the cost of added complexity.

The addition of stops does not change the continuity equation. Both the spring and damper will only be active after the relative motion between the slug and reservoir is larger than the gap (h). The following Heaviside function describes this property:

$$\beta = \begin{cases} 0 \text{ if } \left| y - x + \frac{A_b}{A_a}(x-y) \right| < h \\ 1 \text{ if } \left| y - x + \frac{A_b}{A_a}(x-y) \right| \geq h \end{cases} \tag{2.50}$$

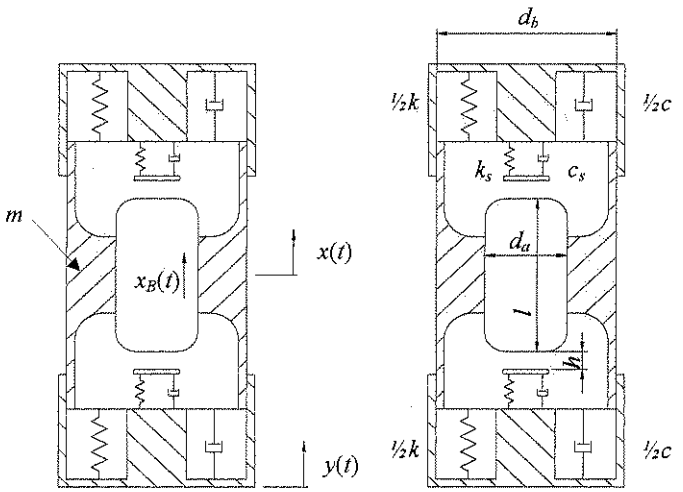

Figure 2.38: Mechanical model of a type II AVAI with slug stops

The spring force is [Equation (B.65)]:

$$f_s = \beta k_s \left\{ y - x + \frac{A_b}{A_a}(x - y) - \text{sign}\left[y - x + \frac{A_b}{A_a}(x - y) \right] h \right\} \tag{2.51}$$

The damping force is [Equation (B.66)]:

$$f_d = \beta c_s \left[\dot{y} - \dot{x} + \frac{A_b}{A_a}(\dot{x} - \dot{y}) \right] \tag{2.52}$$

The reservoir pressure that drives equalization of the fluid is [Equation (B.67)]:

$$p = \frac{1}{2A_a}(f_s + f_d - m_B \ddot{x}_B) \tag{2.53}$$

Equation (2.53) shows that the addition of stops will increase the pressure in the reservoir. Such a system is however non-linear, which makes its practical implementation problematic. The complete equation of motion is [Equation (B.69)]:

$$\ddot{x} = \left(\frac{\omega_n}{\omega_i}\right)^2 \ddot{y} - 2\zeta\omega_n(\dot{x} - \dot{y}) - \omega_n^2(x - y) - \omega_n^2 \frac{k_s}{k}\Delta_d \left(\frac{A_b}{A_a} - 1\right) - 2\zeta_s \omega_n \Delta_v \left(\frac{A_b}{A_a} - 1\right)$$

where: $\zeta = \dfrac{c}{2\left[m + m_B\left(\frac{A_b}{A_a} - 1\right)^2\right]\omega_n}$, $\zeta_s = \dfrac{c_s}{2\left[m + m_B\left(\frac{A_b}{A_a} - 1\right)^2\right]\omega_n}$

$$\omega_n = \sqrt{\frac{k}{m + m_B\left(\frac{A_b}{A_a} - 1\right)^2}}, \quad \omega_i = \sqrt{\frac{k}{m_B\left(\frac{A_b}{A_a} - 1\right)\frac{A_b}{A_a}}} \tag{2.54}$$

$$\Delta_d = \beta\left\{ y - x + \frac{A_b}{A_a}(x - y) - \text{sign}\left[y - x + \frac{A_b}{A_a}(x - y) \right] h \right\}$$

$$\Delta_v = \beta\left[\dot{y} - \dot{x} + \frac{A_b}{A_a}(\dot{x} - \dot{y}) \right]$$

Figure 2.39 shows the force and the relative motion. For this simulation the gap ratio was $h/Y = 10$ and the excitation amplitude (Y) equal to 1. As can be seen the force is zero when the relative motion is less than the gap length.

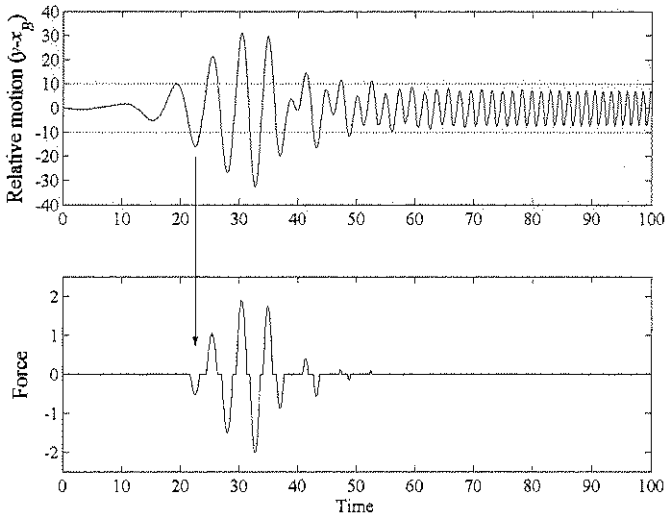

Figure 2.39: Stop force and relative motion of the slug and reservoir ($k_s/k = 0.01$, $h/Y = 10$, $Y = 1$, $\omega_n/\omega_i = 0.5$ and $\zeta = \zeta_s = 0$)

2.2.3 Leakage

The previous models assumed that a perfect seal exists between the slug and the port. The effect of leakage through this space will be considered next. It is assumed that the clearance is small in relation to the diameter of the slug.

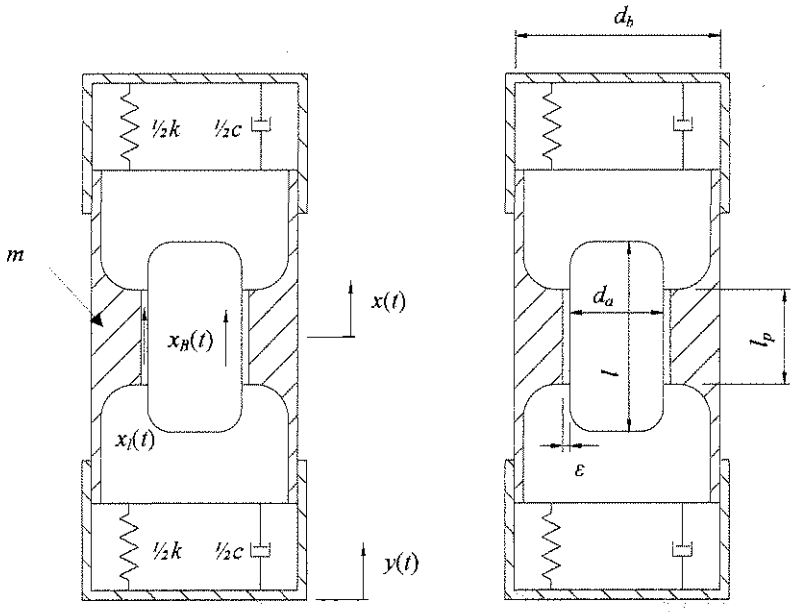

Figure 2.40: Mechanical model of a type II AVAI with leakage

If it is assumed that the gap between the port and the slug is small the leakage area is:

$$A_e = \varepsilon \pi d_a \tag{2.55}$$

where ε is the gap between the slug and the port.

The continuity equation is modified by the leak flow [Equation (B.71)]:

$$x_B = \frac{A_b}{A_a} y + \left(1 + \frac{\varepsilon \pi d_a - A_b}{A_a}\right) x - \frac{\varepsilon \pi d_a}{A_a} x_l \tag{2.56}$$

The kinetic energy now includes the mass of the leak flow [Equation (B.72)]:

$$T = \frac{1}{2}\left(m\dot{x}^2 + m_B \dot{x}_B^2 + m_l \dot{x}_l^2\right)$$
$$\text{where:} \quad m_B = \rho A_a l, \quad m_l = \rho_f \varepsilon \pi d_a l_p \tag{2.57}$$

m is the mass of the port, m_B the mass of the slug. m_l the mass of the fluid in the gap and is a function of the fluid density (ρ_f), area ($\varepsilon \pi d_a$) and the length of the port (l_p). $\dot{x}_l$ is the velocity of the liquid in the gap.

The mass of the leak flow is coupled to the slug and the port through damping created by the velocity dependent shear forces acting on these bodies. This is shown in Figure 2.41.

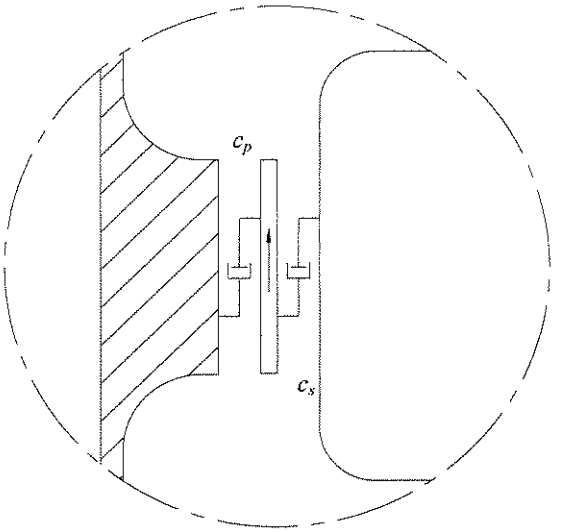

Figure 2.41: Fluid damping

The Rayleigh term is [Equation (B.76)]:

$$R = \frac{1}{2}\left[c\left(\dot{x} - \dot{y}\right)^2 + c_p\left(\dot{x}_l - \dot{x}\right)^2 + c_s\left(\dot{x}_B - \dot{x}_l\right)^2\right] \tag{2.58}$$

c_p is the damping resulting from the shear force between the fluid and the port and c_s the damping resulting from the shear force between the fluid and the slug.

The complete equation of motion is shown in Appendix B and leads to the definition of the following natural frequencies and damping ratios that will be used to non-dimensionalise the transmissibility:

$$\omega_l = \sqrt{\frac{k}{m_l + m_B\left(4\frac{\varepsilon}{d_a}\right)^2}},\quad \omega_i = \sqrt{\frac{k}{m_B\frac{A_b}{A_a}\left(\frac{A_b}{A_a} - 4\frac{\varepsilon}{d_a} - 1\right)}},\quad \omega_\varepsilon = \sqrt{\frac{k}{m_B\left(\frac{A_b}{A_a} - 4\frac{\varepsilon}{d_a} - 1\right)4\frac{\varepsilon}{d_a}}},$$

$$\omega_\varepsilon' = \sqrt{\frac{k}{m_B\frac{A_b}{A_a}4\frac{\varepsilon}{d_a}}},\quad \omega_n = \sqrt{\frac{k}{m + m_B\left(\frac{A_b}{A_a} - 4\frac{\varepsilon}{d_a} - 1\right)^2}},\quad \zeta_s = \frac{c_s}{2\left[m + m_B\left(\frac{A_b}{A_a} - 4\frac{\varepsilon}{d_a} - 1\right)^2\right]\omega_n},\qquad (2.59)$$

$$\zeta_p = \frac{c_p}{2\left[m + m_B\left(\frac{A_b}{A_a} - 4\frac{\varepsilon}{d_a} - 1\right)^2\right]\omega_n}$$

The transmissibility is given by [Equation (B.83)]:

$$\frac{X}{Y} = \frac{AB - CD}{EF - G^2},\qquad \text{where:}$$

$$\frac{A}{k} = i2\frac{\omega}{\omega_n}\left[\zeta_s\left(4\frac{\varepsilon}{d_a} + 1\right)^2 + \zeta_p\right] - \left(\frac{\omega_n}{\omega_l}\right)^2\left(\frac{\omega}{\omega_n}\right)^2$$

$$\frac{B}{k} = 1 + i2\frac{\omega}{\omega_n}\left[\zeta + \zeta_s\frac{A_b}{A_a}\left(\frac{A_b}{A_a} - 4\frac{\varepsilon}{d_a} - 1\right)\right] - \left(\frac{\omega_n}{\omega_i'}\right)^2\left(\frac{\omega}{\omega_n}\right)^2$$

$$\frac{C}{k} = i2\frac{\omega}{\omega_n}\left[\zeta_s\left(\frac{A_b}{A_a} - 4\frac{\varepsilon}{d_a} - 1\right)\left(4\frac{\varepsilon}{d_a} + 1\right) - \zeta_p\right] - \left(\frac{\omega_n}{\omega_\varepsilon}\right)^2\left(\frac{\omega}{\omega_n}\right)^2$$

$$\frac{D}{k} = i2\frac{\omega}{\omega_n}\zeta_s\frac{A_b}{A_a}\left(4\frac{\varepsilon}{d_a} + 1\right) - \left(\frac{\omega_n}{\omega_\varepsilon'}\right)^2\left(\frac{\omega}{\omega_n}\right)^2$$

$$\frac{E}{k} = 1 + i2\frac{\omega}{\omega_n}\left[\zeta + \zeta_p + \zeta_s\left(\frac{A_b}{A_a} - 4\frac{\varepsilon}{d_a} - 1\right)^2\right] - \left(\frac{\omega}{\omega_n}\right)^2$$

$$\frac{F}{k} = i2\frac{\omega}{\omega_n}\left[\zeta_s\left(4\frac{\varepsilon}{d_a} + 1\right)^2 + \zeta_p\right] - \left(\frac{\omega_n}{\omega_l}\right)^2\left(\frac{\omega}{\omega_n}\right)^2$$

$$\frac{G}{k} = i2\frac{\omega}{\omega_n}\left[\zeta_s\left(\frac{A_b}{A_a} - 4\frac{\varepsilon}{d_a} - 1\right)\left(4\frac{\varepsilon}{d_a} + 1\right) - \zeta_p\right] - \left(\frac{\omega_n}{\omega_\varepsilon}\right)^2\left(\frac{\omega}{\omega_n}\right)^2$$

$$\frac{\omega_n}{\omega_l} = \frac{\frac{m_l}{m_B} + \left(4\frac{\varepsilon}{d_a}\right)^2}{\frac{m}{m_B} + \left(\frac{A_b}{A_a} - 4\frac{\varepsilon}{d_a} - 1\right)^2},\quad \frac{\omega_n}{\omega_i'} = \frac{\frac{A_b}{A_a}\left(\frac{A_b}{A_a} - 4\frac{\varepsilon}{d_a} - 1\right)}{\frac{m}{m_B} + \left(\frac{A_b}{A_a} - 4\frac{\varepsilon}{d_a} - 1\right)^2},\qquad (2.60)$$

$$\frac{\omega_n}{\omega_\varepsilon} = \frac{4\frac{\varepsilon}{d_a}\left(\frac{A_b}{A_a} - 4\frac{\varepsilon}{d_a} - 1\right)}{\frac{m}{m_B} + \left(\frac{A_b}{A_a} - 4\frac{\varepsilon}{d_a} - 1\right)^2},\quad \frac{\omega_n}{\omega_\varepsilon'} = \frac{4\frac{\varepsilon}{d_a}\frac{A_b}{A_a}}{\frac{m}{m_B} + \left(\frac{A_b}{A_a} - 4\frac{\varepsilon}{d_a} - 1\right)^2}$$

When studying the effect of the gap on the transmissibility it is important to keep in mind that the mass ratio (m_l/m_B) is also a function of the gap size:

$$\frac{m_l}{m_B} = 4\beta\frac{\varepsilon}{d_a} \qquad \text{where:} \quad \beta = \frac{\rho_f l_p}{\rho l} \tag{2.61}$$

The main objective in using a slug was to exploit the large density of a heavy metal. It can therefore safely be assumed that the density of the fluid will be less than that of the slug. Since the slug is longer than the port, β will always be much less than 1. As the gap increases more of the effort will go towards accelerating the fluid, which has less mass, thereby increasing the isolation frequency. This can clearly be seen in Figure 2.42.

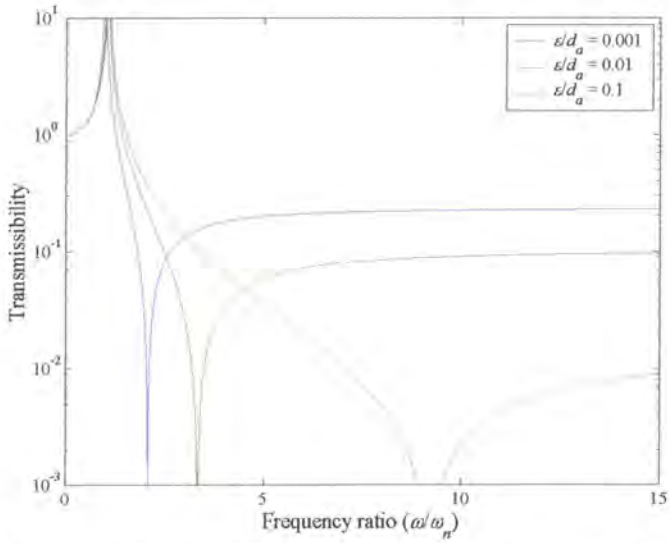

Figure 2.42: Transmissibility for various gap ratios ($\zeta = \zeta_s = \zeta_p = 0$, $m/m_B = 100$, $\beta = 0.01$ and $A_p/A_a = 10$)

Once damping is introduced the situation is very different, as shown in Figure 2.43. The leak flow mass is now coupled to the motion of the slug, equalising the acceleration of the two bodies.

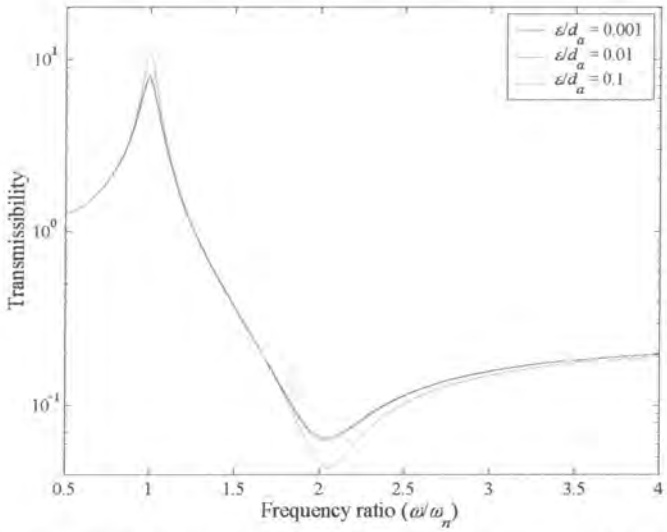

Figure 2.43: Transmissibility for various gap ratios ($\zeta = 0$, $\zeta_s = \zeta_p = 0.001$, $m/m_B = 100$, $\beta = 0.01$ and $A_b/A_a = 10$)

2.2.4 Slug with diaphragm seal

Rolling diaphragm seals are fabric-reinforced rubber seals that allow large axial movement with little damping and stiffness. Such a seal will not allow any leakage therefore ensuring that the slug stays centred with respect to the port. One disadvantage is that the device will become solid during over travel.

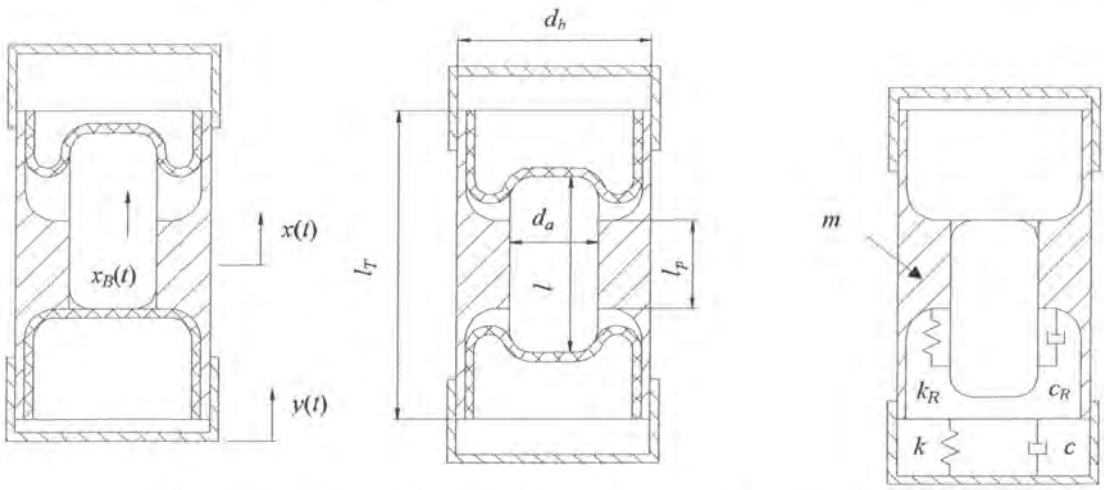

Figure 2.44: Mechanical model of a type II AVAI with a rolling diaphragm seal

By noting that a reinforced diaphragm cannot stretch, the continuity equation can be written as [Equation (B.85)]:

$$\begin{aligned} yA_b &= x_B A_a + \frac{1}{2}(x_B + x)(A_b - A_a) \\ x_B &= -\left(\frac{A_b - A_a}{A_b + A_a}\right)x + \frac{2A_b}{A_b + A_a}y \end{aligned} \tag{2.62}$$

The effect on the transmissibility is that the effective absorber mass is reduced (the diaphragm mass is neglected). In terms of a device without a diaphragm the effective absorber mass ratio is [Equation (B.96)]:

$$M_{ratio} = \frac{4}{\left(\frac{A_b}{A_a} + 1\right)^2} \tag{2.63}$$

The effective mass is therefore reduced for any area ratio larger than 1. Using a diaphragm will therefore increase the overall size of the device. Other practical problems exist such as commercial availability of suitable large-displacement small-diameter diaphragms.

An alternative to a rolling diaphragm is to insert a diaphragm that can stretch, for instance one made of thin latex rubber. In such a case the effective absorber mass will not be affected. There will, however, be relative motion between the latex and the slug, which will lead to damping. In addition, the number of cycles that such a latex diaphragm can be subjected to should be investigated.

2.3 Conclusion

This chapter showed the properties of two novel adaptive AVAI concepts. The type I AVAI used flexible reservoir walls to adapt the isolation frequency of the device. Conceptual design methodologies were illustrated for both damped and undamped fixed and adaptive isolation frequency devices. To determine the effects of tuning, the equations were transformed in terms of constant frequency ratios and the stiffness ratio, which was the only tuning parameter considered. For a fixed frequency device the system of equations is underdetermined and some parameters have to be prescribed or additional constraints should be introduced in the design. For adaptive devices it was shown that specific choice of the area and mass ratios can influence the tuning range. For damped adaptive AVAIs the transmissibility at the isolation frequency was minimised when the area ratio was minimised and the mass ratio maximised.

The type II AVAI used a metal slug to increase the absorber mass without the use of toxic heavy liquids. For this AVAI the main spring stiffness was made adaptive. The design methodology is different from the type I because the travel of the slug is restricted and must enter the design process to ensure that realistic area ratios are chosen. Three additional models were analysed. The first investigated the effect of rubber stops instead of slug springs. The second took account of leakage between the port and the slug. The effect of leakage was to increase the isolation frequency. The third showed the effect of using rolling diaphragm seals to eliminate leakage. The rolling diaphragm seal will result in a larger device since the effective mass is reduced.

3 Adaptive control methods

Several methods for the control of adaptive vibration absorbers have been studied. Most researchers suggested the use of open-loop rough tuning followed by a fine-tuning algorithm (Long *et al.*, 1994 and Franchek, 1995). Other methods that have been suggested include neural network and fuzzy logic control (Sun *et al.*, 1995). In this chapter several variations of the first method's application to the type I and type II AVAI will be discussed. An optimisation approach will be used, in contrast to the above work which used constant step size algorithms. The choice of variation on this method will depend on the characteristics of the input and the AVAI as will be shown. The scenarios investigated are:

1. The machine operates at a constant but unknown excitation frequency for an indefinite period after it is switched on. In such a case the AVAI will be tuned to this frequency at start-up only. An example is a pneumatic drill where the excitation frequency is a function of the supply air pressure and the drill is used at different locations with varying supply pressure.
2. The machine operates with a constant but unknown frequency for a period after which a near instantaneous change in frequency occurs to a new and unknown frequency. An example is if the operational frequency is a function of load in a batch process.
3. The properties of the AVAI changes with time, for instance, as the rubber spring heats up due to hysteresis. As the properties change, the isolation frequency is adapted to compensate. Similar conclusions are reached when the excitation frequency varies slowly with time.
4. A general case that does not require the above assumptions.

The control method that will be investigated is a physical implementation of optimisation where the objective function is the transmissibility (which is calculated from simulated or measured accelerometer data) and the variables are physical properties of the AVAI that can be adapted to minimise the objective function. The available variables can be classified as tuning and damping variables. Tuning variables are those that change the isolation frequency. For tonal excitation the isolator should have the lowest possible damping and therefore tuning only will be considered. In cases where wide-band excitation is present together with prominent tonal excitation, the addition of damping can be considered. In such cases it might even be beneficial to use the damping as a variable in the optimisation process. In this chapter it will be assumed that the excitation is tonal and that the amplitude is not necessarily constant.

3.1 Type I AVAI

If the excitation frequency is tonal and the stiffness is the only variable, the objective function can be written as the transmissibility given by Equation (2.19) with the stiffness ratio the only variable:

$$f(\mu_k)=\left|\frac{\left(1+i2\frac{\omega_e}{\omega_1}\zeta_1\right)\left[1+i\frac{2}{\mu_k}\frac{\omega_1}{\bar{\omega}_2}\frac{\omega_e}{\omega_1}\bar{\zeta}_2-\frac{1}{\mu_k}\left(\frac{\omega_1}{\bar{\omega}_2}\right)^2\left(\frac{\omega_e}{\omega_1}\right)^2\right]-\left(1+i\frac{2}{\mu_k}\frac{\omega_1}{\bar{\omega}_2}\frac{\omega_e}{\omega_1}\bar{\zeta}_2\right)\left(\frac{\omega_1}{\bar{\omega}_i}\right)^2\left(\frac{\omega_e}{\omega_1}\right)^2}{\left[1+\mu_k+i2\frac{\omega_e}{\omega_1}\left(\zeta_1+\frac{\omega_1}{\bar{\omega}_2}\bar{\zeta}_2\right)-\left(\frac{\omega_e}{\omega_1}\right)^2\right]\left[1+i\frac{2}{\mu_k}\frac{\omega_1}{\bar{\omega}_2}\frac{\omega_e}{\omega_1}\bar{\zeta}_2-\frac{1}{\mu_k}\left(\frac{\omega_1}{\bar{\omega}_2}\right)^2\left(\frac{\omega_e}{\omega_1}\right)^2\right]-\mu_k\left(1+i\frac{2}{\mu_k}\frac{\omega_1}{\bar{\omega}_2}\frac{\omega_e}{\omega_1}\bar{\zeta}_2\right)^2}\right| \tag{3.1}$$

where ω_e is the excitation frequency. A plot of the objective function as a function of stiffness ratio is shown in Figure 3.1. From the figure it can be seen that a low initial value will not allow convergence to the global minimum. This condition is caused by the second frequency of maximum transmissibility being lower than the excitation frequency as shown in Figure 3.2 where the transmissibilities for three different initial values are shown. Clearly, an initial condition of 0.2 will not allow for convergence to the minimum value if a local minimisation algorithm is used.

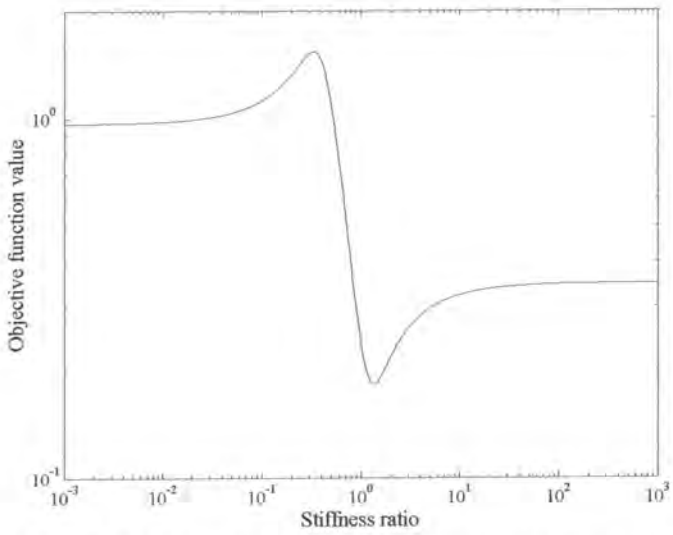

Figure 3.1: Objective function *vs.* stiffness ratio $\omega_e/\omega_1 = 1.4$ ($A_b/A_a = 10$, $m_B/m_y = 0.003$, $\zeta_1 = 0.1$ and $\overline{\zeta}_2 = 0.1$)

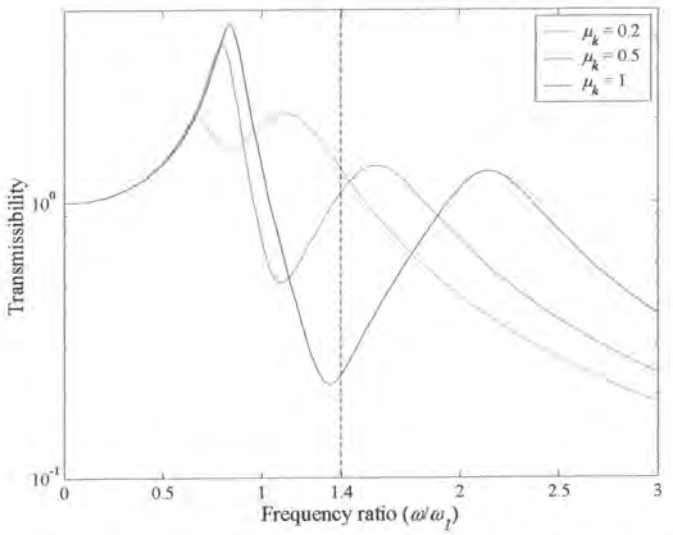

Figure 3.2: Transmissibility *vs.* frequency ratio for three initial values ($A_b/A_a = 10$, $m_B/m_y = 0.003$, $\zeta_1 = 0.1$ and $\overline{\zeta}_2 = 0.1$)

There are a number of solutions to this problem. A global optimisation strategy can be used, but this might be unacceptable in situations where the isolator cannot be allowed to operate close to regions of high transmissibility. Examples of global optimisation strategies are multiple start local optimisations or a genetic algorithm.

If the initial value can be guaranteed to be between the peaks of maximum transmissibility, the search direction of a gradient-based method will always be in the direction of the minimum. The following line search can therefore only find the optimal solution. It is possible that an unconstrained line search method may step too far, in which case the step size must be limited. To ensure that the initial value is between the frequencies of maximum transmissibility, the AVAI can simply be tuned to the maximum stiffness when initialised. The only risk with such a strategy is that it will put the excitation frequency near the first frequency of maximum transmissibility. If properly designed, the transmissibility should still be less than 1 even if tuned to the maximum isolation frequency. This can be seen from Figure 3.1 where for large stiffness ratios (and large isolation frequencies) the transmissibility is less than 1. It is also possible to initialise the optimisation algorithm by using the isolation frequency and stiffness ratio relationship found during a characterisation test. If changes in the physical properties of the device occur over time this relationship will not be exact anymore, but it should put the initial value close to the optimum as well as between the peaks of maximum transmissibility. It also requires that the excitation frequency be measured before initialisation.

It is possible to formulate a constrained optimisation problem to remove the risk posed by the local minimum. The necessary constraint is a lower bound on the stiffness ratio ($\hat{\mu}_k$) and can be calculated from [Equation (2.14)]:

$$\left(\frac{\Omega_2}{\omega_1}\right)^2 \frac{2}{\hat{\mu}_k}\left(\frac{\omega_1}{\bar{\omega}_2}\right)^2 - \frac{1+\hat{\mu}_k}{\hat{\mu}_k}\left(\frac{\omega_1}{\bar{\omega}_2}\right)^2 - 1 - \sqrt{\left[\frac{1+\hat{\mu}_k}{\hat{\mu}_k}\left(\frac{\omega_1}{\bar{\omega}_2}\right)^2 + 1\right]^2 - \frac{4}{\hat{\mu}_k}\left(\frac{\omega_1}{\bar{\omega}_2}\right)^2} = 0 \tag{3.2}$$

where Ω_2 is equal to the excitation frequency ω_e. In practice the above value will be found from a characterisation test and will therefore include the effect of damping. Once the problem has been set for a specific excitation frequency, continuous monitoring is necessary to ensure that the excitation frequency does not change. If the excitation frequency does change, it is necessary to recast the optimisation problem with a new lower bound. Only large changes in excitation frequency will require the process to be restarted, during which time the optimisation algorithm will maintain optimal tuning even if isolator physical properties changed slightly.

It is possible to simulate the control systems suggested above by solving the equation of motion and calculating the objective function from the simulated response. The process is explained in Figure 3.3. The optimisation algorithm calls the objective function. The objective function calculates the transmissibility by solving the equation of motion. The optimisation algorithm now estimates a new stiffness value and recalculates the objective function. During the second and subsequent objective function calls, the Runga-Kutta algorithm is restarted with the final value from the previous simulation as the initial value. This implies that the process of calculating the new stiffness ratio and changing the current stiffness ratio to the new stiffness ratio requires zero time. Although this is physically impossible, the purpose of the simulation is to study the performance of the optimisation algorithm and not the effect of delay and is therefore valid. The effect of delay will be to degrade performance and this simulation therefore represents the best case.

The set of equations that needs to be solved are [Equations (C.1) and (C.2)]:

$$\begin{aligned}\ddot{y}+2\left(\zeta_1+\frac{\omega_1}{\bar{\omega}_2}\bar{\zeta}_2\right)\omega_1\dot{y}-2\frac{\omega_1}{\bar{\omega}_2}\bar{\zeta}_2\omega_1\dot{u}+\omega_1^2\left(1+\mu_k\right)y-\omega_1^2\mu_k u-2\zeta_1\omega_1\dot{x}-\omega_1^2 x=0\\ \ddot{u}+2\bar{\zeta}_2\bar{\omega}_2\left(\dot{u}-\dot{y}\right)+\mu_k\bar{\omega}_2^2\left(u-y\right)-\left(\frac{\bar{\omega}_2}{\omega_1}\right)^2\ddot{x}=0\end{aligned} \tag{3.3}$$

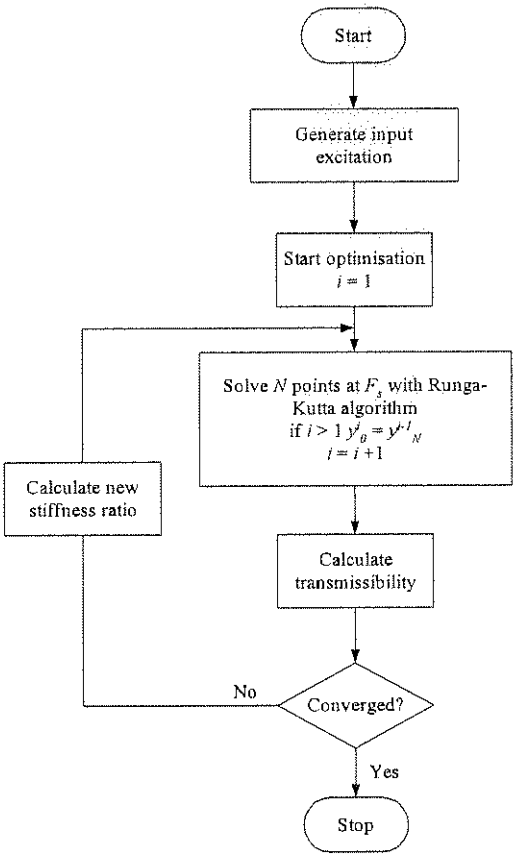

Figure 3.3: Control flow diagram

The properties of the system that was simulated are $\omega_1 = 1$, $A_b/A_a = 10$ and $m_B/m_y = 0.003$. This is the same system as was used in the previous chapter and only serves to illustrate the method. The solution was found with $F_s = 5$ Hz and the transmissibility was estimated using the H_1 estimator. H_1 evaluated at the excitation frequency is (Ewins, 2000):

$$H_1(\omega_e)=\frac{S_{xy}(\omega_e)}{S_{yy}(\omega_e)} \tag{3.4}$$

In a practical system it will be easier to use the ratio of rms output to input as an estimate of the transmissibility. The rms and maximum values calculations are, however, a function of frequency content and the number of data points used. At steady state the signals should only contain the excitation frequency, but due to impulsive excitation when the stiffness ratio is changed the two natural frequencies will also be excited. This has a larger effect on the maximum values calculation than the rms since the rms calculation averages the error. One possible solution is to use a band-pass

filter. Figure 3.4 shows four transmissibility estimates, a simple division of maximum values, a filtered and unfiltered rms and the H_1 estimate. Since the H_1 estimate is calculated at the excitation frequency only, it is considered to be the most accurate. The band-pass filtered rms can approach the H_1 estimate and might be easier to implement in practice.

Figure 3.5 shows that a minimum number of data points will be needed for an accurate estimate using the unfiltered rms method. The number of data points required will depend on the time taken to reach steady state conditions and therefore the damping present in the system.

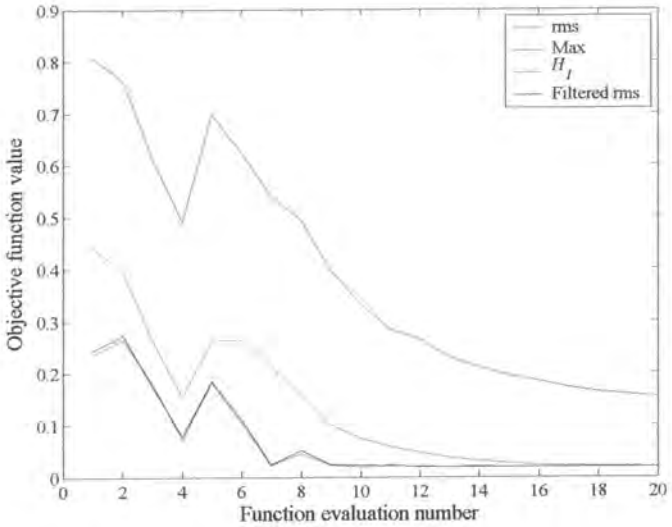

Figure 3.4 Comparison of objective function estimates at low damping ($N = 200$, $\omega_1 = 1$, $A_b/A_a = 10$, $m_B/m_y = 0.003$, $\zeta_1 = 0.01$ and $\overline{\zeta}_2 = 0.01$)

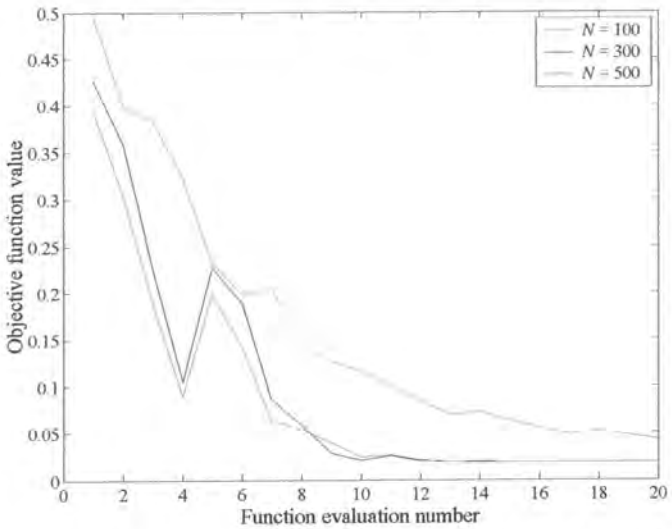

Figure 3.5 Comparison of objective function estimates at low damping for a different number of data points used for the rms transmissibility estimate ($\omega_1 = 1$, $A_b/A_a = 10$, $m_B/m_y = 0.003$, $\zeta_1 = 0.01$ and $\overline{\zeta}_2 = 0.01$)

Another way to formulate the objective function has been described by Long *et al.* (1994). When the angle between the input and output is -90°, the system is close to the minimum transmissibility as

shown in Figure 3.6. At high damping ratios there will be a difference between the optimal value using this method and the actual minimum transmissibility achievable, as indicated in the figure.

The objective function, formulated as the square of the difference between the actual phase angle and the required phase angle (-90°), is shown in Figure 3.7. The device needs to be tuned to the second minimum. Starting at a large stiffness ratio and limiting the step size will ensure that this minimum is reached.

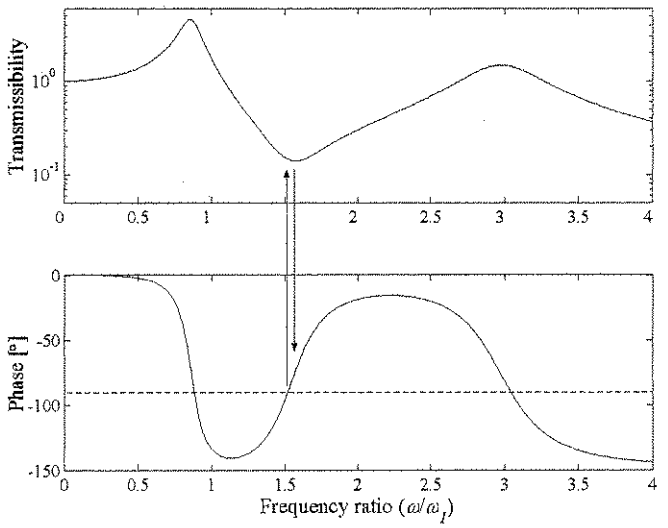

Figure 3.6: Transmissibility and phase angle indicating the difference in tuning frequency ($\omega_1 = 1$, $A_b/A_a = 10$, $m_B/m_y = 0.003$, $\zeta_1 = 0.1$, $\zeta_2 = 0.1$ and $\mu_k = 2$)

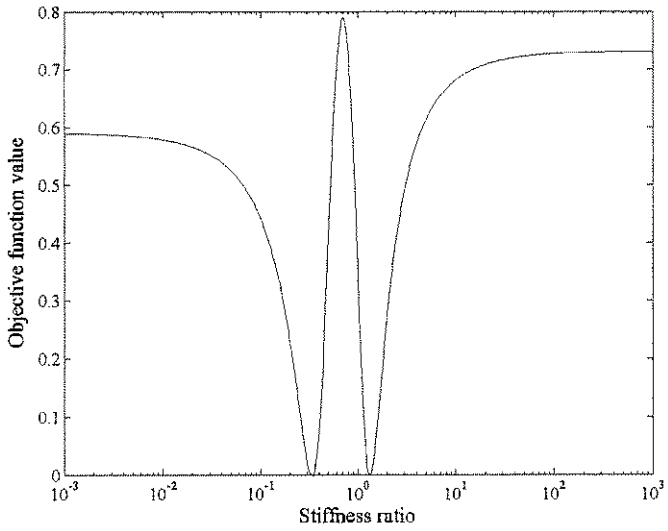

Figure 3.7: Quadrature objective function ($\omega_e = 1.4$, $A_b/A_a = 10$, $m_B/m_y = 0.003$, $\zeta_1 = 0.1$ and $\zeta_2 = 0.1$)

One major advantage of this method is the ease of implementation. The objective function can be formulated by integrating the input and response of the AVAI over a period of time T:

$$f = \frac{1}{T}\int_0^T x(t)\,y(t)\,dt \tag{3.5}$$

3.1.1 Tuning at start-up

A simulation of constant frequency excitation using the Matlab's constrained minimisation algorithm `fmincon.m` is shown in Figure 3.8. The excitation frequency ratio is constant at $\omega_e/\omega_1 = 1.4$. The objective function for this excitation frequency ratio was plotted in Figure 3.1. The simulation shows that an initial value of 0.2 will converge to the local minimum of $\mu_k^* = 0$. When a large initial value is specified, the global optimal value ($\mu_k^* = 1.34$) is approached within a couple of iterations. The results for the various initial values are shown in Table 3.1.

Table 3.1: Results of `fmincon.m` at constant excitation frequency ratio $\omega_e/\omega_1 = 1.4$

Initial value (μ_k^0)	Optimal value (μ_k^*)	$f(\mu_k^*)$
0.2	0.10	1.1088
1.0	1.36	0.1810
5.0	1.32	0.1806

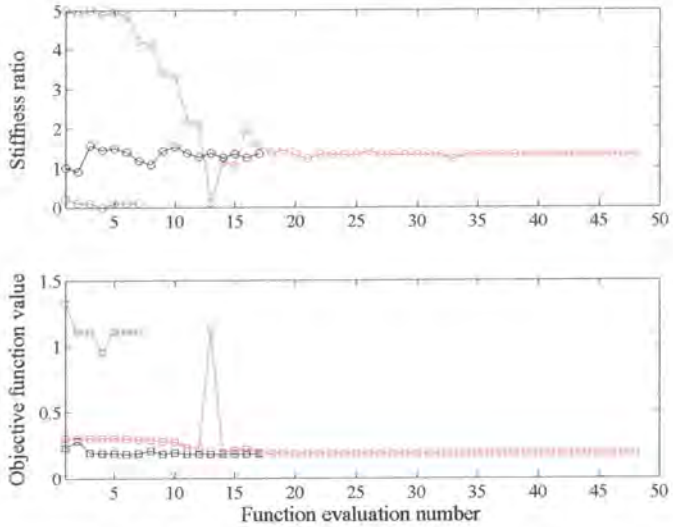

Figure 3.8: Convergence history of `fmincon.m` at constant frequency ratio $\omega_e/\omega_1 = 1.4$, and three initial conditions $\mu_k^0 = 0.2$, 1 and 5 ($\omega_1 = 1$, $A_b/A_a = 10$, $m_B/m_y = 0.003$, $\zeta_1 = 0.1$ and $\zeta_2 = 0.1$)

Recognising that the optimisation problem consists of one variable only, a simple method to use is a unimodal search technique. The search technique involves the efficient minimisation of the interval within which the solution is assumed to fall. If the AVAI is properly designed, the minimum must be in the interval given by the minimum and maximum stiffness ratios. Several methods exist of which the Fibonacci method could be shown to be optimal, but the simpler near-optimal golden section method is often preferred when implemented in optimisation algorithms. The convergence of the `fminbnd.m` algorithm in Matlab is shown in Figure 3.9. The algorithm is based on the golden section method and quadratic interpolation. The algorithm calculates the new stiffness ratio by successive operations that reduce the stiffness ratio interval until a preset convergence tolerance is reached. It can be inefficient when the solution is near one of the bounds and will only give local solutions. This method is easily implemented since the bounds of the stiffness ratio are known.

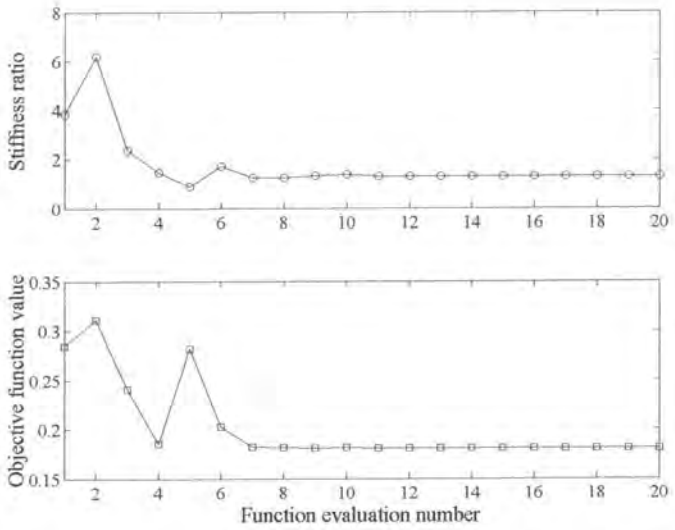

Figure 3.9: Convergence history of `fminbnd.m` at constant frequency ratio $\omega_e/\omega_1 = 1.4$ with bounds 0 and 10 ($\omega_1 = 1$, $A_b/A_a = 10$, $m_B/m_y = 0.003$, $\zeta_1 = 0.1$ and $\bar{\zeta}_2 = 0.1$)

To find the global minimum a genetic algorithm can be used. The result of the freely available algorithm `devec3.m` of Storn (1996) is shown in Figure 3.10.

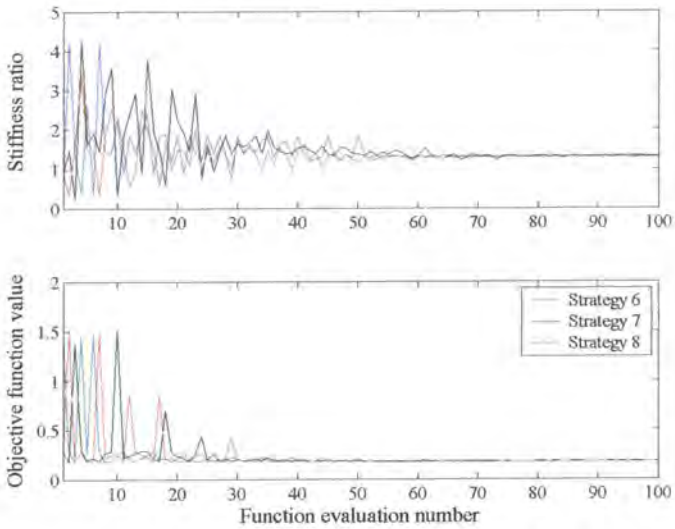

Figure 3.10: Convergence history of `devec3.m` at constant frequency ratio $\omega_e/\omega_1 = 1.4$ ($\omega_1 = 1$, $A_b/A_a = 10$, $m_B/m_y = 0.003$, $\zeta_1 = 0.1$ and $\bar{\zeta}_2 = 0.1$)

The algorithm is based an evolutionary process where the next generation is selected with bias towards the fittest choice of stiffness ratio. The strategies included crossover, which attempts to create a better solution from two previous solutions using parts of each. It differs from the previous technique in that it is suitable for problems with multiple local minima. The algorithm implements nine strategies of which the best three are shown. Some did not converge after 200 iterations. Although the algorithm was able to find the global optimum value, it did so after almost ten times more function evaluations than the previous method. Additionally, the transmissibility was larger than 1 during the optimisation

process. If this cannot be tolerated by the mechanical system under consideration, this method will not be acceptable. The methods discussed previously will ensure that such a condition cannot occur and are therefore safer to use.

3.1.2 Sudden excitation frequency change

If a step change in frequency occurs the algorithm must adapt the stiffness to the new optimal value for that excitation frequency. Since optimisation algorithms are not designed to handle changes in the objective function during optimisation, the standard Matlab routines did not exhibit the desired behaviour. A gradient-based algorithm that does not use explicit line searches was successfully used for this case. Details of the lfopc algorithm can be found in Snyman (1982). The algorithm handles constraints with a penalty function approach.

The gradient is determined using forward-difference (Nocedal & Wright, 1999):

$$\frac{\partial f}{\partial x_i} \approx \frac{f(x+\varepsilon e_i) - f(x)}{\varepsilon} \tag{3.6}$$

where e_i is the i^{th} unit vector and ε is chosen to be a small value. An additional advantage of this algorithm is that the step size can be controlled. This makes it easy to limit the risk that a too low stiffness ratio will be calculated during the optimisation process. A typical result is shown in Figure 3.11 and Table 3.2.

Table 3.2: Results of lfopc at constant excitation frequency ratio

Excitation frequency ratio (ω_e/ω_1)	Optimal value (μ_k^*)	μ_k after 7000 s of excitation at ω_e/ω_1
1.2	0.7710	0.7571
1.4	1.3414	1.3004

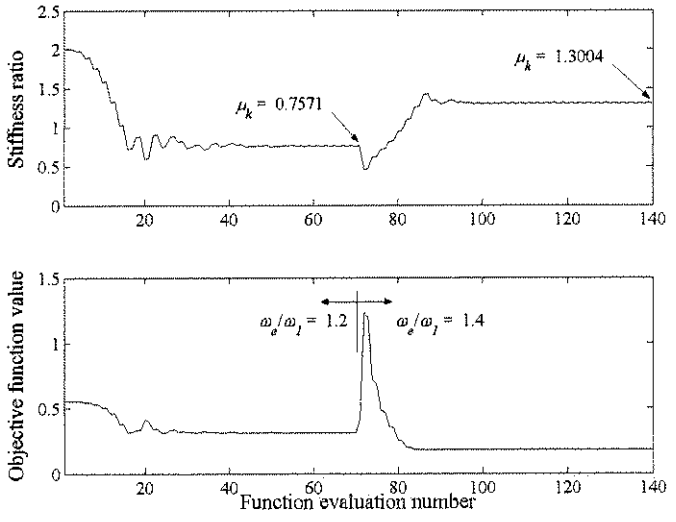

Figure 3.11: Convergence history of lfopc with a frequency step from $\omega_e/\omega_1 = 1.2$ to $\omega_e/\omega_1 = 1.4$ at 7000 s ($\omega_1 = 1$, $A_b/A_a = 10$, $m_D/m_y = 0.003$, $\zeta_1 = 0.1$ and $\bar{\zeta}_2 = 0.1$)

At 7000 seconds the excitation frequency ratio was changed from 1.2 to 1.4. The algorithm adapted the stiffness ratio to the optimum of the new excitation frequency within a couple of function evaluations. The step size was limited to 0.3 while the other parameters were left at their default. The time history is shown in Figure 3.12.

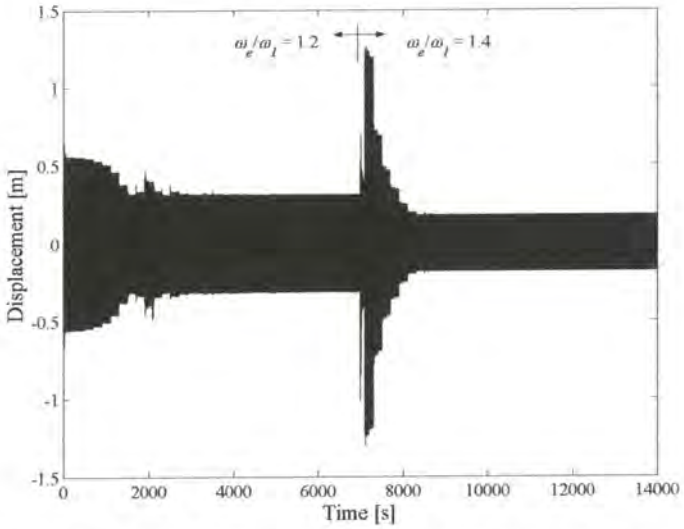

Figure 3.12: Time history of the isolated system displacement for Ifopc with a frequency step from ω_e/ω_1 = 1.2 to 1.4 at 7000 s ($\omega_1 = 1$, $A_b/A_a = 10$, $m_B/m_y = 0.003$, $\zeta_1 = 0.1$ and $\bar{\zeta}_2 = 0.1$)

3.1.3 Slow change in excitation frequency or AVAI properties

When a slow change in excitation frequency occurs the optimisation method will not always have the desired result since optimisation requires that the objective function should only be a function of the variables being optimised. If the optimisation algorithm is not restarted the calculated gradients will be incorrect. Two results are shown in Figure 3.13.

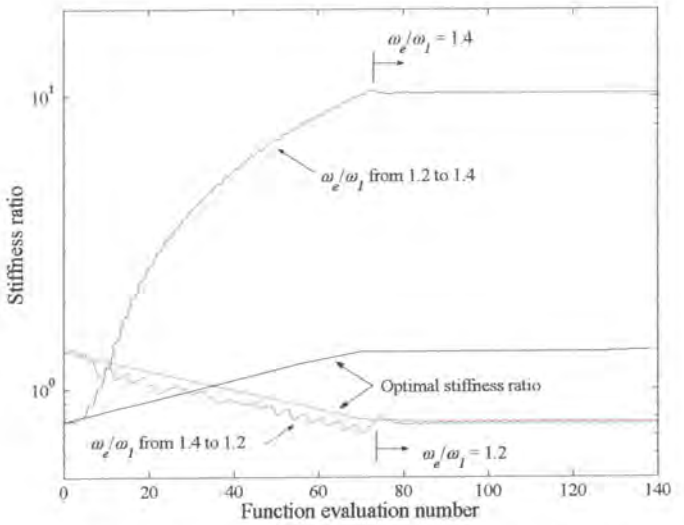

Figure 3.13: The tuning result for a slow change in excitation frequency ($\omega_1 = 1$, $A_b/A_a = 10$, $m_B/m_y = 0.003$, $\zeta_1 = 0.1$ and $\bar{\zeta}_2 = 0.1$)

For a case where the excitation frequency ratio varied from 1.4 to 1.2 over 7000 seconds, the tuning result seems reasonable. For a case where the excitation frequency ratio varied from 1.2 to 1.4, the stiffness ratio calculated was incorrect. For a case where a slow change in frequency is expected, open-loop tuning must be implemented as will be discussed in §3.1.4.

Figure 3.14 shows the effect of a changing system parameter on the convergence history. The primary system natural frequency was changed from 1 to 1.2 during the first 6000 seconds, after which it was kept constant. The algorithm was able to follow the optimal stiffness ratio even with incorrect gradient information. If the change were in the opposite direction the convergence would not have been to the correct value as was the case for a slow change in excitation frequency.

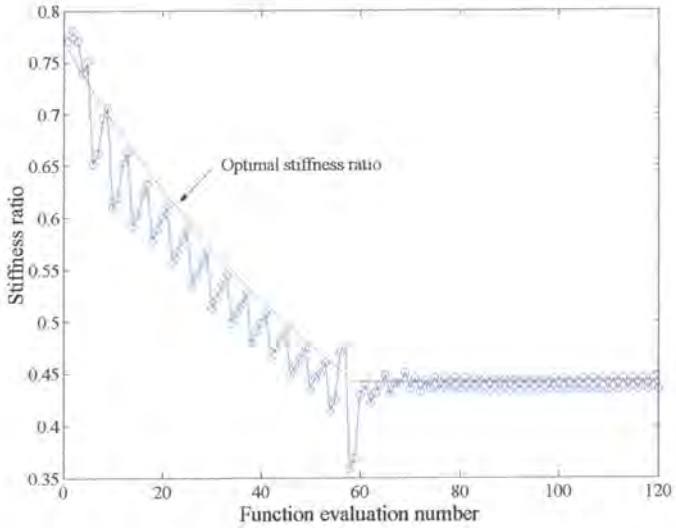

Figure 3.14: Convergence history of lfopc with ω_1 changing from 1 to 1.2 from function evaluation 1 to 60 ($\omega_e = 1.2$, $A_b/A_a = 10$, $m_B/m_y = 0.003$, $\zeta_1 = 0.1$ and $\bar{\zeta}_2 = 0.1$)

3.1.4 General tuning method

Although it has been shown that for certain conditions a restart of the optimisation algorithm after a change in excitation frequency is not necessary, it is the safest option since it will ensure that the optimisation algorithm starts near the optimal point. If the frequency varies slowly or frequently this method will not be efficient. In such a case open-loop rough tuning followed by a fine-tuning algorithm should be used. The rough tuning can be done using either a look-up table or a curve fit of the stiffness ratio (μ_k) *vs.* isolation frequency (ω_i). The rough tuning only needs to set the stiffness ratio near the optimal value as shown in Figure 3.15. If the initial value is close to the optimal value after the change in excitation frequency occurred, convergence could be achieved after only a few objective function evaluations.

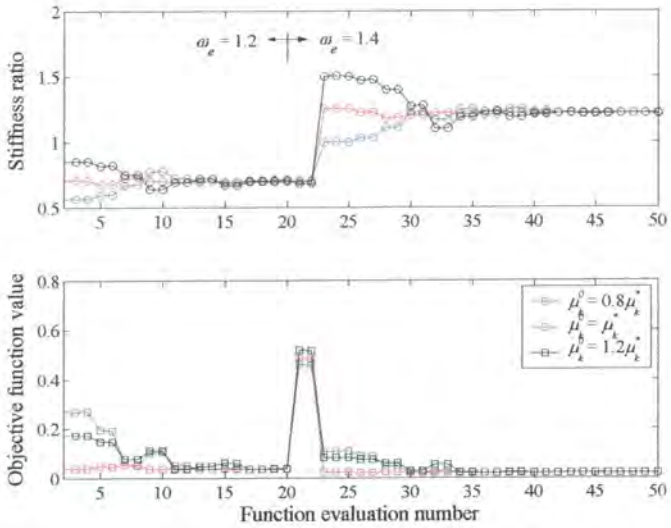

Figure 3.15: Convergence history of lfopc with a frequency step from $\omega_e/\omega_1 = 1.2$ to $\omega_e/\omega_1 = 1.4$ at 2000 s ($\omega_1 = 1$, $A_b/A_a = 10$, $m_B/m_y = 0.003$, $\zeta_1 = 0.1$ and $\bar{\zeta}_2 = 0.1$)

The system can be made more robust by continuous updating of the look-up table using the results of each optimisation process. The flow diagram for such a process is shown in Figure 3.16.

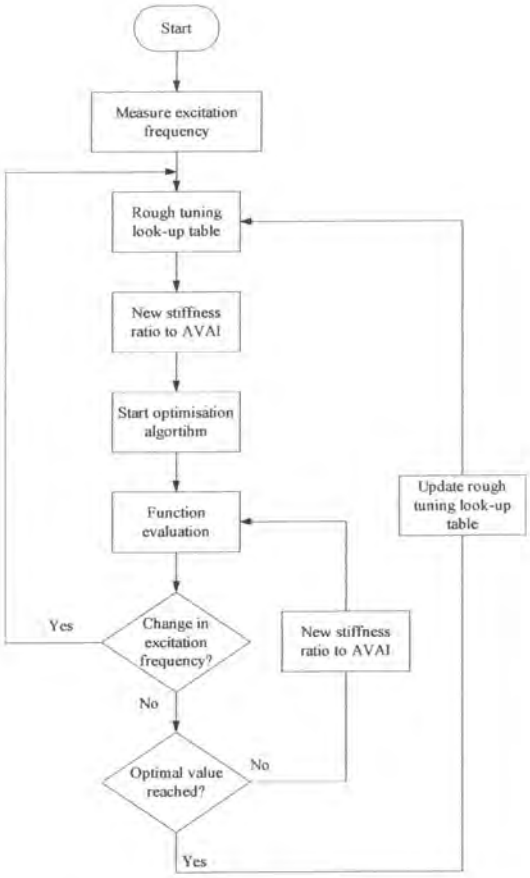

Figure 3.16: General tuning method

During optimisation the excitation frequency must be monitored continuously to make sure than an erroneous value is not entered in the look-up table. The frequency change must be evaluated with a certain tolerance to account for small changes in the excitation frequency and small errors in the estimation process. The maximum error that can be allowed is a function of the bandwidth and the rate of change in frequency.

3.2 Type II AVAI

The control for the type II AVAI is in most respects exactly the same as for the type I. This chapter will not repeat the discussion of the previous paragraphs; instead the few differences will be highlighted. The most important difference is the objective function [Equation (2.48)]:

$$f(\mu_k) = \left| \frac{1 + i\frac{2}{\mu_k}\frac{\omega_e}{\omega_n'}\zeta' - \frac{1}{\mu_k}\left(\frac{\omega_n'}{\omega_i'}\right)^2\left(\frac{\omega_e}{\omega_n'}\right)^2}{1 + i\frac{2}{\mu_k}\frac{\omega_e}{\omega_n'}\zeta' - \frac{1}{\mu_k}\left(\frac{\omega_e}{\omega_n'}\right)^2} \right| \tag{3.7}$$

The objective function is shown in Figure 3.17. If compared to the objective function of the type I AVAI, it can be seen that the problem with the local minimum is reversed and that a large initial stiffness value will make it impossible for a local minimiser to find the optimum stiffness ratio.

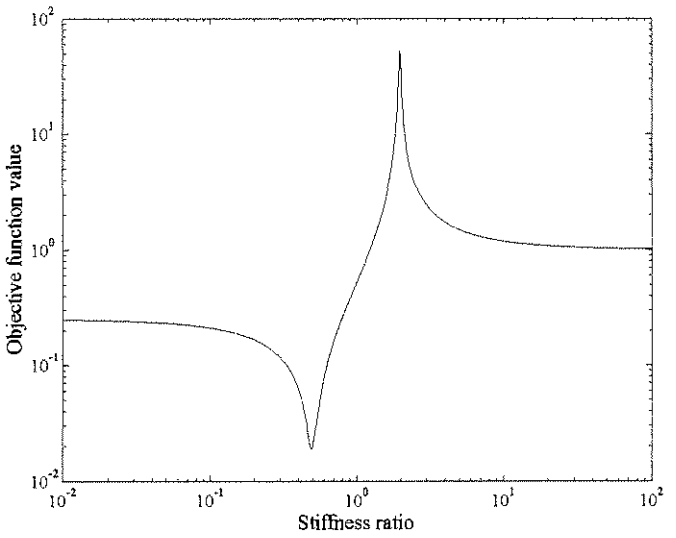

Figure 3.17: Objective function *vs.* stiffness ratio $\omega_e/\omega_n' = 1.4$ ($\omega_n'/\omega_i' = ½$ and $\zeta' = 0.01$)

The techniques to address this problem have been discussed in §3.1. For the last method that was discussed an upper bound on the stiffness ratio ($\hat{\mu}_k$) must be calculated. For the type I AVAI this constraint is [Equation (2.47)]:

$$\hat{\mu}_k = \frac{4\frac{\zeta'^2}{\mu_k} + 4\frac{\zeta'^2}{\mu_k}\left(\frac{\omega_n'}{\omega_i'}\right)^2 - 2\left(\frac{\omega_n'}{\omega_i'}\right)^2}{-\left(\frac{\omega_n'}{\omega_i'}\right)^2 - 1 + \sqrt{\left[\left(\frac{\omega_n'}{\omega_i'}\right)^2 - 1\right]^2 + 8\frac{\zeta'^2}{\mu_k}\left[\left(\frac{\omega_n'}{\omega_i'}\right)^2 + 1\right]}}\left(\frac{\Omega_n}{\omega_n'}\right)^2 \tag{3.8}$$

where Ω_n is equal to the excitation frequency ω_e. To estimate the transmissibility the following equation of motion must be solved [Equation (C.8)]:

$$\ddot{y} + 2\zeta'\omega_n'\dot{y} + \mu_k\omega_n' y = \left(\frac{\omega_n'}{\omega_i'}\right)^2 \ddot{x} + 2\zeta'\omega_n'\dot{x} + \mu_k\omega_n' x \tag{3.9}$$

The results for the lfopc algorithm for four initial conditions are shown in Figure 3.18. No constraint was used to illustrate the problem posed by the local minimum when a high initial value for the stiffness ratio is used.

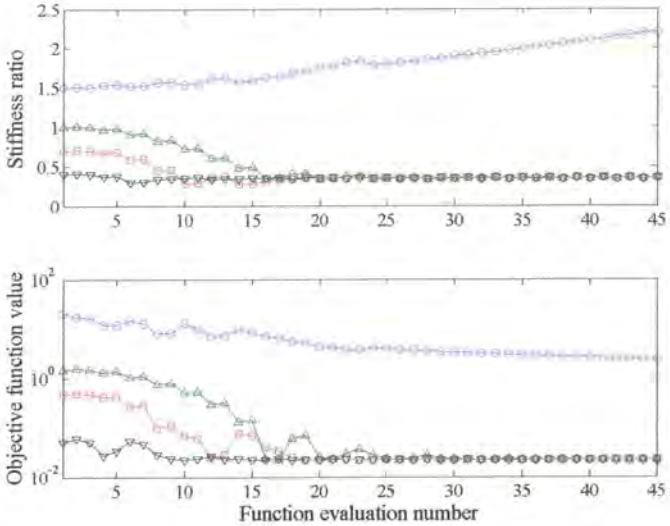

Figure 3.18: Adaptation results for 4 initial conditions $\omega_e/\omega_n' = 1.2$ ($\mu_k^0 = 0.4, 0.7, 1, 1.5$, $\omega_n'/\omega_i' = ½$ and $\zeta' = 0.01$)

For the type II AVAI the same general tuning method as described in Figure 3.16 can be applied to ensure both optimal and fast tuning.

3.3 Conclusion

This chapter showed how optimisation can be used as a control method for the AVAI. Several pitfalls exist which have been discussed in detail. Even though the objective functions differ, the same control methods can be applied to the type I and type II AVAIs. For the most general case it was suggested that open-loop tuning using a look-up table be used as a rough tuning method. If the excitation

frequency remains constant, a fine-tuning algorithm will find a new optimal stiffness for that excitation frequency. If such an optimal value is found, the look-up table is updated. The methods concentrated on using the transmissibility value as the objective function. If the input amplitude is known to be constant, it is possible to use only one sensor to measure the response of the system to provide the objective function value.